Electrophysiological characterization of catecholamine-containing GFP-expressing dissociated mouse area postrema neurons and their response to glucagon-like peptide-1 receptor agonists

by

Samantha Lee

A thesis submitted to the Faculty of Graduate Studies of the University of Manitoba

in partial fulfilment of the requirements of the degree of

MASTER OF SCIENCE

Department of Biological Sciences

University of Manitoba

Abstract

The area postrema (AP) is a hindbrain sensory circumventricular organ that participates in energy balance regulation. Catecholamine-containing AP neurons are a key subpopulation that inhibit food intake and appear to mediate the appetite-reducing effects of glucagon-like peptide-1 (GLP-1) receptor agonists. Neither the electrophysiological properties nor the electrical response of CA-containing neurons to GLP-1 receptor agonists has been characterized. Therefore, we carried out patch clamp experiments on dissociated neuronal cultures from transgenic mice (TH-GFP). Voltage-clamp recordings revealed subtle differences in K^+ current, Na^+ current, and I_H properties between TH and nonTH neurons. In current-clamp configuration, application of 1 μM GLP-1 or 1 μM Exendin-4 activated the majority of TH neurons tested. Our results suggest that TH neurons are an electrophysiologically heterogeneous population and confirm that GLP-1 receptor agonists activate most TH neurons. Together, it appears that TH neurons play multiple roles in integrating satiety information to ultimately reduce food intake.

Dedication and Acknowledgements

This thesis is dedicated to Michael Becker, who stood by me through blood, sweat, and many tears.

Thank you to my committee members Dr. Jim Hare and Dr. Gilbert Kirouac for your valuable input. Thank you Dr. Quinton Pitman and Ian Spreadbury for your experimental guidance. Thank you Dr. Toshihiko Yada and Dr. Shigetoma Suyama for hosting me during my stay in Japan. Thank you Dr. Mark Belmonte and Dr. Dirk Weihrauch for your personal guidance. Thank you Ainsley Chan and Razvan Purza for your kind support. Thank you Dr. Mark Fry for your patience.

Table of contents

List of Figures

List of Tables

List of abbreviations

aCSF	Artificial cerebrospinal fluid
ARC	Arcuate nucleus
AgRP	Agouti-related protein
ANGII	Angiotensin II
AP	Area postrema
AT_1	Angiotensin II type-I receptor
BBB	Blood-brain barrier
CA	Catecholamine
CCK	Cholecystokinin
CNS	Central nervous system
CTZ	Chemoreceptor trigger zone
CVO	Circumventricular organ
ENaC	Epithelia sodium channel
ERS	Exteneral recording solution
GABA	Gamma aminobutyric acid
GFP	Green fluorescent protein
GHSR	Growth hormone secretagogue receptor
GLP-1	Glucagon-like peptide 1
ICV	Intracerebroventricular
I_H	Hyperpolarization activated current
I_K	Non-inactivating K^+ current

I_{NaT}	Transient Na^+ current
I_{NaP}	Persistant Na^+ current
IRS	Internal recording solution
I_{TO}	Transient K^+ current
I_{TOTAL}	Total voltage-gated K^+ current
IP	Intraperitoneal
NPY	Neuropeptide Y
NTS	Nucleus of the solitary tract
PB	Phosphate buffer
PBN	Parabrachial nucleus
POMC	Proopiomelanocortin
RAMP	Receptor-activity modifying protein
SFO	Subfornical organ
TEA	Tetraetylammonium
TH	Tyrosine hydroxylase
TTX	Tetrodoxin
$V_{1/2ACT}$	Voltage of half activation
$V_{1/2INACT}$	Voltage of half inactivation
VLM	Ventrolateral medulla

1. Introduction

Obesity has become a modern day epidemic, surpassing malnutrition as a leading cause of death (WHO, 2016). Advances in technology and economic development have increased access to highly processed food and decreased physical activity (Zobel et al., 2016). These commodities contribute to greater caloric consumption and reduced physical activity, which together result in weight gain. In Canada, over half of adults and a quarter of youth are reported as either overweight (BMI $\geq$ 25 kg/m^2) or obese (BMI $\geq$ 30 kg/m^2). This raises concern because health problems related to excess weight such as cardiovascular disease, type II diabetes, cancer, and joint problems (Harvard Health Publications, 2007), create a financial burden on health care systems. Canada spends an estimated 4 to 7 billion dollars, or about 4% of the annual health care budget, treating obesity-related diseases (Government of Canada, 2011); this represents more than what is spent on health research or other basic services such as vision care (Canadian Institute for Health Information, 2015). It is clear that we need effective strategies to prevent obesity and help individuals lose weight in order to improve their health and alleviate financial strain.

Despite increased efforts in promoting the adoption of a healthy diet and daily exercise regimen, the numbers of overweight and obese individuals have not begun to decline (Statistics Canada, 2014). Physiological factors that contribute to regulation of energy balance include genetics, circadian rhythm, and pregnancy (Levin, 2005, 2007). The central nervous system (CNS) is also well-recognized to contribute to energy balance. Central mechanisms that govern food intake and energy balance include feelings of reward, direct neural communication with the gut, and sensing of circulating peripheral

peptides and hormones by the CNS (Berthoud, 2002). Disruption of any of these circuits may result in miscommunication about energy balance state and lead to obesity. Obesity itself may further potentiate these disruptions and cause changes within the CNS that lead to resetting of central weight regulatory mechanisms in obese individuals to favour weight stasis over weight loss. For example, when obese individuals attempt to loss weight, these central compensatory mechanisms may include increased feelings of hunger and increased cravings for pleasurable food working against weight loss (Levin, 2007; Thomas et al., 2013). Because of this, weight loss is often negligible and difficult to sustain long-term (Salam et al., 2016). In order to reduce the current prevalence of obesity, and better prevent individuals from becoming overweight and obese in the future, it is crucial we have a deeper understanding of how the CNS governs energy balance.

This introduction will review our current knowledge of how the CNS regulates energy balance. It will first review well-known peripheral satiety signals and present how the hypothalamus integrates these signals into a neuronal circuit to regulate energy balance. This introduction will then discuss how the blood-brain barrier (BBB) limits the ability of the hypothalamus to detect peripheral satiety signals and present the circumventricular organs (CVOs) as alternative sites for the first order detection of such signals. From there, the remainder of the introduction will focus on the area postrema (AP), a brainstem sensory CVO implicated in energy balance regulation; this section will introduce glucagon-like peptide-1 (GLP-1), an incretin hormone and satiety signal, and the notion that catecholamine (CA)-containing area postrema (AP) neurons detect circulating GLP-1. Finally, a series of experiments will explore the possibility that

CA-containing AP neurons can be identified by their electrophysiological properties, and investigate how they are electrically modulated by GLP-1.

1.1 CNS regulation of energy balance

The hypothalamus is a key CNS centre regulating many aspects of homeostasis including energy balance. Pioneering work conducted by Hetherington and Ranson (1940) and Anand and Brobeck (1951) first demonstrated that the hypothalamus plays an essential role in the regulation of food intake and body weight. Since then, much work has been invested into furthering the notion of the hypothalamus in energy balance, leading to the identification of the arcuate nucleus (ARC) of the hypothalamus as the most important centre in the determination of hunger and satiety. Neurons of the ARC are thought to possess the ability to detect and respond to circulating satiety signals, peptides and hormones that are released from the periphery into the circulation to signal current energy state.

1.1.1 Conventional satiety signals

Currently, dozens of peripheral signals are recognized to influence appetite. This section of the introduction will focus on two well-studied satiety signals (ghrelin and leptin) and the notion that they modulate satiety at the level of the ARC.

The orexigenic (appetite stimulating), 28 amino acid peptide, ghrelin, was first discovered by Kojima et al., 1999 as an endogenous ligand for the G-protein coupled growth hormone secretagogue receptor (GHSR). Ghrelin is released from the stomach in response to hunger (Date et al., 2000), with plasma levels peaking just prior to a meal and

decreasing afterwards (Cummings et al., 2001). Both peripheral and central injection of ghrelin in rats increase food intake as well adiposity (Tschöp et al., 2000; Shintani et al., 2001). Increased food consumption is also observed in humans following a subcutaneous administration of ghrelin (Druce et al., 2006). Furthermore, ghrelin-induced food intake in rats can be attenuated by intracerebroventricular (ICV) injection of an anti-ghrelin immunoglobin G (Bagnasco et al., 2003). Cells within the ARC express the GHSR (Willesen et al., 1999; Bagnasco et al., 2003; Zigman et al., 2006). Mice lacking the GHSR show subtle deficits in energy balance including reduced gastric emptying (Yang et al., 2013), a decrease in food-anticipatory activity (Lamont et al., 2013), decreased body weight, and decreased levels of adipose tissue (Lin et al., 2011).

Leptin is a 167 amino acid anorexigenic (appetite inhibiting) peptide synthesized by and secreted from white adipocytes (Green et al., 1995) in proportion to total body weight (Weigle et al., 1997), and elicits an opposing response to ghrelin. Intraperitoneal (IP) injection of leptin into mice decreases food intake, body fat, and total weight (Halaas et al., 1995). IP injections of leptin can also restore a healthy body weight in ob/ob mice (Halaas et al., 1995), which possess a mutation in the leptin gene (*ob*) resulting in overeating and obesity (Ingalls et al., 1950). Neurons within the ARC express the leptin receptor (Ob-R) (Tartaglia et al., 1995). Viral mediated knockdown of the leptin receptor in rats results in increased food intake and body weight (Bian et al., 2013).

1.1.2 NPY/Melanocortin circuit

Two key neuronal populations within the ARC are thought to largely dictate satiety. These populations may be identified by their main peptide product and include

orexigenic neuropeptide Y (NPY)-containing neurons and anorexigenic proopiomelanocortin (POMC)-containing neurons. Together, these populations make up the NPY/melanocortin circuit (Figure 1.1), which is considered to be the most important circuit in central regulation of energy balance.

NPY/AgRP neurons are located in the ventromedial ARC and contain the orexigenic peptides NPY and agouti-related protein (AgRP). NPY/AgRP neurons utilize NPY and GABA as neurotransmitters in signalling hunger to higher neuronal centres. Repeated injections of NPY into the paraventricular nucleus of the hypothalamus in rats significantly increase food intake, body weight, and adiposity (Glenn Stanley et al., 1986). Furthermore, mice with a homozygous knock-out of the gene encoding NPY show reduced food intake after fasting when compared to wild-type mice (Bannon et al., 2000).

Within higher neuronal centres of the hypothalamus NPY may bind one or more of the receptors belonging to the Y receptor family including Y1 (Kopp et al., 2002), Y2 (Stanić et al., 2011), Y4 (Kishi et al., 2005), or Y5 (Nichol et al., 1999). Mice lacking the Y1 (Pedrazzini et al., 1998) or Y5 receptor (Criscione et al., 1998; Marsh et al., 1998) show reduced food intake. Furthermore, administration of a Y1 receptor antagonist in mice lacking the Y5 receptor nearly abrogates the orexigenic effects of NPY administration (Marsh et al., 1998).

NPY neurons are thought to possess the ability to detect and respond to circulating satiety signals. NPY neurons express the GHSR (Willesen et al., 1999). Activation of GHSR not only depolarizes NPY neurons but also increases action potential frequency (Cowley et al., 2003). As well, *in vitro* administration of ghrelin is able to increase NPY mRNA expression in brain tissue (Goto et al., 2006). Increased NPY

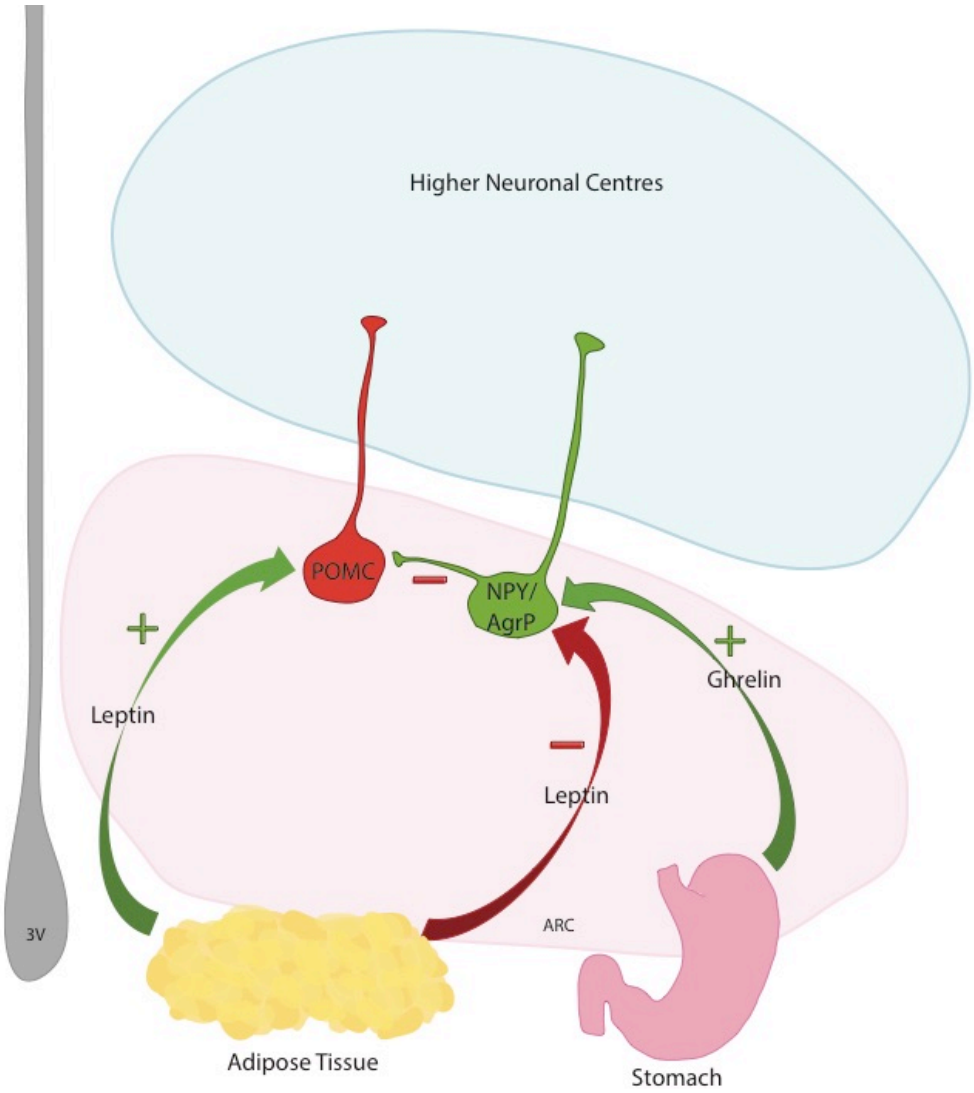

Figure 1.1 NPY/Melanocortin circuit detects peripheral satiety signals and signals to higher neuronal centres. NPY/AgRP neurons and POMC neurons make up the NPY/melanocortin circuit. NPY/AgRP neurons stimulate appetite and as such are activated by ghrelin (Cowley et al., 2003) and inhibited by leptin (Nagamori et al., 2003). Conversely, POMC neurons inhibit appetite and are activated by leptin (Cowley et al., 2001). NPY/AgRP neurons release the inhibitory neurotransmitter, GABA, onto POMC neurons when they are activated (Cowley et al., 2003). This decreases appetite-inhibiting signalling from POMC neurons and shifts the balance of the NPY/melanocortin circuit to favour food intake.

mRNA expression is also seen when a single dose of ghrelin is administered via ICV injection in rats (Shintani et al., 2001). When stimulated by ghrelin, NPY neurons release the inhibitory neurotransmitter GABA onto anorexigenic neurons within the hypothalamus, potentiating the appetite stimulating effects of ghrelin (Cowley et al., 2003). Mice lacking the vesicular GABA transporter are unable to release the inhibitory neurotransmitter GABA onto anorexigenic neurons. These mice are resistant to diet-induced obesity and have reduced body weight and food intake after IP injection of ghrelin (Tong and Pelletier, 1992).

NPY neurons also express the leptin receptor (Håkansson et al., 1996), allowing counter regulation. Activation of leptin receptors causes hyperpolarization of the membrane potential resulting in neuronal inhibition (Nagamori et al., 2003). Leptin is also able to attenuate the stimulatory effects of ghrelin in a time-dependent manner (van den Top et al., 2004; Kohno et al., 2007; Williams et al., 2010; Yang et al., 2010). Lastly, leptin application has been shown to reduce NPY mRNA expression (Morrison et al., 2005; Bian et al., 2013).

POMC neurons are found within the ventrolateral ARC (Pelletier and Dube, 1977; Jacobowitz and O'Donohue, 1978) and utilize POMC and it's peptide cleavage products, such as α-MSH, in signalling to higher centres. Specific deletion of the ribonuclease Dicer-1 in rat POMC neurons results in cell death and leads to obesity, glucose intolerance, and decreased physical activity (Greenman et al., 2013). ICV injection of α-MSH into the third ventricle of rats has been demonstrated to reduce food intake and body weight (McMinn et al., 2000). Thus far, the MC3 and MC4 melanocortin receptors have been shown to have the largest roles in appetite regulation. Mice lacking MC4

develop adult onset obesity, hyperphagia, and glucose intolerance (Huszar et al., 1997). Deletion of MC3 in mice results in a metabolic syndrome characterized by increased levels of adipose tissue and decreased motor activity (Butler et al., 2000).

Specific receptors for AgRP do not exist. Instead, AgRP released by NPY/AgRP neurons acts as a competitive antagonist at melanocortin receptors within the hypothalamus. ICV injection of a c-terminal fragment of AgRP or a MC3 and MC4 antagonist into rats results in hyperphagia (Rossi et al., 1998).

POMC neurons are also thought to possess the ability to detect circulating satiety signals. POMC neurons within the hypothalamus express the Ob-R (Cheung et al., 1997). Activation of the leptin receptor changes the mRNA expression within POMC neurons. Expression of POMC mRNA has been shown to be positively correlated to leptin mRNA (Mizuno et al., 1998). Further to this, Mizuno et al. (1998) have demonstrated that POMC mRNA expression is decreased in leptin insufficient (ob/ob) and leptin insensitive (db/db) mice. Application of exogenous leptin to neurons in brain slices results in membrane depolarization and increased action potential firing frequency in POMC neurons (Cowley et al., 2001; Wang et al., 2008; Williams et al., 2010). Leptin also acts indirectly on POMC neurons. Leptin application decreases the frequency of GABA-mediated inhibitory postsynaptic currents from orexigenic neurons, lifting tonic inhibition on POMC neurons (Cowley et al., 2001), thus increasing appetite inhibition. Mice with a specific knockout of the leptin receptor in POMC neurons are obese, hyperglycemic, and insensitive to insulin and restoration of the leptin receptor recovers glucose and insulin control (Berglund et al., 2012).

In spite of the wealth of information supporting this model, a significant question remains: how do satiety signals gain access to the brain through the blood brain barrier (BBB)?

1.1.3 The BBB

The BBB is a highly selective barrier between the CNS and peripheral circulation and is composed of a tight endothelium surrounded by pericytes and astrocytic endfeet (Reese and Karnovsky, 1967; Abbott et al., 2006). Only select substances, such as lipophilic compounds and water, are able to passively diffuse through this layer. This restricted access means that most peptides, such as satiety signals, cannot come into direct contact with neurons in the CNS. This poses a dilemma because while ARC neurons express receptors for, and are able to respond to satiety signals, the ARC is protected by the BBB (Peruzzo et al., 2000), so it is unknown how these peripherally circulating compounds can reach ARC neurons. A few controversial theories that try to reconcile this discrepancy have been proposed.

One theory is that certain peptides and hormones can be actively transported across the BBB. Leptin was one the first satiety signals proposed to be transported across the BBB via a saturable mechanism (Banks et al., 1996; Koistinen et al., 1998). This mechanism was believed to involve the short form of the leptin receptor as it is expressed on microvessles in the brain (Bjørbæk et al., 1998). However, in rats lacking the short leptin receptor, leptin still enters the CNS, suggesting that there must be another means of entry (Takaya et al., 1996). Ghrelin has also been suggested to enter the CNS by means of a transport protein, however, brain to blood transport of ghrelin is favoured over blood

to brain transport (Banks et al., 2002), and transport of ghrelin into the CNS is too slow to support its observed, more immediate effects on feeding, suggesting that it too must influence the brain via an alternative mechanism (Grouselle et al., 2008).

An alternative method of entry was subsequently proposed such that that the integrity of BBB is labile to changes in energy balance state. For example, obese mice lose the ability to transport ghrelin across the BBB, while fasting promotes ghrelin transport (Banks et al., 2008). More recently, decreases in blood glucose have been shown to reorganize the BBB to favour increased access of peptides to the CNS (Langlet et al., 2013a). A major concern with this theory is that circulating satiety signals do not have consistent access to the CNS (how does leptin get transported into the sated brain), so how these signals would otherwise be transduced remains unknown.

Together, the limitations of the above notions suggest that there must be another means for circulating signals to freely access and modulate neurons of the ARC. Recently, a great deal of attention has been focused on sensory CVOs, areas of the brain that offer a promising avenue of access to the CNS.

1.1.4 Circumventricular organs

CVOs are specialized, midline structures found near the ventricles of the brain. These organs are privileged because unlike the rest of the brain, they lack a complete BBB. For example, the capillary endothelium in CVOs contains large fenestrations, allowing constituents of the circulation that would not normally contact the CNS, such as proteins, to enter CVOs. The role of these fenestrated capillaries to allow diffusion of non-lipid soluble plasma components into the CNS is supported by a study that

demonstrated the vital stain, Evan's blue, marks CVOs after intravenous administration (Mullier et al., 2010; Morita and Miyata, 2012; Langlet et al., 2013b). Due to this unique vasculature, CVOs provide a means by which the periphery and CNS can communicate with one another and therefore, are often referred to as the "windows of the brain" (Gross and Weindl, 1987).

There are a total of 8 CVOs that are divided into sensory and secretory groups (for review see McKinley et al., 2003a). The sensory CVOs include the AP, subfornical organ (SFO), and vascular organ of the lamina terminalis. These CVOs "listen" to the periphery by detecting circulating molecules, peptides, and hormones that signal homeostatic state (Hendel and Collister, 2005; Shi et al., 2007; Fry and Ferguson, 2009). This information is then communicated to autonomic control centres in order to maintain or regain homeostasis. The CNS is also capable of "talking" to the periphery via secretory CVOs that facilitate the release of centrally synthesized hormones and peptides into the peripheral circulatory system. Secretory CVOs include the posterior pituitary, pineal gland, and median eminence (Yao et al., 2011; Glanowska and Moenter, 2015; Simoes et al., 2016). Some also consider the subcomissural organ to be a secretory CVO, however, this is debated as it lacks the "leaky" vasculature that characterizes the other CVOs (Petrov et al., 1994; Rodríguez et al., 1998). The remainder of this thesis will focus on the AP.

1.2 The AP

The AP is of considerable interest because of its functions in emesis, cardiovascular regulation, and in particular, energy balance. The AP is located on the

dorsal aspect of the medulla. In rodents, the AP is situated midline over the central canal on the wall of the fourth ventricle and is subdivided into 4 morphologically distinct zones: the dorsal mantle, the central area, the ventral junction, and the lateral area. To contrast, in humans and other larger mammals, the AP is a bilateral structural that wraps up along the walls of the fourth ventricle (Leslie, 1986; reviewed in McKinley et al., 2003). In these animals, the AP does not have a distinct lateral region. Despite the anatomical differences between rodents and primates, the AP retains relatively similar connectively and function (Leslie, 1986).

In all mammals the AP is part of the dorsal vagal complex, which also includes the nucleus of the solitary tract (NTS) and dorsal motor nucleus of the vagal nerve (Kalia and Sullivan, 1982; reviewed in Palkovits, 1985). This group of nuclei serve to integrate information from visceral sensory neurons and appropriately regulate the activity of visceral organs including the gut and heart.

The AP is distinct from the other sensory CVOs in that it receives direct input from visceral afferent neurons (Morest, 1967), in addition to input from a number of higher brain centres including the NTS, the parabrachial nucleus (PBN), and the dorsomedial and paraventricular hypothalamic nuclei (Shapiro and Miselis, 1985; Geerling et al., 2010). These brain nuclei are important in integrating and relaying autonomic information, and support the role of the AP in regulating homeostasis. Much of the output from the AP is directed towards the adjacent NTS, PBN and ventrolateral medulla (VLM; Shapiro and Miselis, 1985; Cunningham et al., 1994). Nuclei in the forebrain (such as the lateral hypothalamus) also receive synaptic input from the AP (Potes et al., 2010). These targets contribute to the regulation of energy

balance, hydromineral balance, and activity of afferent autonomic vagal neurons, and thus place the AP in a position to be a key regulator of homeostasis. In particular, reciprocal connections with the NTS have been postulated to play an important role in transducing information that the AP has collected by detecting circulating compounds, especially noxious compounds that trigger emesis (Hay and Bishop, 1991a, 1991b; reviewed in Miller and Leslie, 1994).

1.2.1 Emesis

The AP is well recognized for its role in the control of emesis. The AP contains the chemoreceptor trigger zone (CTZ), an area of the brain that detects circulating emetic compounds, which can be either endogenously or exogenously derived.

The first studies examining the role of the CTZ in emesis demonstrated that abalation of the AP in cats and dogs reduces the probability of emesis occurring following ICV administration of epinephrine, apomorphine, or emetine (Borison, 1959; Bhargava et al., 1961); all compounds well-recognized to potently stimulate emesis. Ionophoretic application of many emetic compounds including leucine enkaphalin, cholecystokinin (CCK), and NPY, onto the AP has been shown to stimulate AP neurons as demonstrated by an increase in the frequency of recorded extracellular action potentials (Carpenter et al., 1988). It is important to note that many of the emetic compounds in this study, including CCK and NPY, also function as satiety signals. More recent research has focused on the emetic properties of the cancer drug cisplatin, which induces both an acute (viscerally-mediated) and delayed (centrally-mediated) phase of emesis (Horn, 2009). Cisplatin has been shown to increase cFos activation within the AP

(De Jonghe and Horn, 2009) and ablation of the AP prevents only the delayed phase of cisplatin-induced emesis (Percie du Sert et al., 2009). This is not surprising, as many studies have demonstrated that despite receiving input from vagal afferent neurons, the CTZ does not play a significant role in in initiating emesis triggered by vagal afferent stimulation (Andrews et al., 2001; Hagbom et al., 2011). Finally, the CTZ also contributes to the development of conditioned taste aversion, which occurs when food intake is paired with a noxious substance. If the AP is either ablated or cooled before administration of the profoundly emetic substance, lithium chloride, conditioned taste aversion fails to fully develop (Eckel and Ossenkopp, 1993; Wang et al., 1997). In particular, Shinpo et al. (2012) have demonstrated that a population of neurons expressing a hyperpolarization activated current (I_H) plays an important role in the development of conditioned taste version and feelings of nausea in rats.

1.2.2 Cardiovascular regulation

There is vast literature on the role of the AP in cardiovascular regulation and it is beyond the scope of this thesis to provide an in depth review. Instead, this section will briefly highlight some key findings that strongly support the role of the AP in cardiovascular regulation.

The AP exerts a tonic influence over cardiovascular regulation. In dogs, AP lesions produce acute tachycardia and hypertension followed by a prolonged period of hypotension due to decreased cardiac output and reduced peripheral resistance (Ferrario et al., 1979). Lability of mean atrial pressure is also reduced in AP-lesioned dogs (Pollick et al., 1987). Based on these observations, it was suggested that the AP contains a

pathway that facilitates increased sympathetic activity (Ferrario et al., 1979). This pathway likely involves direct excitation of vasomotor neurons as inhibition of the baroreceptor receptor reflex is not necessary for AP stimulation to increase sympathetic activation (Barnes and Ferrario, 1980). In agreement with the above, is the observation that stimulation of the AP in cats increases coronary resistance, heart rate, and blood pressure (Gatti et al., 1988). Observations in rats also support the view that the AP exerts tonic influence over cardiovascular regulation. For example, hypotension and bradycardia have been observed in rats following AP lesion (Ferguson and Marcus, 1988; Skoog and Mangiapane, 1988; Curtis et al., 2003) and lesioning of the AP in a spontaneously hypertensive rats significantly reduces blood pressure (Mangiapane et al., 1989).

Cardiovascular regulation can be further modulated at the level of the AP by circulating vasoactive peptides. The AP expresses receptors for many such peptides (Quirion et al., 1986; Privitera et al., 2003; Hindmarch et al., 2011) and is well recognized to mediate their effects. The best studied of these peptides is angiotensin II (ANGII). ANGII is a peripheral peptide hormone synthesized and released in response to decreased blood pressure. AP neurons express ANGII type I receptors (AT_1) and are excited by ANGII application (Papas et al., 1990). In particular, the AP most strongly participates in ANGII-dependent regulation of the baroreceptor reflex. For example, ANGII microinjections into the AP increase blood pressure and heart rate. The ability of ANGII to acutely reset the baroreceptor reflex (Xue et al., 2003) and chronically elevate blood pressure (Fink et al., 1987) is dependent on an intact AP. Moreover, an intact AP is required for lorsartan (an AT_1 antagonist) to be fully effective (Collister and Osborn, 1998). In addition to sensing circulating ANGII, the AP detects a number of other

vasoactive peptides including arginine vasopressin (Xue et al., 2003; Yang et al., 2006) and adrenomedullin (Allen et al., 1997). These peptides, like ANGII, have been demonstrated to modulate the baroreceptor reflex at the level of the AP.

Another means by which the CNS monitors cardiovascular status is to sample plasma sodium concentration and appropriately adjust salt intake and excretion. AP neurons have been demonstrated to directly detect plasma sodium. For example, increased cFos expression is observed in the AP following elevations in plasma sodium concentration and neurons that become activated also express epithelial sodium channels (ENaCs) (Miller et al., 2013). ENaCs are highly concentrated in the AP and are believed to play a role in sensing plasma osmolarity. Blockade of ENaCs also produces increased cFos expression in the AP (Miller et al., 2015); however, these neurons appear to comprise a separate population from those that are activated by increased sodium. These two neuronal populations project to different areas of the PBN, a higher brain centre involved in regulating sodium appetite. Detection of increased sodium by the AP also stimulates the neurohypophysial release of oxytocin and vasopressin, which are involved in regulating hydromineral balance (Huang et al., 2000). Given the relationships described above, it is not surprising that lesioning of the AP in rats disrupts hydromineral balance, resulting in increased sodium appetite without a change in natriuresis (Contreras and Stetson, 1981; Kosten et al., 1983; Watson, 1985), and that dehydration strongly influences gene regulation in the AP (Hindmarch et al., 2011).

1.2.3 Energy balance

The AP has long been recognized to influence food intake and food preference.

Early studies conducted in the 1980s demonstrated that lesioning the AP results in an acute period of reduced food intake (hypophagia) and lower adult body weight (Hyde and Miselis, 1983). In these studies, AP-lesioned rats were also observed to over-consume highly palatable foods (those high in sugar and fat), but only when presented with them for a short period of time (Edwards and Ritter, 1981). Over-ingestion of these foods in AP-lesioned rats was not the result of concomitant damage to vagal afferent neurons, as subdiaphragmatic vagotomy failed to elicit a similar feeding response (Edwards and Ritter, 1986). And so it was postulated that circulating gastric signals may play a role acting via the AP (Edwards and Ritter, 1986).

Indeed, many subsequent studies have demonstrated that the AP expresses a variety of satiety signal receptors and that these signals directly act on AP neurons to alter food intake (Hindmarch et al., 2011). For example, the GHSR is expressed in the AP (Zigman et al., 2006) and peripheral administration of either ghrelin (Takayama et al., 2007) or a GHSR agonist (Pirnik et al., 2011) induces c-fos expression in the AP. Central infusion of ghrelin into the fourth ventricle or directly into the AP and surrounding areas produces a hyperphagic response ARC (Faulconbridge et al., 2003) and ablation of the AP abolishes the orexigenic effect of peripheral ghrelin injection (Gilg and Lutz, 2006). Ghrelin directly alters the electrophysiological properties of dissociated AP neurons (Fry and Ferguson, 2009) and it is likely that *in vivo*, AP neurons signal ghrelin-related information to higher order brain structures involved in regulating food intake, such as the NTS (Li et al., 2006). Together, these observations underscore the importance of the AP as a primary detection centre for peripherally circulating ghrelin and strongly support its role in food intake.

A great deal effort has been invested into understanding the mechanism of amylin action at the AP. Amylin is an anorexigenic peptide secreted from pancreatic beta cells together with insulin. Single cell qPCR analysis has demonstrated that the calcitonin receptor and members of the receptor-activity modifying protein (RAMP) class, which together form the amylin receptor, are co-expressed in individual AP neurons (Liberini et al., 2016). High levels of amylin binding have been reported in the AP (Sexton et al., 1994; Christopoulos et al., 1995) and both peripheral (Barth et al., 2004) and central (Rowland et al., 1997) administration of amylin activate AP neurons as determined by increased levels of cFos immunostaining. Lesioning of the AP abolishes the hypophagic effect of both acute (Rowland and Richmond, 1999) and chronic (Lutz et al., 2001) peripheral amylin administration. Similarly, injection of amylin antagonist directly into the AP attenuates the anorectic effects of peripheral amylin treatment (Mollet et al., 2004). Interestingly, other satiety signals, as well as macronutrients (Michel et al., 2007), modulate the degree of the hyperphagic response produced by amylin at the AP. Specifically, leptin and insulin act synergistically to potentiate the anorectic effect of amylin, while meals high in protein but low in fat or carbohydrates attenuate amylin's effect on food intake. Leptin and amylin likely share neural pathways originating from the AP as the receptors for these peptides are co-expressed in AP neurons (Liberini et al., 2016; Smith et al., 2016). Finally, increased cFos expression following amylin treatment is also observed in many other higher brain areas known to regulate food intake, including the NTS and lateral PBN, but is attenuated after AP ablation (Riediger et al., 2004). The above studies provide further evidence that the AP is a first order centre in the detection and integration of peripheral energy balance information and support the role of

the AP in energy balance.

1.3 GLP-1

Many overweight and obese individuals are either in a prediabetic state or have type II diabetes (Daousi et al., 2006; Tuso, 2014). Because of this, interest in incretins (peptide hormones that help to lower blood glucose) and incretin mimetics has increased. GLP-1 is both an incretin *and* appetite-reducing satiety signal. The following section will focus on the biology of GLP-1, its known actions, and function of the GLP-1 receptor. This section will then provide evidence that GLP-1 receptors are expressed in the AP, that the AP mediates the anorectic actions of GLP-1, and that a specific subpopulation of AP neurons is responsible for detection of GLP-1.

1.3.1 GLP-1 history

GLP-1 is part of the glucagon superfamily of peptide hormones and is well-conserved between animals. GLP-1 is derived from cleavage of proglucagon, which also gives rise to glucagon, oxyntomodulin, and glucagon-like peptide-2. GLP-1 was first identified in anglerfish from cloned prepropglucagon cDNA as a glucagon-related peptide (Lund et al., 1983), and then humans (Novak et al., 1987) and rats (Drucker and Brubaker, 1989). Two equally active, N-terminal truncated forms of GLP-1 exist: a 29 (7-36) amino acid version and 30 (7-36) amino acid version that includes a c-terminal glycine (Suzuki et al., 1989). Since then, GLP-1 has been demonstrated to contribute to many important physiological functions, most notably regulation of blood glucose and energy homeostasis.

1.3.2 GLP-1 and glucose homeostasis

GLP-1 was first recognized as an incretin hormone and as such, is well recognized to have a variety of peripheral functions that together, contribute to the regulation of blood glucose. While it has been shown that GLP-1 is produced centrally and used as a peptide neurotransmitter (Larsen et al., 1997a), only peripherally circulating GLP-1 will be considered in this section. In mammals, intestinal-L cells within the distal jejunum, ileum, and colon (Eissele et al., 1992) release GLP-1 into circulation following a satiating meal. GLP-1 receptors are expressed on pancreatic beta cells and binding of GLP-1 stimulates transcription of proinsulin mRNA, synthesis of insulin, and release of insulin (Holst et al., 1987; Fehmann and Habener, 1992). Mice with a null mutation of the GLP-1 receptor are glucose intolerant (Scrocchi et al., 1996), highlighting the importance of GLP-1 in regulating insulin secretion and blood glucose. GLP-1 can help counteract the effects of type II diabetes. For example, GLP-1 can re-establish glucose sensitivity in pancreatic beta cells that have lost the ability to appropriately respond to rising levels of glucose (Holz et al., 1993) and GLP-1 appears to increase insulin sensitivity in muscle and adipose tissue, resulting in greater glucose utilization (Sandhu et al., 1999). Systemic administration of GLP-1 also promotes pancreatic cell proliferation, importantly, the growth of new pancreatic beta cells (Perfetti et al., 2000). GLP-1 can also counteract the effects of leptin on pancreatic beta cells, which include reducing proinsulin transcription and insulin release. Finally, GLP-1 has also been demonstrated to inhibit glucagon secretion in rodents, furthering its ability to lower blood glucose (Komatsu et al., 1989; Fridolf et al., 1991).

GLP-1 also plays an important role in regulation of gastric motility and secretion.

In humans, GLP-1 has been shown to reduce motility in the small intestine and pyloric valve (Näslund et al., 1998; Schirra et al., 2006). The observed reduction in motility appears to be at least in part, dependent on nitric oxide signalling (Tolessa et al., 2001). Because GLP-1 release is stimulated by the presence of nutrients in the ileum and contributes to inhibition of the upper gut, GLP-1 has been proposed to play a role in the ileal brake mechanism, which slows meal absorption ensuring maximal nutrition is obtained (Wen et al., 1995; reviwed in Schirra and Göke, 2005). This slowed nutrient absorption also helps to regulate spikes in blood glucose following meal consumption. Another way to slow meal absorption is to slow the chemical breakdown of food in the stomach. GLP-1 receptors have been identified on rat gastric glands (Uttenthal and Blázquez, 1990) and administration of GLP-1 reduces gastric acid secretion in both rats and humans (Hansen et al., 1988; O'Halloran et al., 1990). In humans, decreased gastric acid secretion depends on intact vagal innervation, suggesting that the CNS at least in part plays a role in GLP-1 dependent regulation of gastric acid secretion. Interestingly, these studies also noted that in humans, GLP-1 administration increased feelings of satiety (Näslund et al., 1998), a role best attributed to action within the CNS.

1.3.3 GLP-1 and energy balance

The CNS plays an important role in mediating the effects of circulating GLP-1. In particular, the CNS is a key site regulating the anorectic actions of GLP-1. GLP-1 receptors are expressed throughout the brain, with particularly high densities in areas that regulate food intake including the AP, ARC, ventromedial, and paraventricular hypothalamus (Richards et al., 2014). In addition to the periphery, a population of NTS

neurons also synthesizes GLP-1 centrally (Larsen et al., 1997b). These neurons project to satiety and rewarding processing areas of the brain (Alhadeff et al., 2012; Gu et al., 2013) that are behind the BBB and therefore unlikely to detect circulating GLP-1. Central administration of either GLP-1 or the GLP-1 receptor agonist, Exendin-4, has been shown to reduce food intake and lower body weight in both normal and obese rats (Tang-Christensen et al., 1996; Turton et al., 1996; Davis et al., 1998; Meeran et al., 1999) and peripherally administered Exendin-4 and Liraglutide (a long acting GLP-1 receptor agonist used clinically) retain their anorexigenic properties even after subdiaphragmatic vagotomy (Osaka et al., 2005), supporting the notion that anorexigenic effects of GLP-1 are due to central, but not peripheral actions. Moreover, destruction of key feeding areas with monosodium glutamate in neonatal rodents completely abolishes the anorexigenic actions of centrally acting GLP-1 (Tang-Christensen et al., 1998).

1.3.4 GLP-1 Receptor

Currently, there is only one known receptor for GLP-1, which is a G-protein coupled receptor. The third intracellular loop of the GLP-1 receptor possesses distinct binding domains for both G_s and $G_{i/o}$ proteins (Hällbrink et al., 2001), allowing the activation of different intracellular cascades. The direct effects of GLP-1 binding are best studied in pancreatic beta cells, wherein the effects of GLP-1 binding have largely been attributed to increased cAMP levels (Drucker et al., 1987; reviewed in Gromada et al., 1998). Binding of GLP-1 has been demonstrated to modulate K_{ATP} channels in a glucose-dependent manner. Inhibition of K_{ATP} channels results in membrane depolarization and activation of voltage-dependent Ca^{2+} channels (Holz et al., 1993). Increased cAMP,

together with activation of phospholipase C in response to GLP-1, have also been proposed to mobilize intracellular Ca^{2+} stores that then activate a Ca^{2+}-dependent nonselective cation current in pancreatic beta cells (Holz et al., 1995, 1999, Leech and Habener, 1997, 1998). The direct effects of GLP-1 on neurons are less well studied. In peripheral ganglionic neurons, GLP-1 inhibits the opening of voltage-dependent K^+ channels, reducing both transient and persistent K^+ current, resulting in neuronal depolarization (Gaisano et al., 2010). Conversely, in neurons of the CNS, GLP-1 does not appear to alter whole cell potassium currents. Instead, GLP-1 activates a nonselective cation current and depresses calcium current in these neurons, resulting in an overall depolarization of membrane potential (Acuna-Goycolea and van den Pol, 2004).

1.4 GLP-1 and the AP

Recently, the AP has been recognized as a key site of circulating GLP-1 action. Firstly, it has been shown that GLP-1 receptor mRNA is strongly expressed within the AP (Merchenthaler et al., 1999), that GLP-1 receptors are present on AP neurons (Richards et al., 2014), and centrally injected radiolabelled GLP-1 binds to these receptors (Orskov et al., 1996). Secondly, peripheral injection of GLP-1 induces c-fos expression in the AP (Parker et al., 2013) and ablation of the AP alters the response to Exendin-4 (Baraboi et al., 2010), a GLP-1 receptor agonist.

Moreover, recent evidence suggests that CA-synthesizing neurons of the AP are a key subpopulation of neurons acting to inhibit food take. A large portion of AP neurons that are activated by feeding, as determined by c-fos immunoreactivity, are CA-synthesizing neurons (Rinaman et al., 1998). In particular, it is thought that the CA-

synthesizing neurons may mediate the effects of GLP-1 acting on the AP as it has been shown by *in-situ* hybridization and immunohistochemistry that 90% of CA-synthesizing AP neurons express GLP-1 receptors (Yamamoto et al., 2003; Holst, 2007). Importantly, intravenous injection of GLP-1 activates CA-synthesizing neurons. (Schreihofer et al., 1997; Yamamoto et al., 2003). GLP-1 sensitive CA-synthesizing neurons have been shown to specifically project to important autonomic control sites including the NTS, PBN, and VLM. In particular, catecholaminergic projections from the AP activate gastric sensory NTS neurons, resulting in reduced gastric motility and anorexia (Shapiro and Miselis, 1985; Yamamoto et al., 2003; Hollis et al., 2004), suggesting that GLP-1 sensitive CA-synthesizing AP neurons play an important role in regulating feelings of satiety.

While CA-containing AP neurons have demonstrated roles in emesis (Yoshikawa and Yoshida, 2002), cardiovascular regulation (Miller et al., 2015), and energy balance, this population of neurons has never been electrophysiologically characterized. Previous studies performed by Funahashi et al., 2002a, 2002b have demonstrated that AP neurons can be classified into subpopulations based on K^+ current properties and presence of a hyperpolarization activated current (I_H). Voltage-gated K^+ channels play important roles in regulating neuronal excitability. Outwards K^+ current is activated at depolarized potentials and augments action potential firing patterns and frequency (Gean and Shinnick-Gallagher, 1989; Spain et al., 1991; Wu and Barish, 1999; Luther et al., 2000; Shibata et al., 2000; Yue and Yaari, 2004; Yuan et al., 2005). Conversely, I_H is activated at hyperpolarized membrane potentials and contributes towards the production of action potentials following after-hyperpolarization and pacemaker activity in neurons

(McCormick and Pape, 1990; Erickson et al., 1993). CA-containing neurons in other brain regions have previously been demonstrated to have unique intrinsic properties that allow them to be electrophysiologically distinguished from surrounding neurons. For example, dopamine-containing neurons in the ventral tegmental area and substania nigra fire spontaneous action potentials more slowly, exhibit a larger I_H, and have a larger I_A than non-dopamine neurons (for review see Shi, 2009) In the AP, biochemical phenotype of any neuron has never been correlated with electrical phenotype.

1.5 Objectives

The experiments described in this thesis (1) compare ionic currents and membrane properties between CA-containing and nonCA AP neurons and (2) investigate how the membrane potential and action potential firing frequency of CA-containing AP neurons is modulated by GLP-1. These experiments are the first to investigate if electrical phenotype can be used to identify the biochemical phenotype of AP neurons. Additionally, these experiments examine the electrophysiological effects of GLP-1 on CA-containing AP neurons for the first time. These data are important because it will increase our current knowledge of how the CNS contributes to energy balance. Moreover, these data will provide potential new targets for the development of treatments to combat weight gain and obesity. Finally, if these data identify an electrophysiological signature in TH neurons, it will allow researchers to circumvent the use of transgenic animals or immunochemistry in identifying CA-containing neurons.

1.6 Hypotheses

1.6.1 Hypothesis 1: TH-containing neurons can be electrically identified from nonTH neurons

Given that (1) AP neurons can be grouped according to K^+ current properties and the presence of I_H and (2) that TH-containing neurons in other brain regions have unique ionic current and action potential properties compared to surrounding neurons, it is possible that TH AP neurons will also have distinct differences in membrane properties that will allow them to be electrically identified from nonTH AP neurons. In order to test this hypothesis, transgenic mice will be used to identify TH-containing AP neurons in a dissociated neuronal culture. Both TH and nonTH neurons will be subjected to voltage-clamp experiments to measure properties of K^+ current, I_H, and Na^+ current. Cell-attached and current clamp experiments will be used to investigate differences in action potential firing properties including spontaneous action potential firing frequency and pattern, as well as membrane properties including resting membrane potential and input resistance.

1.6.2 Hypothesis 2: GLP-1 receptor agonists will modulate the electrophysiological properties of TH neurons

Previous cFos studies have demonstrated that CA-containing neurons are activated following peripheral GLP-1 administration (Yamamoto et al., 2002, 2003). Therefore, it is expected that GLP-1 receptor agonists GLP-1 and Exendin-4 will stimulate TH neurons. In order to test this hypothesis and gain insight into ionic mechanisms, TH neurons will be subjected to continuous current-clamp recordings to measure changes in action potential firing frequency and membrane potential.

2. Methods

This section describes 3 sets of experiments that (1) confirm GFP expression is an accurate indicator of TH expression, (2) use voltage clamp and cell-attached recordings to characterize ionic currents and spontaneous action potential firing properties of TH and nonTH neurons, and (3) use cell-attached and current clamp recordings to examine the effects of GLP-1 receptor agonists on membrane potential and action potential firing frequency in TH and nonTH neurons.

Animals

All animal protocols conformed to the standards of the Canadian Council on Animal Care and were approved by the University of Manitoba. All experiments utilized 4-9 week old male and female transgenic TH-eGFP C57BL/6 mice obtained from a colony maintained at the University of Manitoba and housed under standard conditions with free access to water and chow. Mice from this colony express enhanced green fluorescent protein (GFP) under the control of the tyrosine hydroxylase (TH) promoter (Dr. Kazuto Kobayashi at RIKEN; Matsushita et al., 2002). TH is the first and rate-limiting enzyme in the synthesis in CAs. Therefore, the detection of GFP expression using epifluorescence microscopy (Figure 2.1) allows visual identification of neurons that contain TH (and thus CA neurotransmitters).

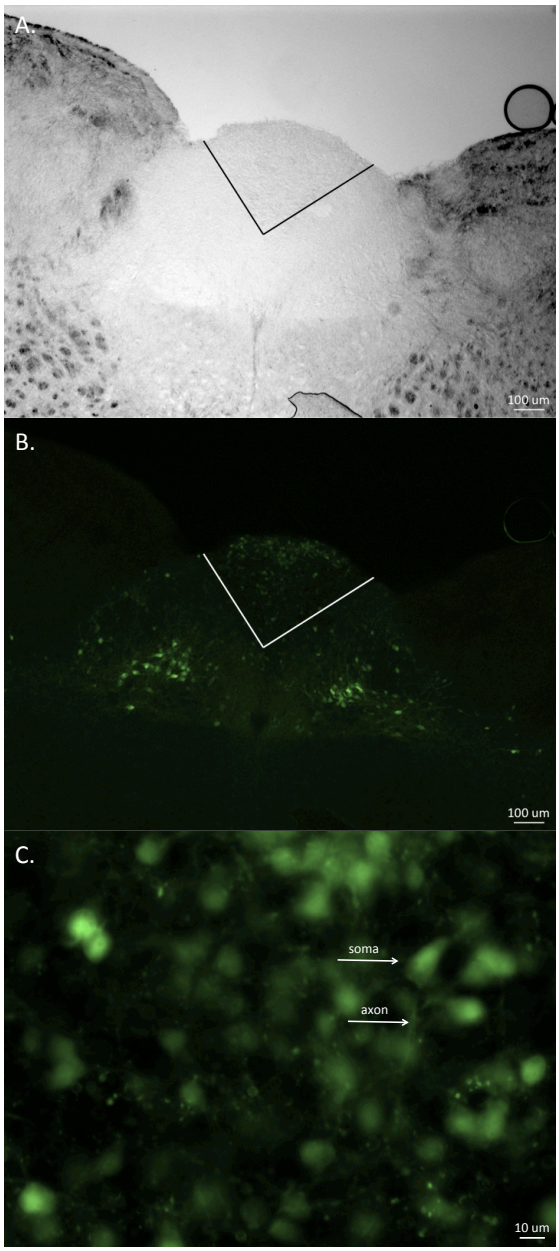

Figure 2.1 GFP-expressing TH-synthesizing AP neurons. (**A**) A 35μm section of fixed mouse brain stem containing AP visualized at 5x with bright phase contrast. White lines delineate the AP. (**B**) Same section visualized at 5x under epifluorescence with filters for GFP. Many faint GFP neurons are visible within the AP. Note the many bright GFP neurons in the adjacent NTS as well. (**C**) GFP positive neurons in the AP visualized at 40x. Axon and cell soma are indicated by arrows.

2.1 Immunohistochemistry

In the first set of experiments, immunohistochemistry for TH was carried out to confirm that GFP was an accurate indicator of TH expression. Mice (N=2 females) were decapitated, the brain removed and immediately placed into ice-cold, oxygenated artificial cerebrospinal fluid (aCSF) (Table 2.1) for 2 minutes to cool the brain. The cerebellum and underlying brainstem were removed from the forebrain and placed into ice-cold 0.1 M phosphate buffer (PB) (Table 2.2) containing 4% paraformaldehyde. After 4 hrs of fixation at 4 °C, 15 μM to 30 μM coronal sections through the AP were prepared using a vibratome (Leica Microsystems Inc. Concord, ON). Sections were washed in 0.1 M PB four times, for 5 min each and then incubated with blocking solution containing 10% goat serum and 0.3% Triton-X-100 for 1 hr at 4 °C. Sections were then incubated with primary antibody overnight with gentle shaking at 4 °C. The following day, sections were washed with ice-cold blocking solution four times and incubated with secondary antibody for 1 hr at 4 °C, protected from light. After incubation, sections were sequentially washed with vehicle, 0.1 M PB, and 0.05 M PB. Sections were mounted on glass slides and allowed to air dry before mounting media (Polysciences Inc., Warrington, PA) was applied. Images were acquired on a Zeiss Apotome (Carl Zeiss Canada, Toronto, ON) using AxioVision LE software v4.9.1 (Carl Zeiss Canada, Toronto, ON). Neurons were visually identified and only those in focus and within the bounds of the AP were counted.

Table 2.1 aCSF composition

Compound	Final Concentration (mM)
NaCl	87
Sucrose	75
KCl	2.5
NaH_2PO_4	1.25
$MgCl_2$	7
$CaCl_2$	0.5
$NaHCO_3$	25
Glucose	25

pH 7.4 when bubbled with 5% CO_2/95% O_2

Table 2.2 0.1M PB pH 7.4 composition

Compound	Final Concentration (mM)
$NaH_2PO_4 \bullet H_2O$	22.5
$NaHPO_4$	76.8

2.2 Dissociated neuronal cultures

For the second and third sets of experiments in this thesis, dissociated cultures of AP neurons from TH-eGFP mice were prepared essentially as previously described (Fry and Ferguson, 2009; Huang et al., 2015). Briefly, mice were decapitated, the brain removed from the skull and placed into ice cold, aCSF for 60 s to cool the brain. Cyanoacrylate glue was then applied to the ventral surface of the brain and allowed to cure while the brain was re-submerged in aCSF for another 60 s. The cured cyanoacrylate glue was gentled peeled from the brain in order to remove the meninges. Removal of the meninges facilitated slicing, presumably by reducing mechanical shearing. After removal of the meninges, the cerebellum and underlying brainstem were cut from the forebrain and glued onto a Leica VT 1000S vibratome (Leica Microsystems Inc. Concord, ON). A slice of 600-700 µM that contained the AP was prepared and transferred into Hibernate A media (Brain Bits, Springfield, IL) supplemented with 1X B27 (Invitrogen, Burlington, ON). The AP was carefully dissected away from surrounding brain tissue and placed into 5 mL Hibernate A containing 10 mg of papain (Worthington, Lakewood, NJ). The AP was incubated for 25 minutes at 30°C, with gentle agitation at 12 minutes.

After incubation, the AP was washed twice in 2 mL Hibernate A/B27 to remove remaining enzyme. The AP was then transferred into 1 mL of fresh Hibernate A/B27 and triturated with a 100 µl pipette tip in order to liberate individual neurons. The suspension sat undisturbed for 60 s, allowing larger tissue pieces to settle while individual neurons remained in suspension. Without disturbing tissue that had settled to the bottom, the HibernateA/B27 containing suspended cells was removed, placed in a new tube, and the volume adjusted to 2 mL with fresh Hibernate/B27. The neuronal suspension was then

centrifuged at approximately 300g for 4 minutes to pellet cells. The pelleted cells were re-suspended in 0.4 mL pre-warmed Neurobasal A medium (Invitrogen, Burlington, ON) supplemented with 1X B27 and Glutamax (Invitrogen, Burlington, ON). Afterwards, 50 μl of the cell suspension was plated onto 8 glass-bottomed 35 mm culture dishes and allowed to settle for 2-3 hours in a tissue culture incubator at 37C and 5% CO_2. After settling, an additional 2 mL of warmed supplemented Neurobasal A/B27 was added to each culture dish. Media was changed the day after plating, and every second day thereafter. For all experiments, dishes were used within 2-5 days of culturing.

2.3 Electrophysiological properties of TH and nonTH neurons

In the second part of this study, whole-cell voltage-clamp recordings were carried out to determine if significant differences in voltage-gated ion current properties (including K^+ current, Na^+ current, and I_H) or membrane properties (including resting membrane potential and input resistance) existed between GFP-labeled putative TH neurons (hereinafter TH neurons) and non-labeled AP neurons (nonTH neurons). In addition, cell-attached recordings were carried out to determine if there was a difference in spontaneous action potential frequency between TH and nonTH neurons.

For voltage clamp experiments, recording electrodes were fabricated from thin-walled borosilicate glass using a PIP 6 vertical pipette puller (HEKA, Chester, NS) or Flaming-Brown micropipette puller (P-97; Sutter Instruments, Novato, CA) and had resistances between 3 and 6 MΩ. Series resistances of <20 MΩ were accepted and compensated by >60% at 10 or 100 μs, and monitored during recordings for changes

>25%. Different voltage-gated ion currents were isolated using specific recording solutions and/or voltage clamp protocols.

For continuous cell-attached recordings, electrodes were fabricated from thick-walled borosilicate glass (Sutter Instruments, Novato, CA) using a Flaming-Brown micropipette puller (P-97; Sutter Instruments, Novato, CA) and had sizes between 3.5 and 7.5 MΩ. During cell-attached experiments, neurons were perfused with external recording solution (ERS, Table 2.3) at a rate of 2.5 mL/min using a perfusion pump system.

Measurement of K^+ current

To measure voltage-gated K^+ current without contamination from voltage-gated Na^+ currents, all K^+ current recordings (N=2 males, 3 females) were carried out in a physiological external recording solution (ERS; Table 2.3) containing 0.8 μM tetrodotoxin (TTX) to block voltage-gated Na^+ current and used a physiological internal solution (IRS; Table 2.4). Total voltage-gated K^+ current (I_{TOTAL}) is composed of a non-inactivating K^+ current (I_K) and transient K^+ current (I_{TO}). I_K and I_{TO} cannot be pharmacologically isolated from one another, so a voltage clamp must be used to inactivate I_{TO}, leaving I_K intact. I_K can then be digitally subtracted from I_{TOTAL} to reveal I_{TO}. To accomplish the above, two voltage-clamp protocols were devised based on previous experiments investigating these currents in AP neurons (Funahashi et al., 2002a). Specifically, to record I_{TOTAL}, neurons were held at a hyperpolarized potential of -100 mV for 500 ms and then subjected to a series of 500 ms depolarizing voltage steps from -60 mV to +30

Table 2.3 Physiological ERS composition

Compound	Final Concentration (mM)
NaCl	140
KCl	2
$MgCl_2$	1
$CaCl_2$	2
Hepes acid	10
Glucose	10

pH adjust to 7.4 with NaOH, osmolarity adjusted to 300 mOsm using sucrose.

Table 2.4 Physiological IRS composition

Compound	Final Concentration (mM)
CH_3KSO_3	122
$MgCl_2$	6
EGTA	10
HEPES acid	10
Na_2ATP	4
NaGTP	0.3
Phosphocreatine	14

pH adjust to 7.4 with KOH, osmolarity adjusted to 290 mOsm using CH_3KSO_3

mV in 10 mV increments. To inactivate I_{TO} and record I_K, neurons were held at a depolarized potential of -40 mV for 500 ms and then subjected to the same series of depolarizing voltage steps. Traces of I_K were subtracted from I_{TOTAL} to reveal I_{TO}. Mean peak current of I_K and I_{TO} were taken within the first 300 ms of current onset for each voltage step and absolute peak current measured at the +30 mV depolarizing voltage step. Normalized curves of mean peak current density (nA/pF) were plotted and fitted to a Boltzmann function of the form:

$$G/G_{max}=1/(1+\exp[(V-V_{1/2ACT})/k])$$

to measure the voltage of half activation ($V_{1/2ACT}$) and slope factor (k). Decay time constants of I_{TO} were analyzed by fitting I_{TO} to a double exponential decay function of the form:

$$I = A_1^{-x/\tau 1} + A_2^{-x/\tau 2} + Y_0$$

that describes current as a function of time where A_1 and A_2 represent the proportion of current made up of τ_1 and τ_2, τ_1 and τ_2 represent the "fast" and "slow" time constants of current decay (note: by definition τ_1 is smaller than τ_2), respectively, and Y_0 represents current offset (or I_{TO} remaining after most of the current is inactivated). Voltage protocols and samples traces are shown in Figure 3.1.

Measurement of voltage-gated Na^+ current

In order to obtain voltage-gated Na^+ current recordings that were not contaminated by other voltage-gated currents, all recordings (N=2 males, 4 females) were conducted using a combination of ERS (table 2.5) and IRS (table 2.6) that pharmacologically block voltage-gated K^+ current, voltage-gated Ca^{2+} current, and I_H. To

evaluate the voltage-dependence of transient Na^+ current (I_{NaT}) activation, neurons were hyperpolarized to -110 mV for 500 ms and then subjected to a series of 100 ms depolarizing voltage steps from -80 mV to +50 mV in 10 mV increments (Figure 3.7 A). In order to evaluate the voltage-dependence of I_{NaT} inactivation, neurons were subjected to a protocol consisting of a series of 500 ms increasing voltage steps from -100 mV to 0 mV in 10 mV increments followed by a 100 ms depolarizing voltage step to +20 mV (Figure 3.7 C). Mean peak conductance was calculated from Ohm's Law:

$$g = I/V_m - E_{Na}$$

where I is peak I_{NaT}; V_m is the membrane potential; and E_{NA} is the equilibrium potential. Normalized conductance curves were generated and fitted to a Boltzmann function:

$$G/G_{max}=1/(1+\exp[(V-V_{1/2ACT})/k])$$

to measure the voltage of half activation ($V_{1/2ACT}$) (or voltage of half inactivation, $V_{1/2INACT}$) and slope factor (k).

Time dependent recovery from inactivation was evaluated by subjecting neurons to a pair of 10 ms depolarizing pulses of +30 mV with a variable interpulse interval of 1-1000 ms. Fractional recovery was calculated by dividing the peak sodium current measured during the second pulse by the peak sodium current measured during the first pulse. Fractional recovery was plotted against interpulse interval and fitted to a double exponential function of the form:

$$I = A_1^{-x/\tau 1} + A_2^{-x/\tau 2} + Y_0$$

where A_1 and A_2 represent the proportion of current made up of τ_1 and τ_2, τ_1 and τ_2 represent "fast" and "slow" time constants of fractional recovery, respectively, and Y_0 represents the maximal fractional recovery reached.

Table 2.5 Composition of ERS for I_{Na} recording

Compound	Final Concentration (mM)
NaCl	30
TEA	110
$MgCl_2$	1
$CaCl_2$	2
CsCl	1
BaCl	1
CdCl	0.3
HEPES	10
Glucose	10

pH adjusted to 7.3 using, osmolarity adjusted to 300 mOsm using sucrose.

Table 2.6 Composition of IRS for I_{Na} recording

Compound	Final Concentration (mM)
CH_3O_3SCs	130
$MgCl_2$	6
$CaCl_2$	10
HEPES	10
EGTA	1
Na_2ATP	2
NaGTP	0.2
Phosphocreatine	14

pH adjusted to 7.2 using CsOH

Finally, to measure persistent Na^+ current (I_{NaP}), neurons were subjected to a 1300 ms depolarizing voltage ramp from -100 mV to +30 mV (Figure 3.11 A). Peak I_{NaP} was measured directly from these traces.

Measurement of I_H

In voltage clamp, I_H current is characterized by a slowly activating sustained inward current that begins activating near -60 mV (Pape, 1996; Funahashi et al., 2002b). To determine if I_H was present, AP neurons (obtained from the same mice used for K^+ current experiments) were held at -60 mV and then subjected to a 500 ms depolarizing potential of -40 mV followed by a series of 500 ms hyperpolarizing voltage steps from -80 mV to -140 mV in 20 mV increments (Figure 3.11 A). All I_H recordings were conducted using the same ERS (Table 2.3) containing TTX, and IRS (Table 2.4) used in K^+ current recording.

Spontaneous action potential frequency

Continuous cell-attached recordings (N=2 males, 2 females) were carried out with the aim of quantifying spontaneous action potential frequency in in TH and nonTH neurons. In these experiments, no current was injected into the membrane patch, allowing spontaneous action potential firing to be monitored. Activity was monitored for 3-5 minutes and a 100s sample from each recording was used to compare spontaneous action potential frequency and coefficient of variation (a measure of spontaneous action potential firing pattern) between TH and nonTH neurons.

2.4 GLP-1 receptor agonist application

In the third part of this study, current-clamp recordings (N=14 males, 7 females) were carried out to characterize membrane properties such as resting membrane potential and input resistance, and investigate changes in membrane potential and action potential frequency in TH neurons following application of either GLP-1 or Exendin-4.

For these experiments, recording electrodes were fabricated from thick-walled borosilicate glass (Sutter Instruments, Novato, CA) using a Flaming-Brown micropipette puller (P-97; Sutter Instruments, Novato, CA) and had resistances between 5 and 10 MΩ. Series resistances of <40 MΩ were accepted. During all experiments, neurons were perfused with external recording solution (ERS) at a rate of 2.5 mL/min using a perfusion pump system.

Resting membrane potential was measured when no current was injected into the neuron. Input resistance is a measure of cell excitability calculated from Ohm's law. In order to measure input resistance, neurons were subjected to a series of 500 ms current injections of 0 pA to -5 pA from baseline. The deflection in membrane potential from baseline was plotted against injected current and fitted to a linear slope to find input resistance.

In experiments that investigated response to GLP-1 receptor agonists, neurons were held at a potential where they fired action potentials infrequently or not at all (about -60 mV to -50 mV). A 3-5 minute period of baseline recording was acquired before peptide application. Membrane potential and action potential frequency were calculated using 100 s time periods. Neurons were considered to respond to GLP-1 receptor agonists if membrane potential depolarized by at least 5 mV or if action potential frequency

increased by at least 1 Hz. These effects were considered to be due to GLP-1 if they occurred within 120 s of GLP-1 reaching the recording dish. For some experiments, a longer latency to response was accepted if there was a clear response and recovery. For statistical analysis, the responses of all neurons (responding and nonresponding) as a population were compared before and after treatment in order to avoid first categorizing neurons into responding and nonresponding groups and then conducting statistical analysis.

2.5 Peptides

TTX was purchased from Sigma Aldrich (Sigma Aldrich), reconstituted in water and stored at -20 °C until use. GLP-1, Exendin-4, Exendin-3 were purchased from Phoenix Pharmaceuticals (Phoenix Pharmaceuticals, Burlingame, CA) or Abcam (Abcam, Toronto, ON), reconstituted in ERS and stored at -20 °C until use. All peptides were applied at a concentration of 1 μM. These concentrations were chosen because they are near the top of the dose response curve (Raufmansq et al., 1991; Serre et al., 1998; Acuna-Goycolea and van den Pol, 2004; Korol et al., 2014; Farkas et al., 2016) and therefore expected to exert maximal effects.

2.6 Data Analysis

Spike2 software (v6.18, Cambridge Electronic Design, Cambridge, UK) was used to concatenate and analyze continuous cell attached and current clamp recordings. All statistical analyses were performed using OriginPro software (OriginPro 2016 and 2017 student version, Originlab, Northhamptom, MA, USA) unless otherwise noted. Two-

sample t-tests were used to determine the significance of normally distributed data, Mann-Whitney tests and Kruskal-Wallis ANOVA were used to determine the significance of non-normally distributed data, Fisher's exact tests (Graphpad.com) were used to determine the significance of partitioning in categorical data, and paired-sample t-tests were used to determine the significance of GLP-1 receptor agonist response. Normally distributed data are plotted as mean ± standard error. Non-normally distributed data are plotted as box plots, where the box ranges from Q1 to Q3, the middle bar represents median, and the whiskers represent the 95% confidence interval. In some sets of data, outliers were determined using an online calculator (miniwebtool.com/outlier-calculator) and subsequently removed. This calculator considered outliers to be values that fell below Q1-1.5xIQR or above Q3-1.5xIQR, where IQR is the interquartile range (represented by the length of the box). GLP-1 receptor agonist response data are plotted as joined points that represent baseline (set to 0) and change (compared to baseline) following peptide application. Level of significance is $p < 0.05$ unless otherwise specified.

2.7 Validation of flow-through system

During cell-attached and current-clamp recordings investigating the action of GLP-1 receptor agonists, a perfusion system was used to supply neurons with fresh ERS (Figure 2.2). This system allowed for switching between ERS or ERS containing peptide.

Initial positive control experiments sought to determine the efficacy of the flow through system used in cell-attached and current clamp recordings. In these experiments,

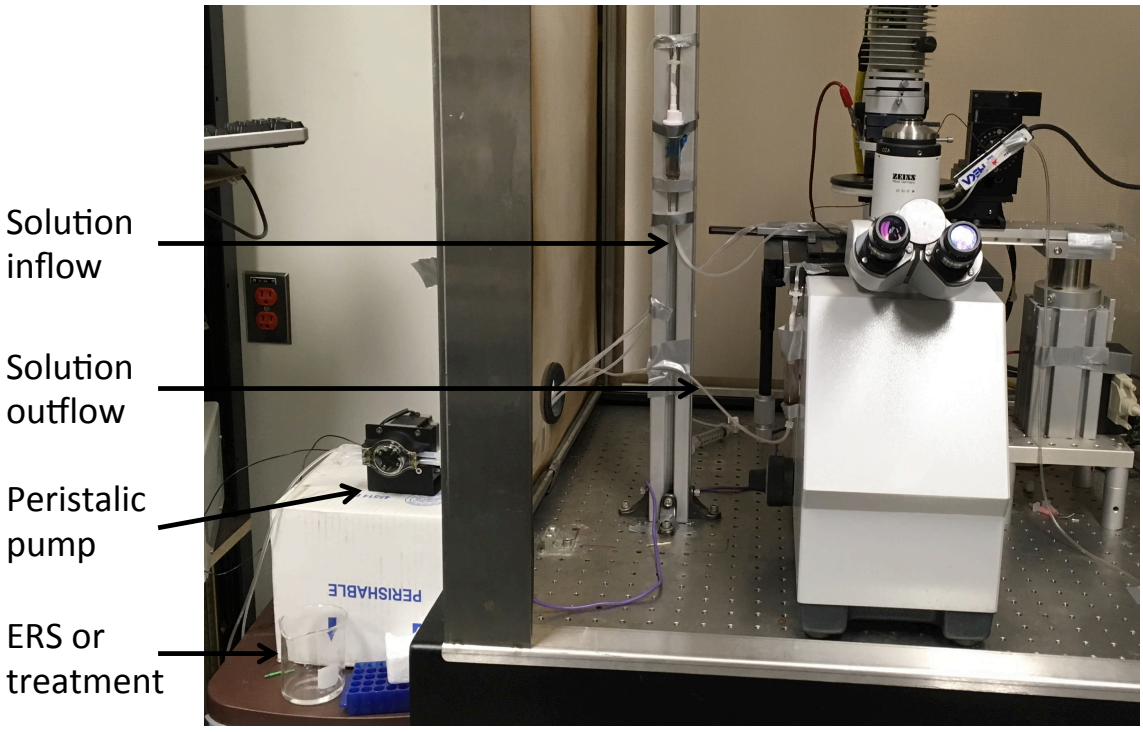

Figure 2.2 Flow-through system used in continuous cell attached and current clamp experiments. A peristaltic pump was used to control solution inflow and outflow at a continuous rate of 2.5 mL/min. Solution was held in a container. In order to change solutions, the inflow line was switched from one container to another.

ERS containing 15 mM KCl, a K^+ concentration expected to depolarize neurons (according to the Goldman-Hodgkin-Katz equation), was applied to neurons in cell-attached configuration. Recordings indicated a 126.0 ± 14.5 second latency for ERS containing 15 mM KCl to reach the cell after switching solutions and a period of 135.7 ± 2.1 seconds for washout (n=3). An example recording from a positive control experiment is shown in Figure 2.3 A.

Negative control experiments (n=3) were also carried out in cell-attached configuration to investigate the effect of switching between two containers of ERS to ensure that changing solutions did not cause perturbation of neurons. In these experiments, spontaneous action potential frequency was observed to change by 0.4 ± 0.4 Hz. The change in spontaneous action potential frequency was not significantly different from baseline according to a paired-sample t-test (p=0.3889). An example recoding from a negative control experiment is shown in Figure 2.3 B.

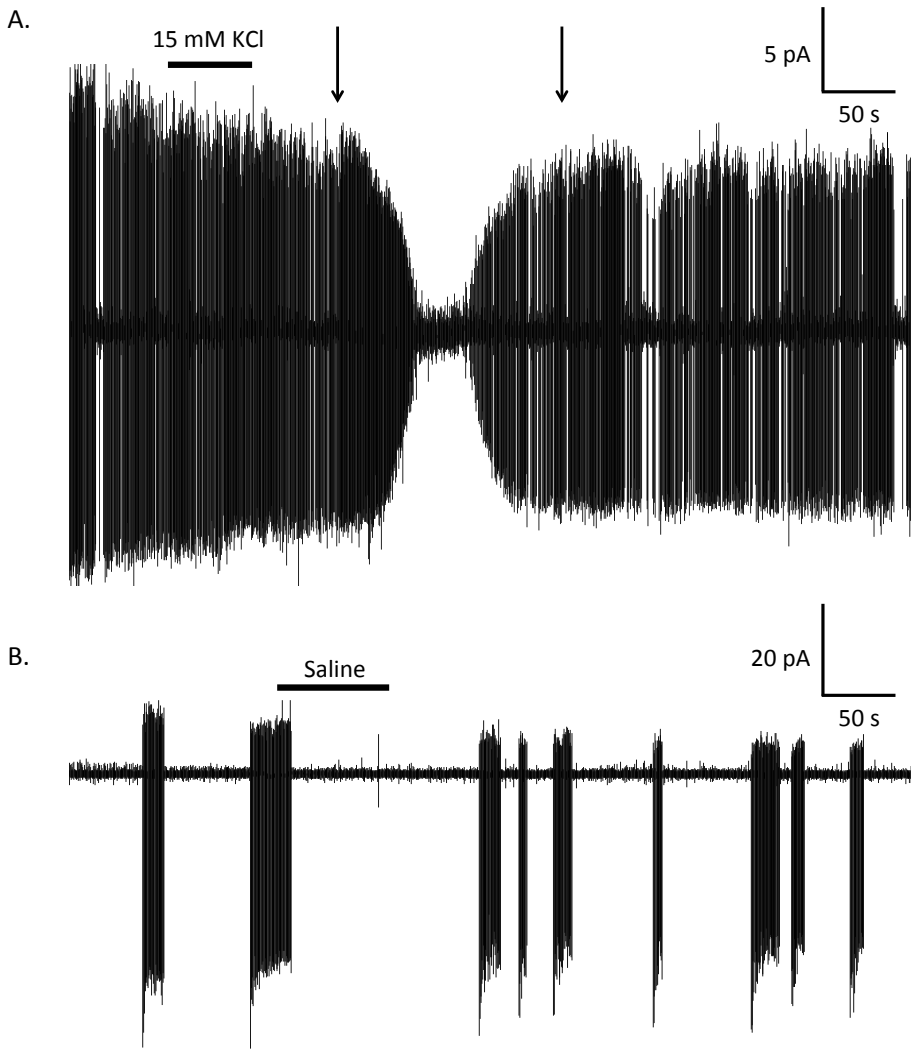

Figure 2.3 Validation of flow through system. (A) Example cell-attached recording from a positive control experiment. ERS containing 15 mM KCl depolarizes the neuron causing it to fire more frequent action potentials. Eventually, the neuron becomes too depolarized to continue firing action potentials and activity stops. As the ERS containing 15 mM KCl is washed out of the dish, the neuron begins to repolarize and fire spontaneous action potentials again. Arrows indicate time at which 14 mM KCl first hits the cell (first arrow) and the point of complete washout (second arrow) **(B)** Example cell-attached recording from a negative control experiment. Normal ERS was perfused over the neuron and did not cause a significant change in spontaneous action potential firing.

3. Results

Previously, Funahashi et al., 2002a, 2002b demonstrated that AP neurons could be grouped into subpopulations based on K^+ current properties and the presence of I_H. In the present study, we aimed to determine if such electrical phenotypes correlated with biochemical phenotypes of AP neurons. Specifically, we used patch clamp experiments to electrophysiologically characterize voltage-gated ion currents in TH and nonTH AP neurons. In particular, we investigated differences in K^+ current properties, I_H, and Na^+ current properties between TH and nonTH AP neurons. Intriguingly, while previous studies have suggested that TH AP neurons respond to GLP-1, the electrophysiological effects of GLP-1 on TH AP neurons have never been investigated. Therefore, we also aimed to characterize the effects of GLP-1 on action potential firing frequency in TH AP neurons.

3.1 Immunohistochemistry

In the first set of experiments, immunochemistry was carried out to confirm that GFP expression could be used as an indicator of TH expression. A total of 8 slices were obtained from 2 animals. We observed that 72.0 ± 3.3 % of neurons expressed both GFP and TH, 17.9 ± 3.5 % expressed only GFP, and the remaining 10.1 ± 3.3 % expressed only TH.

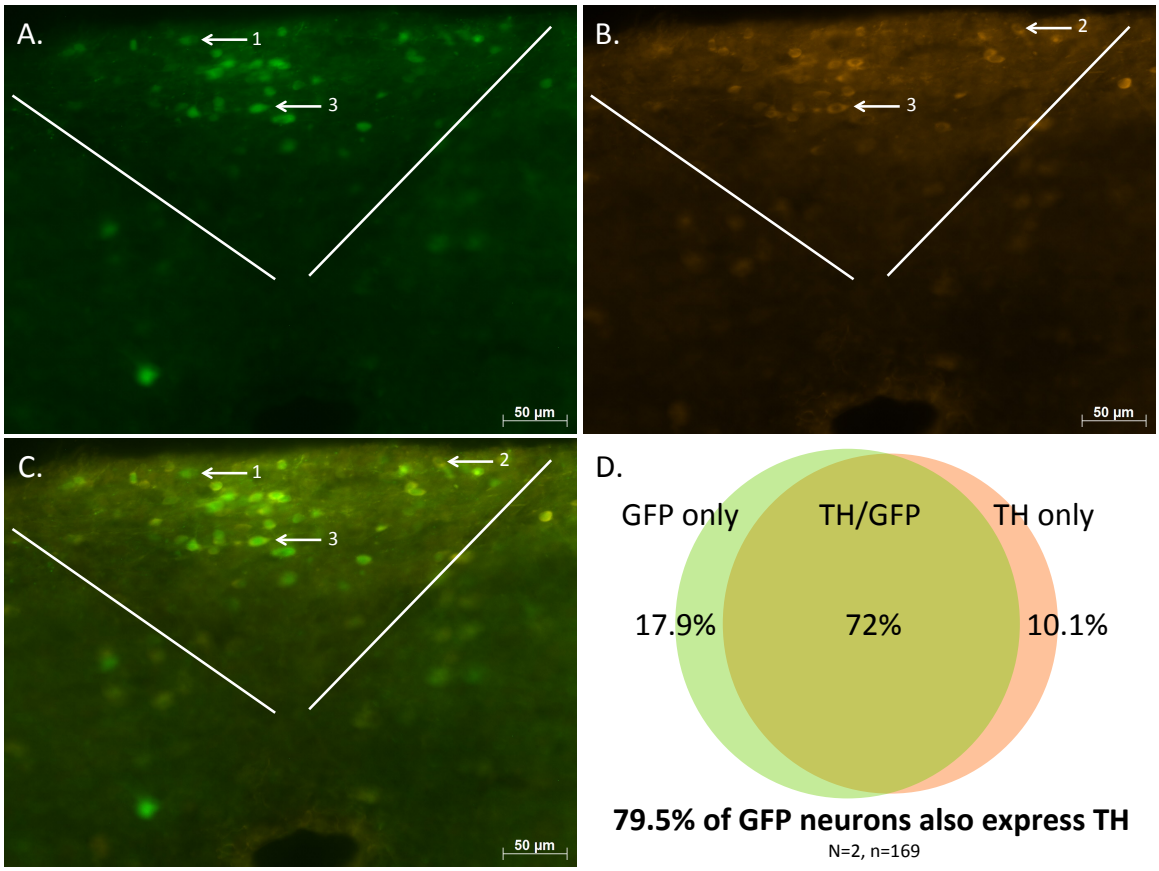

Figure 3.1 Immunohistochemistry for tyrosine hydroxylase in mouse AP. (A) Fluorescence from TH-GFP positive neurons. **(B)** Fluorescence following immunohistochemistry for TH. **(C)** Overlap of GFP and TH fluorescence. **(D)** Venn diagram demonstrating overlap between GFP-positive and TH-positive neuronal populations. White lines in A, B, and C outline the edges of the AP. Arrow 1 indicates a GFP-only neuron. Arrow 2 indicates a TH-only neuron. Arrow 3 indicates a neuron expressing GFP and staining for TH.

3.2 Electrophysiological characterization of TH and nonTH neurons

In the second set of experiments, electrophysiological recordings were carried out to characterize properties of K^+ current, Na^+ current, I_H, and spontaneous action potential firing in TH and nonTH neurons.

3.2.1 Analysis of K^+ current properties in TH and nonTH neurons

Separation of I_K and I_{TO}

The first series of experiments sought to investigate K^+ current properties. In order to investigate the properties of I_K and I_{TO} separately, we carried out specific voltage clamp protocols to electrically activate, or inactivate, I_{TO} in individual neurons. Example current traces of I_{TOTAL}, I_K, and I_{TO} are shown in Figure 3.2.

Analysis of I_K in TH and nonTH neurons

Normalized mean peak I_K density (pA/pF) was fitted to a Boltzmann curve and compared between TH (n=44) and nonTH neurons (n=42) to analyze voltage dependence of I_K activation. The resulting curves exhibited $V_{1/2ACT}$ = -3.6 ± 0.7 mV and slope factor k=7.1 ± 0.2, and $V_{1/2ACT}$=-7.2 ± 0.8 mV and slope factor k=7.7 ± 0.2, for TH neurons and nonTH neurons, respectively (Figure 3.3 A). The $V_{1/2ACT}$ was depolarized (two-sample t-test, p=0.001), and slope factor k smaller (two-sample t-test, p=0.02), in TH neurons compared to nonTH neurons. Repeated two-sample t-tests (with Bonferonni correction) demonstrated that the normalized mean peak I_K density (pA/pF) was significantly lower ($p<0.005$) in TH neurons between -40 mV and -10 mV versus nonTH neurons (Figure 3.3

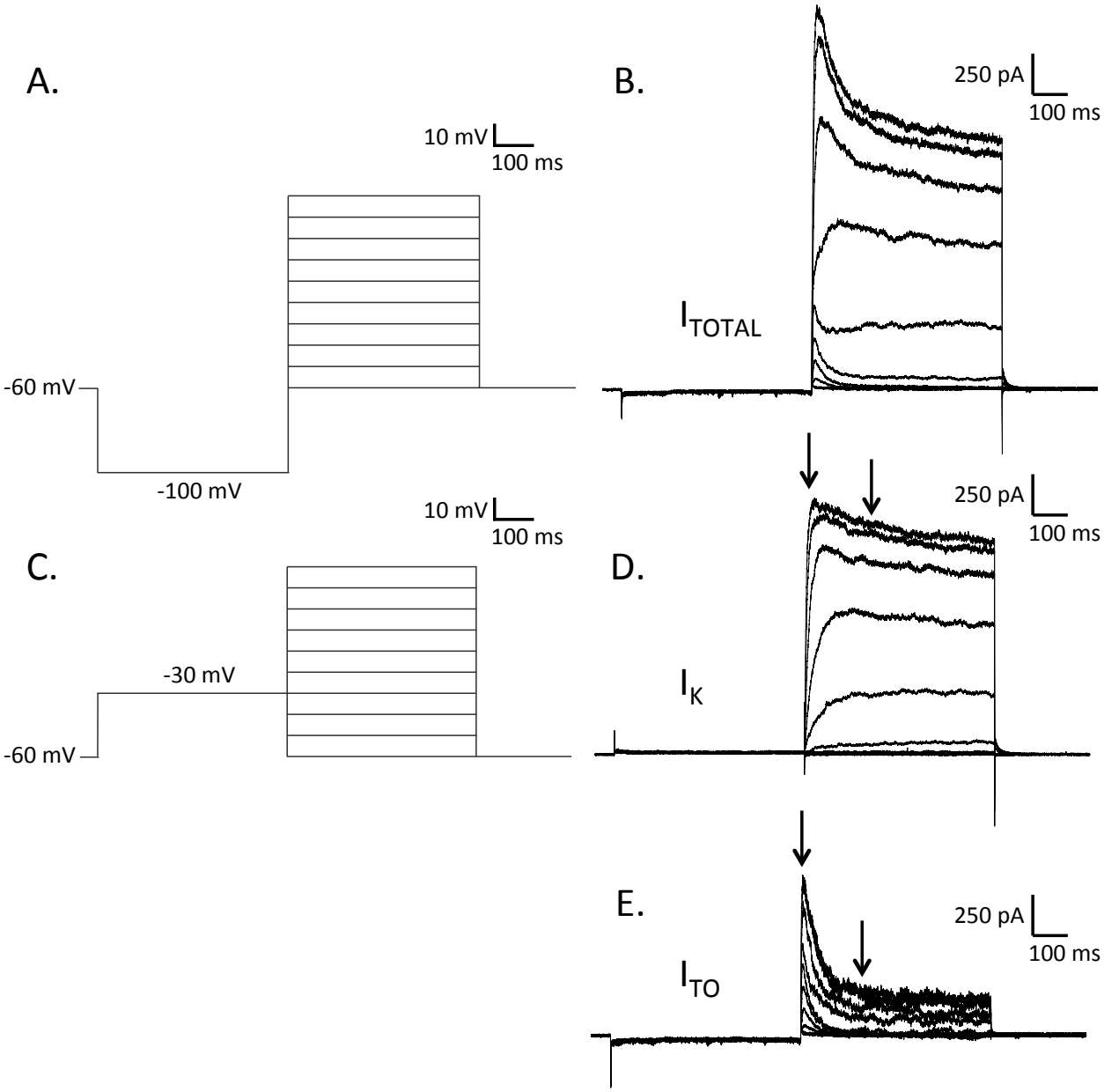

B). Mean peak I_K density at +30 mV was 291.6 ± 29.6 pF/pA in TH neurons. This value was

Figure 3.2 Voltage clamp protocols for separating K^+ currents in AP neurons. (**A**) Voltage clamp protocol for measuring I_{TOTAL} (**B**) Traces of I_{TOTAL} elicited by A. (**C**) Voltage clamp protocol for measuring I_K. (**D**) Traces of I_K elicited by C. (**E**) Traces of I_{TO} revealed by subtracting D from B. Arrows indicate range used to determine peak current.

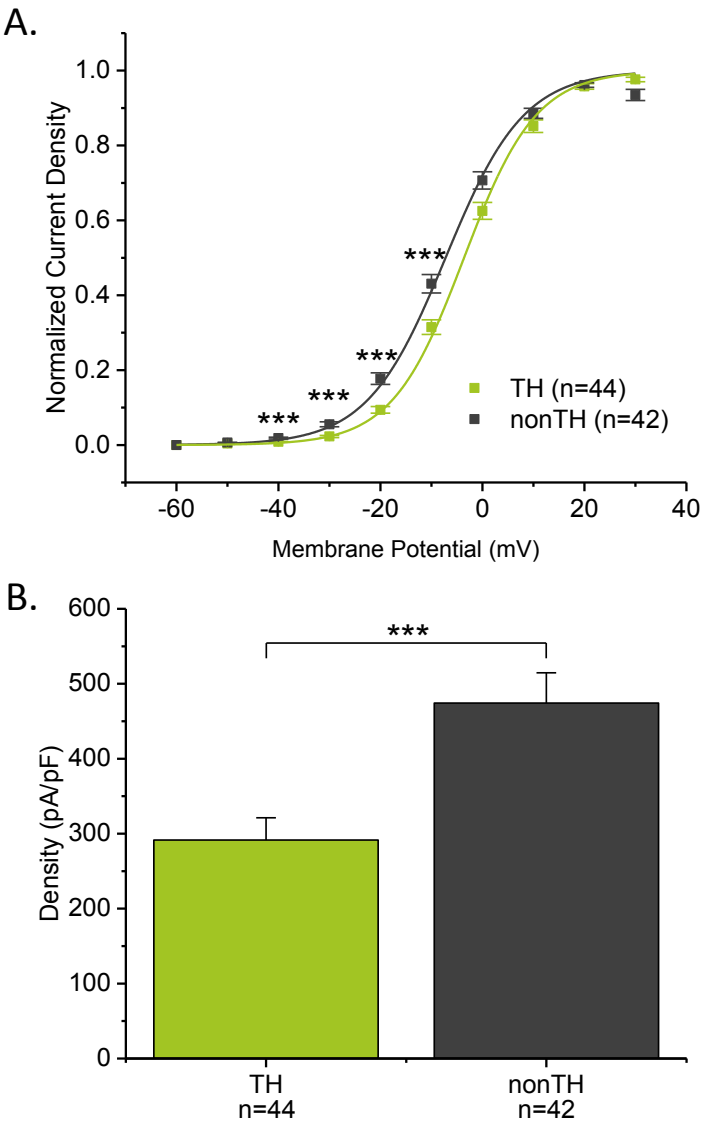

Figure 3.3 Analysis of mean peak I_K density in TH and nonTH neurons. (A) Normalized activation curve of peak I_K density. Data were fitted using Boltzmann curves. Repeated two-sample t-tests with Bonferroni correction indicated that the voltage dependence of I_K activation ($p<0.005$) was significantly depolarized in TH neurons (n=44) compared to nonTH neurons (n=43) (indicated by an asterisk). **(B)** Peak current density of I_K current at 30 mV was lower (two-sample t-test, p=4.2E-4) in TH neurons (n=44) compared to nonTH neurons (n=43).

significantly lower (two-sample t-test, p=4.2E-4) than that measured in nonTH neurons, which we found to be 474.3 ± 40.4 pF/pA (Figure 3.3B). Because previous studies (Hay and Lindsley, 1995; Funahashi et al., 2002a) have focused on differences in I_{TO} between AP neurons, we next analyzed the properties of I_{TO}.

Analysis of I_{TO} in TH and nonTH neurons

Normalized mean peak I_{TO} density (pA/pF) was also fitted to a Boltzmann curve in order to compare voltage dependence of I_{TO} activation between TH (n=44) and nonTH neurons (n=41). The resulting curves displayed $V_{1/2ACT}$ = -2.7 ± 0.8 mV and slope factor k=10.5± 0.4, and $V_{1/2ACT}$=-4.5 ± 1.3 mV and k=10.4 ± 0.4, for TH neurons and nonTH neurons, respectively (Figure 3.4A). There was no significant difference in $V_{1/2ACT}$ (two-sample t-test, p=0.22) or slope factor k (two-sample t-test, p=0.51) between TH and nonTH neurons. Repeated two-sample t-tests with Bonferroni correction indicated that normalized mean peak I_{TO} density was depolarized in TH neurons compared to nonTH neurons between -50 mV and -30 mV ($p<0.005$). Interestingly, we found that mean peak I_{TO} density at + 30 mV of 134.6 ± 13.3 pF/pA in TH neurons was significantly lower (two-sample t-test, p=1.7E-7) than the density of 292.3 ± 24.8 pF/pA measured in nonTH neurons (Figure 3.4B). Because previous studies (Funahashi et al., 2002a, 2006) have demonstrated that AP neurons can be classified as having either a fast or slow I_{TO}, we next sought to investigate the time course of I_{TO} in TH and nonTH neurons.

To evaluate the time course of I_{TO} inactivation in TH and nonTH neurons, the trace of I_{TO} at +30 mV was fitted to a double exponential decay function. An example

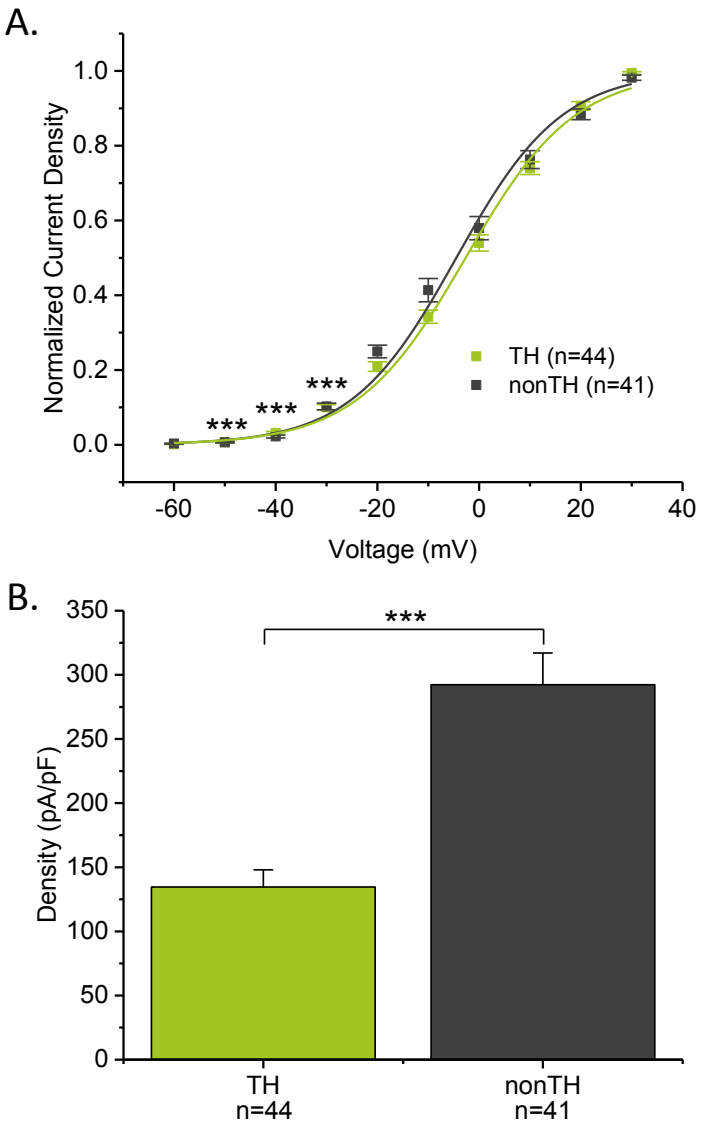

Figure 3.4 Analysis of mean peak I_{TO} density in TH and nonTH neurons. (**A**) Normalized activation curve of mean peak I_{TO} density. Data were fitted using Boltzmann curves. Repeated two-sample t-tests with Bonferroni correction indicated that the voltage dependence of I_K activation ($p<0.005$) was significantly depolarized in TH neurons (n=44) compared to nonTH neurons (n=41) (indicated by an asterisk). (**B**) A two-sample t-test revealed absolute peak I_{TO} density at 30 mV was significantly lower ($p=1.7E-7$) in TH (n=44) neurons compared to nonTH (n=41) neurons.

trace of I_{TO} at +30 mV and fitting are shown in Figure 3.5. Mann-Whitney tests were used to compare median values of individual I_{TO} components between TH (n=35) and nonTH neurons (n=33). The median values of τ_1 and τ_2 were 19.8 ms and 125.9 ms in TH neurons, and 20.3 ms and 137.6 ms in nonTH neurons. Neither the values of τ_1 (p=0.54) or τ_2 (p=0.14) differed significantly between TH and nonTH neurons (Figure 3.6 A and B). Likewise, the percentage of I_{TO} made up of τ_1 (p=0.069) versus τ_2 (p=0.64) was also similar between TH and and nonTH neurons (Figure 3.6 C and D). In TH neurons, I_{TO} was comprised of 41.9% A_1 and 31.4% A_2 and in nonTH neurons I_{TO} was composed of 28.8% A_1 and 34.7% A_2. Interestingly, the median Y_0 (representing the amount of steady-state non-inactivated I_{TO} at +30 mV) accounted for 28.7% of I_{TO} in TH neurons and contributed a significantly smaller portion (p=0.012) than the 35.0% of I_{TO} composed of Y_0 in nonTH neurons (Figure 3.6 E).

Previous studies (Funahashi et al., 2002a, 2006) fitted I_{TO} to a single exponential function and categorized neurons as fast or slow based on an arbitrary τ value. In this study, a double exponential decay function was used and neurons were categorized as fast if the proportion of I_{TO} made up by the "fast" τ was larger than the proportion made up by the "slow" τ (ie. $A_1>A_2$) (Figure 3.7 A and B). Our results indicate that TH and nonTH neurons are heterogeneous populations composed of both fast I_{TO} and slow I_{TO} neurons (Fisher's exact test, p=0.22). Of 35 TH neurons, 22 expressed predominantly fast I_{TO}, while the remaining 13 expressed predominantly slow I_{TO}. Similarly, of 33 nonTH neurons, 15 expressed predominantly fast I_{TO} and 18 expressed predominantly slow I_{TO} (Figure 3.7 C).

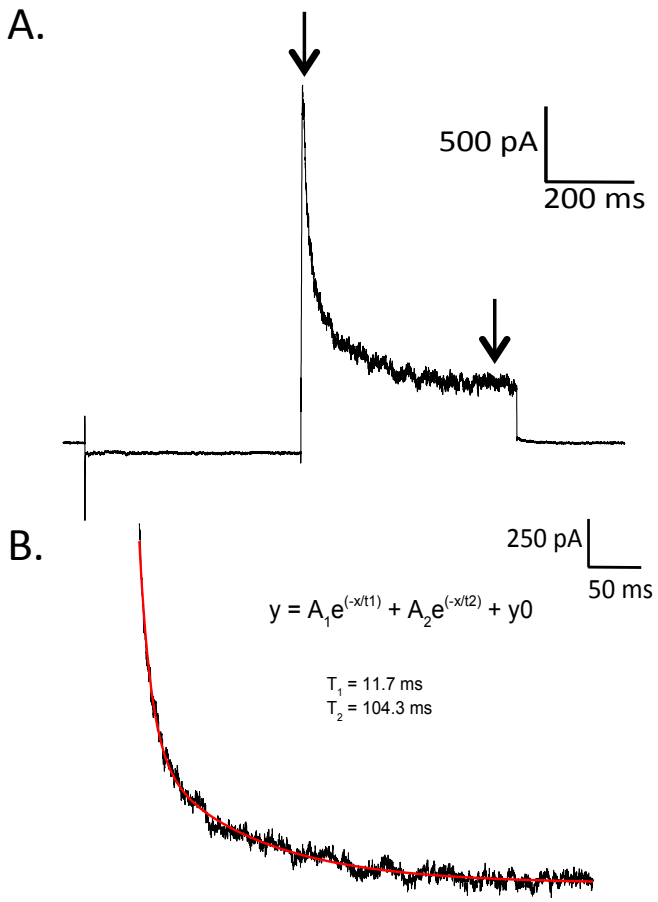

Figure 3.5 I_{TO} fitting to a double exponential decay function. (**A**) I_{TO} current traces elicited at +30 mV were fitted I_{TO} to a double exponential decay function. The arrows indicate the beginning and end of the trace that were using for fitting. (**B**) I_{TO} (black line) was fitted to a double-exponential decay function (red line). Neurons that could not be adequately fitted to a double exponential decay (n=4 TH and n=4 nonTH) were excluded from I_{TO} component analysis. Neurons with τ_1 or τ_2 values that fell below Q1-1.5xIQR or above Q3-1.5xIQR were identified as outliers (n=3 TH and n=3 nonTH) and also excluded from I_{TO} component analysis. Finally, neurons (n=2 TH and n=1 nonTH) with τ_1 or τ_2 values that were not consistent with previous literature (Cooper and Shrier, 1989; Hay and Lindsley, 1995; Funahashi et al., 2002a) values were also excluded from analysis.

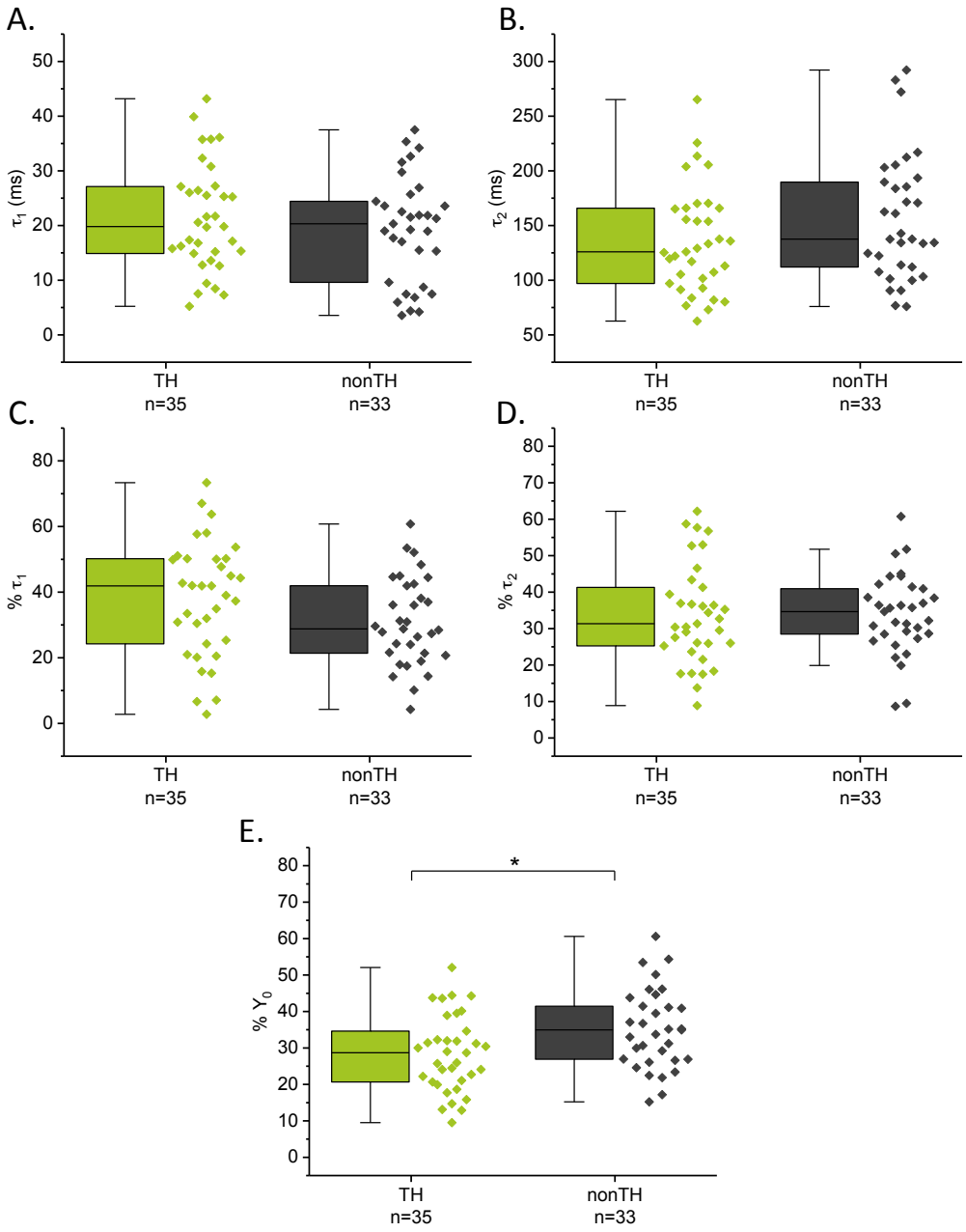

Figure 3.6 Comparison of I_{TO} properties in TH and nonTH neurons. (A) T_1 values did not differ between TH and nonTH neurons. **(B)** T_2 values were not significantly different between TH and nonTH neurons. **(C)** T_1 made up a similar percentage of I_{TO} in TH and nonTH neurons. **(D)** The percentage of I_{TO} made up of T_2 did not differ between TH and nonTH neurons. **(E)** Y_O made up a smaller percentage (Mann-Whitney, p=0.012) of I_{TO} in TH neurons (n=35) compared to nonTH neurons (n=33).

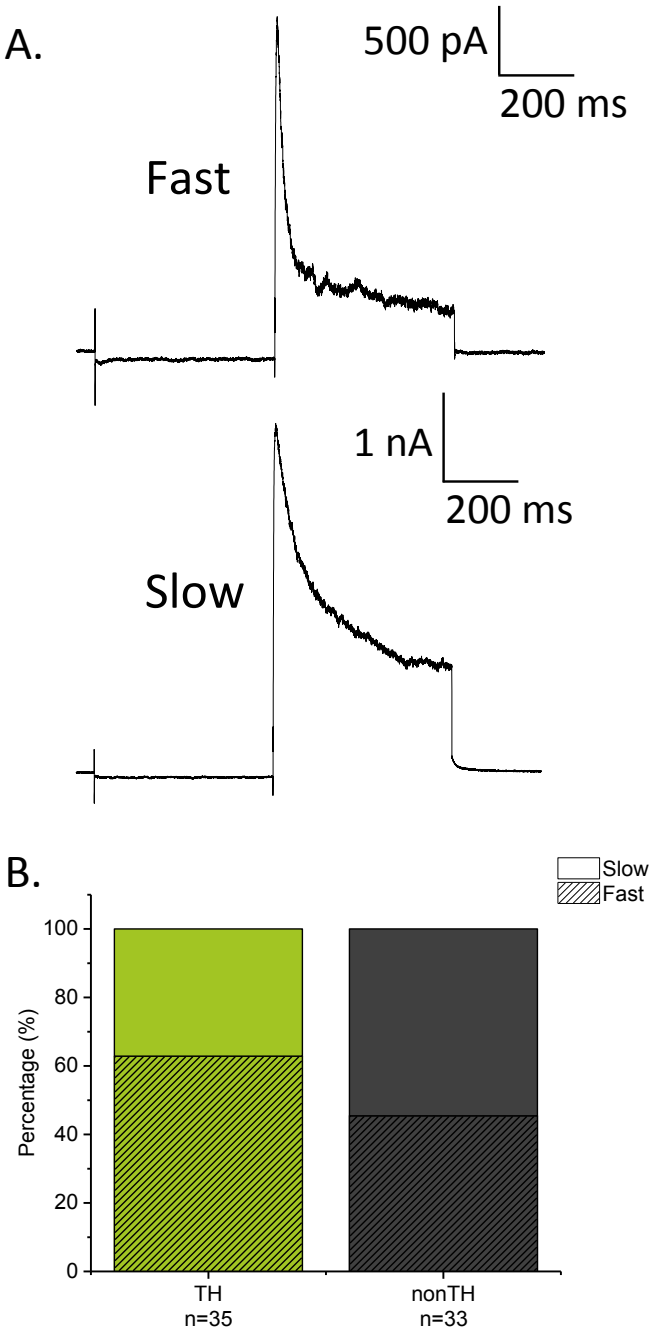

Figure 3.7 Comparison of percentage of neurons with fast vs slow I_{TO} in TH and nonTH neurons. (A) Example current traces of fast or slow I_{TO}. **(B)** TH (n=33) and nonTH (n=33) neuronal populations contained similar (Fisher's exact test, p=0.22) percentages of neurons with fast I_{TO}.

3.2.2 Analysis Na^+ Current Properties in TH and nonTH neurons

Because voltage-gated Na+ current also critically determines electrical excitability, we next investigated whether Na^+ current properties could be used to electrophysiologically identify the biochemical phenotype of AP neurons.

Voltage-dependence of I_{NaT} in TH and nonTH neurons

The first series of experiments sought to investigate the voltage-dependence of transient Na^+ current (I_{NaT}) using specific voltage clamp protocols to either activate, or inactivate, I_{NaT}. Protocols used to investigate the voltage dependence of I_{NaT} activation and inactivation and example current traces are shown in Figure 3.8 A, B, C, and D.

Normalized mean peak conductance curves for activation and inactivation of I_{NaT} were fitted to a Boltzmann curve and compared between TH and nonTH neurons (Figure 3.8 E). For activation of I_{NaT}, the resulting curves of TH (n=17) and nonTH (n=15) neurons exhibited $V_{1/2ACT}$ = -18.5 ± 0.9 mV and slope factor k=6.2 ± 0.1, and $V_{1/2ACT}$ = -18.4 ± 1.3 mV and slope factor k=5.8 ± 0.3, respectively. Neither the values of $V_{1/2ACT}$ (two-sample t-test; p=0.93) nor slope factor k (two-sample t-test, p=0.12) were significantly different. For inactivation of I_{NaT}, the resulting curves of TH (n=18) and nonTH (n=13) neurons exhibited $V_{1/2INACT}$ = -48.2 ± 1.1 mV and slope factor k= 4.9 ± 0.2, and $V_{1/2INACT}$ = -50.0 ± 1.7 and slope factor k= 5.6 ± 0.3, respectively. Similarly, the values $V_{1/2INACT}$ (two-sample t-test, p=0.35) or slope factor k (two-sample t-test, p=0.068) did not differ between TH and nonTH neurons for I_{NaT} inactivation. Interestingly, peak I_{NaT} was -1.6 ± 0.3 nA in TH neurons, which we found to be significantly

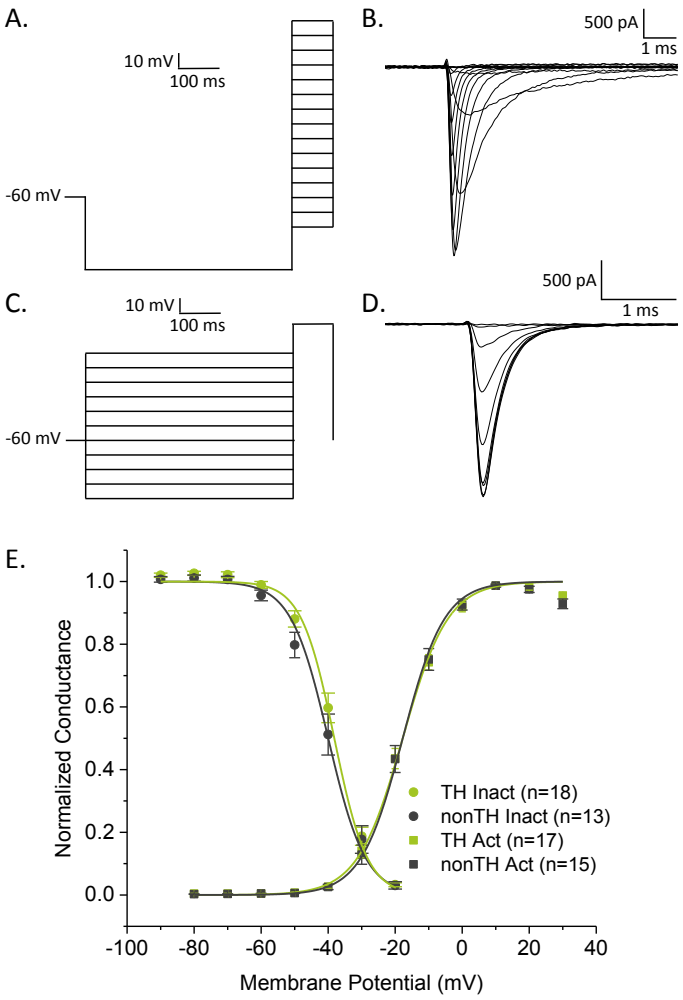

Figure 3.8 Voltage-dependence of activation and inactivation of I_{NaT} in TH and nonTH neurons. (A) Voltage clamp protocol for activation of I_{NaT}. **(B)** Example current traces elicited from A. **(C)** Voltage clamp protocol for inactivation of I_{NaT}. **(D)** Example current traces elicited from C. **(F)** Normalized conductance curves for voltage-dependence of activation and inactivation of I_{NaT} fitted to Boltzmann curves. There was no significant difference in the voltage of half activation (t-test, p=0.93) or slope factor k (t-test, p=0.12) between TH (n=17) and nonTH (n=15) neurons. Similarly, voltage of half inactivation and slope factor k did not significantly differ between TH (n=18) and nonTH (n=13) neurons.

(two-sample t-test, p=0.033) lower than peak I_{NaT} of -2.6 ± 0.3 nA in nonTH neurons. Consistent with the above, is our finding that peak I_{NaT} density in TH neurons of -0.30 ± 0.03 nA/pF is significantly reduced (two-sample t-test, p=0.011) compared to peak I_{NaT} density -0.46 ± 0.05 nA/pF in nonTH neurons (Figure 3.9 B).

We next sought to determine if there was a difference in time-dependent recovery from inactivation of I_{NAT} between TH (n=13) and nonTH (n=10) neurons. Example current traces from time dependent recovery protocols are shown in Figure 3.10 B. The values of A1 and A2 were -0.73 ± 0.03 and -0.31 ± 0.02 in TH neurons, and -0.81 ± 0.03 and -0.24 ± 0.02 in nonTH neurons. While the values of A1 were similar (two-sample t-test, p=0.12) between TH and nonTH neurons, we found that A2 accounted for a significantly (two-sample t-test, p=0.039) larger proportion of the fractional recovery in TH neurons compared to nonTH neurons, suggesting that TH neurons recovery slightly, but significantly more slowly than nonTH neurons (Figure 3.11 C). Neither the values of τ_1 (5.1 ± 0.6 ms in TH neurons and 4.7 ± 0.7 ms in nonTH neurons; two-sample t-test, p=0.66332) or τ_2 (325.7 ± 38.1 ms in TH neurons and 231.5 ± 61.0 ms in nonTH neurons; two-sample t-test, p=0.19) differed significantly between TH and nonTH neurons. The values of Y_0 were also similar (two-sample t-test, p=0.47). In TH neurons, Y_0 was 98.5 ± 1.0, and in nonTH neurons Y_0 was 97.6 ± 0.4.

Analysis of I_{NaP}

Finally, we examined differences in I_{NaP} properties between TH (n=15) and nonTH (n=16) neurons. The voltage clamp protocol used to elicit I_{NaP} and an example trace of I_{NaP} are shown in Figure 3.11 A and B. Peak I_{NaP} was -26.5 ± 3.0 pA in TH

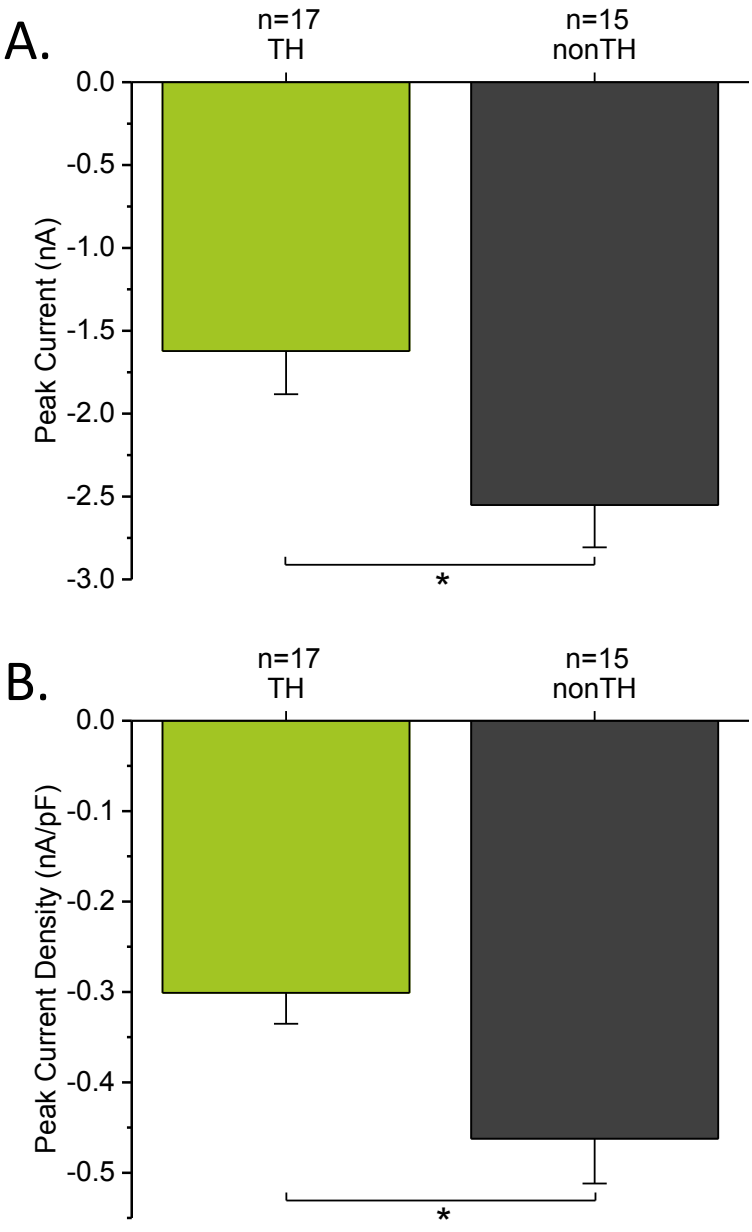

Figure 3.9 Peak I_{NaT} and peak I_{NaT} density in TH and nonTH neurons. (A) Peak I_{NaT} was significantly lower (two-sample t-test, p=0.033) in TH neurons compared to nonTH neurons. **(B)** Peak I_{NaT} density was also significantly lower (two-sample t-test, p=0.011) in TH neurons vs nonTH neurons.

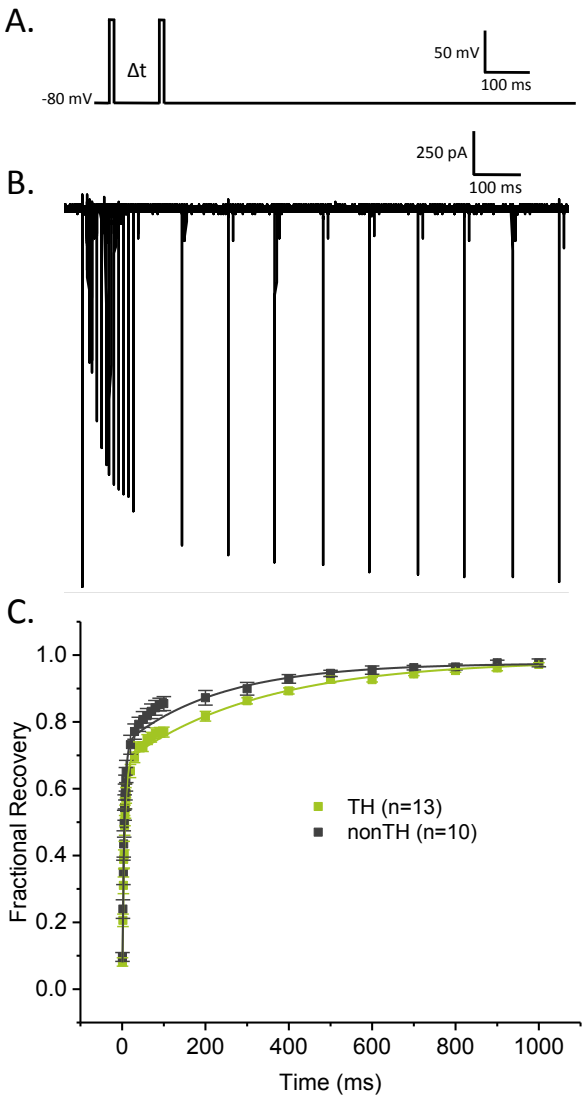

Figure 3.10 Time-dependent recovery from inactivation of I_{NaT} in TH and nonTH neurons. (A) Voltage clamp protocol for investigating time-dependent recovery. The interpulse interval (Δt) increased from 1 ms to 1000 ms. **(B)** Example current trace elicited from A. **(C)** Time-dependent recovery of I_{NaT} fitted to a double exponential function. There was no significant difference in A1, τ_1, τ_2, or Y0 between TH and nonTH neurons. However, A2 made up a significantly larger proportion of fractional recovery in TH vs nonTH neurons (two-sample t-test, p=0.039), contributing to the observed "slower" recovery from inactivation.

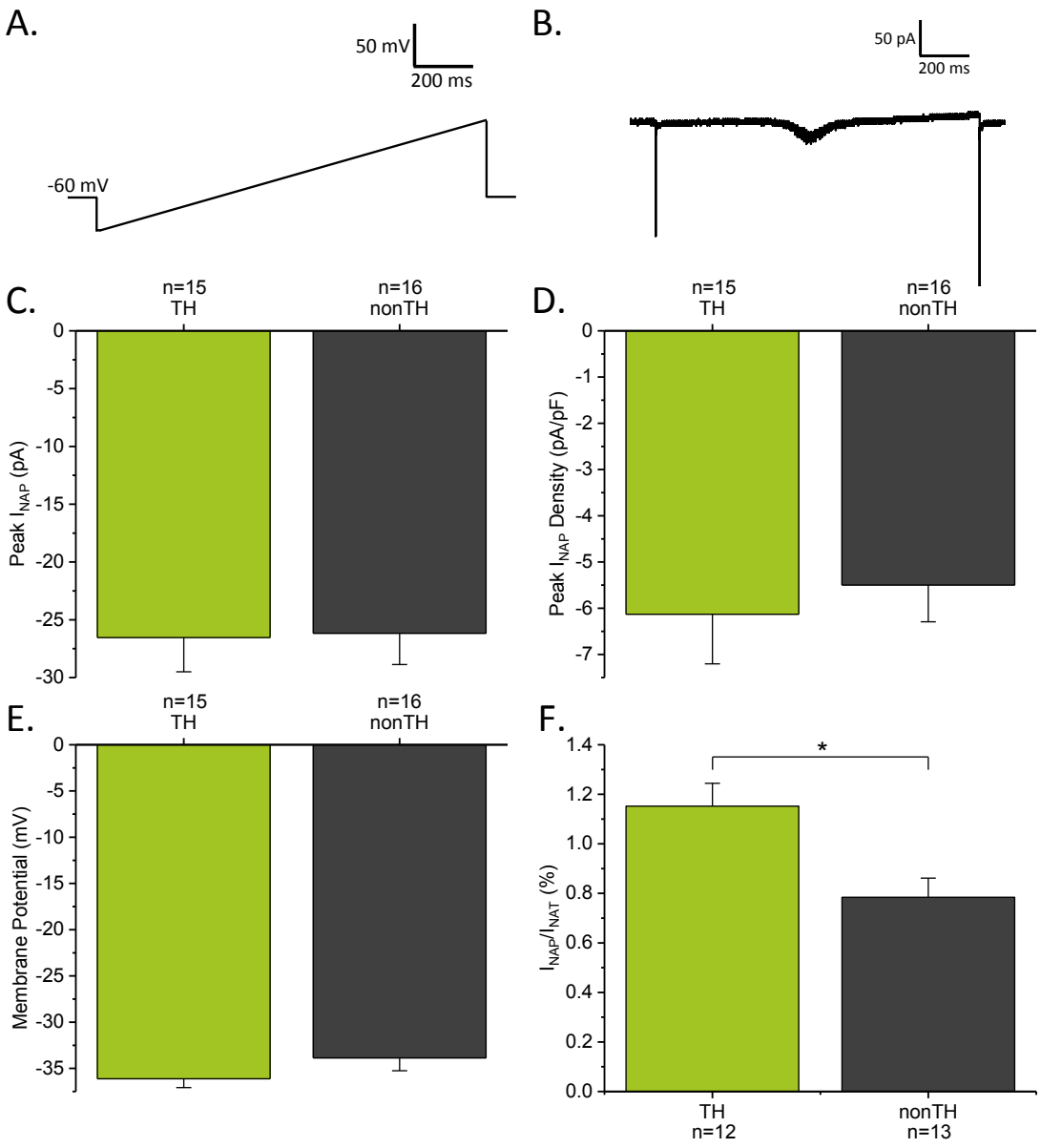

Figure 3.11 Comparison of I_{NaP} properties between TH and nonTH neurons. (A) Voltage clamp protocol used to measure I_{NaP}. **(B)** Current trace of I_{NaP} elicited from protocol shown in A. **(C)** Peak I_{NaP} was similar between TH and nonTH neurons. **(D)** Peak I_{NaP} density was also similar between TH and nonTH neurons. **(E)** The membrane potential which peak I_{NaP} occurred at did not differ between TH and nonTH neurons. **(F)** I_{NaP} made up a significantly greater percentage of I_{NaT} in TH neurons compared to nonTH neurons.

neurons, and was not significantly different (two-sample t-test, p=0.93) from peak I_{NaP} of -26.2 ± 2.7 pA in nonTH neurons (Figure 3.11 C). Peak I_{NaP} density was similar between TH and nonTH neurons (two-sample t-test, p=0.64). In TH neurons, peak I_{NaP} density was -6.1 ± 1.1 pA/pF, while it was in -5.5 ± 0.8 pA/pF in nonTH neurons (Figure 3.11 D). Peak I_{NaP} occurred at membrane potential of -36.1 ± 1.0 mV in TH neurons, which was not significantly different (two-sample t-test, p=0.20) from the membrane potential of -33.9 ± 1.0 mV at which peak I_{NaP} occured in nonTH neurons (Figure 3.11 E).

I_{NaP} is often expressed as a percentage of I_{NaT}. We found that peak I_{NaP} made up a significantly greater percentage (two-sample t-test, p=0.0054) of peak I_{NaT} in TH neurons (n=12) compared to nonTH neurons (n=13). In TH neurons, I_{NaP} made up 1.2 ± 0.09 % of I_{NaT}, while in nonTH neurons, I_{NaP} made up 0.8 ± 0.08% of I_{NaT} (Figure 3.11 F).

3.2.3 Presence of I_H in TH and nonTH neurons

As previous work has also indicated that specific subpopulations of AP neurons express I_H (Funahashi et al., 2002b; Shinpo et al., 2012), we next sought to determine if the presence of I_H correlated with biochemical phenotype. The protocol used to elicit I_H and an example current trace are shown in Figure 3.12 A and B. Significantly fewer TH neurons expressed I_H compared to nonTH neurons (Fisher's exact test, p=0.0028; Figure 3.12 C). Of 40 TH neurons tested, only 2 expressed I_H. In contrast, 12 of the 38 nonTH neurons tested expressed I_H.

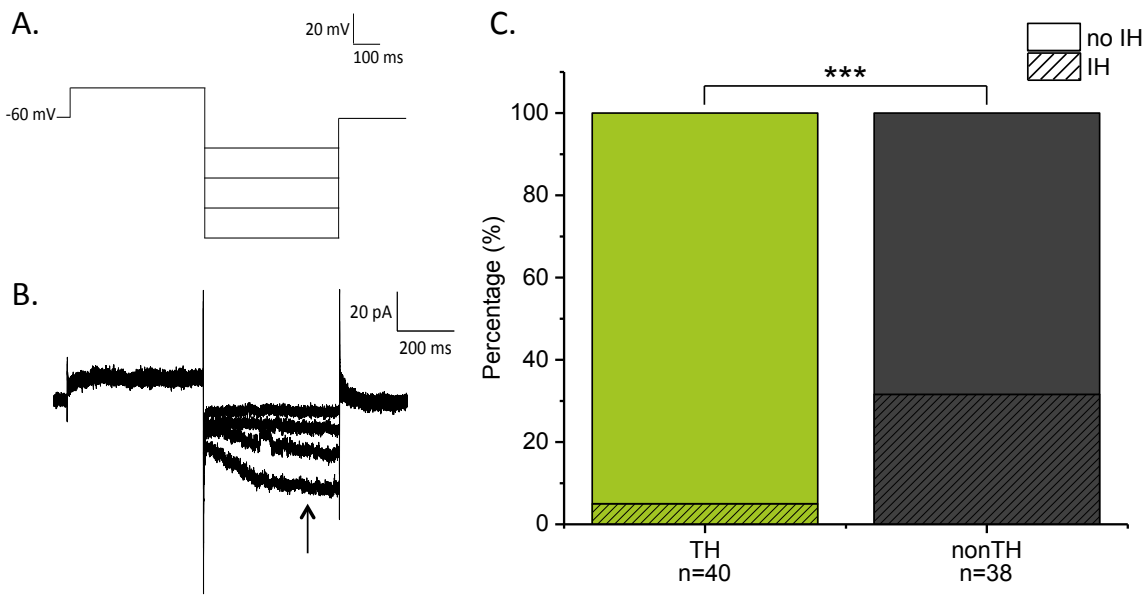

Figure 3.12 Comparison of proportion of neurons with I_H in TH and nonTH neurons. (A) I_H was activated with a -40 mV depolarizing prepulse followed by a series of hyperpolarizing voltage steps from -80 mV to -140 mV. **(B)** Traces of I_H elicited by A. I_H current is indicated by the arrow. **(C)** Neurons were categorized as either having I_H present or lacking I_H. A significantly lower (Fisher's exact test, p = 0.0028) percentage of TH neurons (n=40) were found to have I_H current than nonTH neurons (n=38).

3.2.4 Analysis of spontaneous action potential firing properties in TH and nonTH neurons

The subtle differences in K^+ current and Na^+ current properties we observed between TH properties and nonTH neurons suggested that spontaneous action potential firing may differ between TH and nonTH neurons. Therefore, we next investigated spontaneous action potential firing properties in TH and nonTH neurons. Example recordings of spontaneous action potential activity in TH and nonTH neurons are shown in Figure 3.13 A and B, respectively. Spontaneous action potential frequency was 0.89 Hz in TH neurons (n=11) and 1.11 Hz in nonTH neurons (n=15) (Figure 3.13 C). There was no significant difference (Mann-Whitney, p=1.0) between TH and nonTH neurons in spontaneous action potential frequency. Similarly, Mann-Whitney tests (p=0.43) revealed that coefficient of variation did not differ between TH (n=9) and nonTH (n=14) neurons. Coefficient of variation was 1.32 in TH neurons and 1.39 in nonTH neurons (Figure 3.13 D).

3.3 GLP-1 Receptor agonist response in TH and nonTH neurons

In the third set of experiments, current-clamp recordings were carried out to investigate the response of TH and nonTH neurons to GLP-1 receptor agonists.

3.3.1 Analysis of membrane properties in TH and nonTH neurons

In some experiments, membrane properties including resting membrane potential and input resistance were investigated in TH and nonTH before peptide application. An example recording of resting membrane potential is shown in Figure 3.14 A. Resting

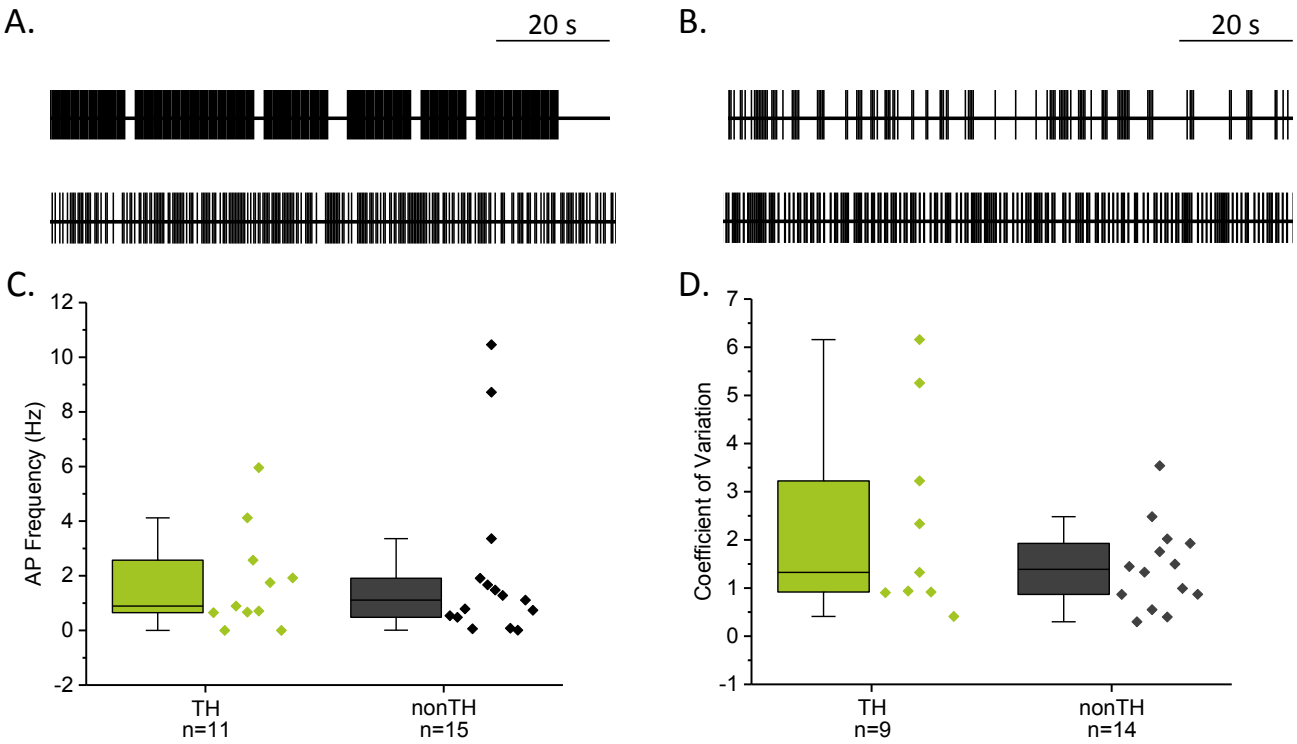

Figure 3.13 Spontaneous action potential firing properties in TH and nonTH neurons. (A) and (B) illustrate various spontaneous action potential firing patterns observed in TH and nonTH neurons, respectively. Each "tick" mark represents a single action potential. (C) There was no significant (Mann-Whitney, p=1.0) difference in the frequency of spontaneous action potentials between TH (n=11) and nonTH neurons (n=15). (D) Coefficient of variation did not significantly (Mann-Whitney, p=0.43) differ between TH (n=9) and nonTH neurons (n=14).

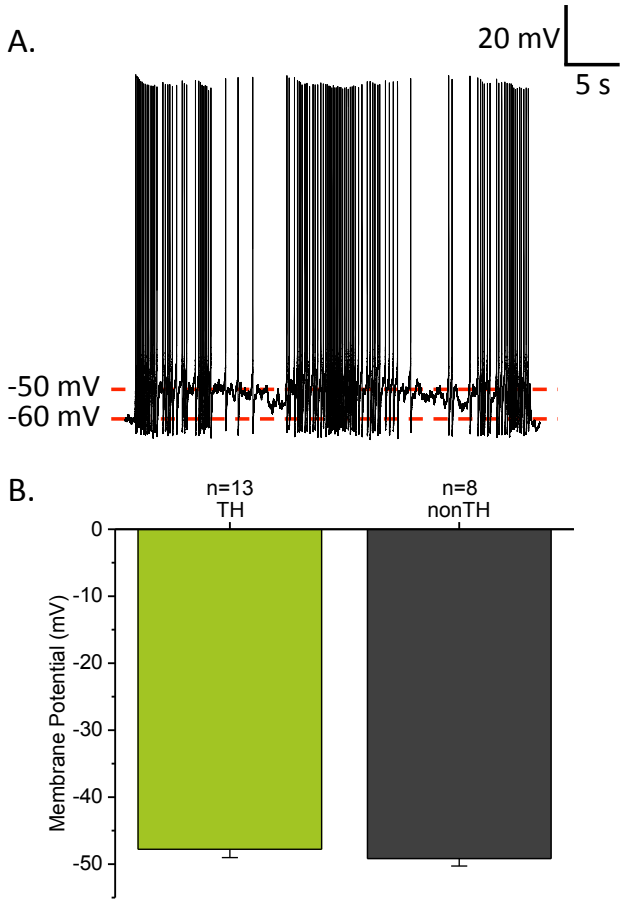

Figure 3.14 Resting membrane potential of TH and nonTH neurons. (A) An example recording of resting membrane potential. The neuron was held near -60 mV with negative current injection. The current injection was removed which allowed the cell to return to its natural resting membrane potential of approximately -50 mV. **(B)** Resting membrane potential of TH neurons (n=13) is similar (two-sample t-test, p=0.46) to resting membrane potential of nonTH neurons (n=8).

membrane potential of -47.8 ± 1.3 mV in TH neurons (n=13) was not significantly different from resting membrane potential of -49.2 ± 1.2 mV in nonTH neurons (n=8) (two-sample t-test, p=0.46) (Figure 3.14 B). The current clamp protocol used to investigate input resistance and example recording are shown in Figure 3.15 A and B. Input resistance of TH neurons (n=13) was 6.3 ± 1.2 GΩ and was not significantly (two-sample t-test, p=0.59) different from input resistance in nonTH neurons (n=8) of 5.3 ± 1.1 GΩ (Figure 3.15 C).

3.3.2 Application of 1 μM GLP-1 onto TH neurons

In current clamp configuration, we first investigated response to the endogenous GLP-1 receptor agonist, 1 μM GLP-1. We found that 4 of 6 TH neurons tested responded to 1 μM GLP-1 treatment according to a membrane depolarization at least 5 mV or an increase in action potential frequency of at least 1 Hz. An example recoding from a TH neuron that responded is shown in Figure 3.16 A. The remaining 2 TH neurons did not respond to 1 μM GLP-1 application according to our criteria. An example recording from a TH neuron that did not respond is shown in Figure 3.16 B. Mean membrane potential changed by 5.7 ± 2.5 mV compared to baseline in TH neurons as a population (n=6) following 1 μM GLP-1 application. While this change was not significant (paired-sample t-test p=0.074), it did trend towards being more depolarized (Figure 3.16 C).
In only responding neurons (n=4), membrane potential depolarized by 9.3 ± 1.6 mV compared to baseline, while in only the neurons that showed no response (n=2) membrane potential hyperpolarized by -1.6 ± 0.9 mV compared to baseline. Action

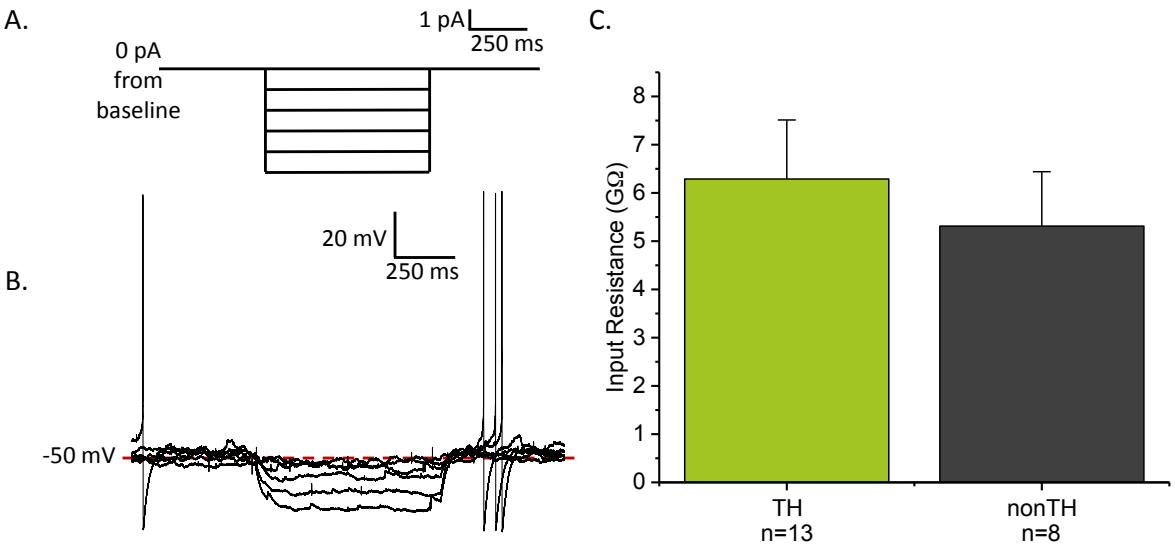

Figure 3.15. Input resistance of TH and nonTH neurons. (A) Current clamp protocol for measuring input resistance in AP neurons. **(B)** Traces of membrane potential elicited from A. (C) Input resistance was not significantly (t-test, p=0.59) different between TH (n=13) and nonTH neurons (n=8).

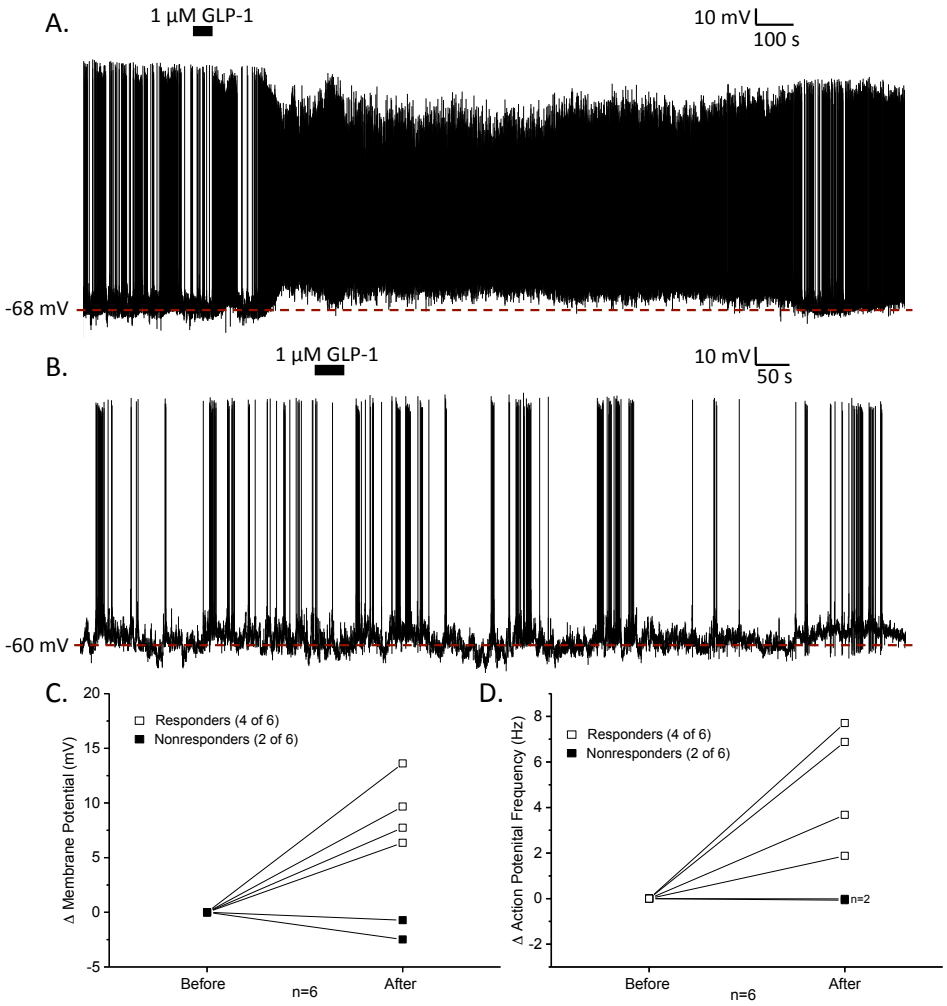

Figure 3.16 Response of TH neurons to 1 µM GLP-1 application. Of 6 TH neurons tested with 1 µM GLP-1, 4 responded and 2 showed no response according to pre-established criteria. **(A)** Example recording from a TH neuron that responded. **(B)** Example recording from a TH neuron that did not respond. **(C)** Membrane potential was not significantly (paired-sample t-test; p=0.074) different compared to baseline in TH neurons as a population (n=6). Neurons that responded (n=4) are indicated by open squares, neurons that did not respond (n=2) by closed squares. **(D)** Action potential frequency was not significantly (paired-sample t-test, p=0.059) different from baseline in TH neurons as a population (n=6). Neurons that responded (n=4) are indicated by open squares, neurons that did not respond (n=2) by closed squares.

it did trend towards an increase (Figure 3.16 D). Action potential frequency increased by 3.8 ± 0.7 Hz compared to baseline in TH neurons that responded (n=4), while in neurons that did not respond (n=2) action potential frequency remained near (0.0 ± 0.0 Hz) baseline values. Average latency to response was 53.3 ± 19 s after application of GLP-1. Of the 4 neurons that responded, only 1 neuron recovered. In this neuron, the duration of response was 1503.6 seconds.

3.3.3 Application of 1 μM Exendin-4 onto TH neurons

Because GLP-1 is susceptible to rapid degradation (Mentlein, 1999), we also investigated the response to the stable exogenous GLP-1 receptor agonist, Exendin-4. We observed that 8 of the 13 TH neurons tested with 1 μM Exendin-4 responded according to membrane depolarization of at least 5 mV or an increase in action potential frequency of at least 1 Hz. An example current-clamp recoding from a TH neuron that responded is shown in Figure 3.17 A. The remaining 5 TH neurons showed no response to Exendin-4 application according to our criteria. An example current-clamp recoding from a TH neuron that did not respond is shown in Figure 3.17 B. Membrane potential significantly (paired-sample t-test p=0.0013) depolarized by 5.5 ± 1.4 mV in TH neurons as a population (n=13) compared to baseline following 1 μM Exendin-4 application (Figure 3.17 C). In only the responding TH neurons (n=8), membrane potential depolarized by 8.2 ± 1.4 mV compared to baseline, while in only the TH neurons that showed no response (n=5) membrane potential depolarized by 1.3 ± 1.1 mV compared to baseline. A significant (paired-sample t-test, p=9.5E-4) concomitant increase in action potential frequency of 2.5 ± 0.7 Hz compared to baseline was also observed in TH neurons as a

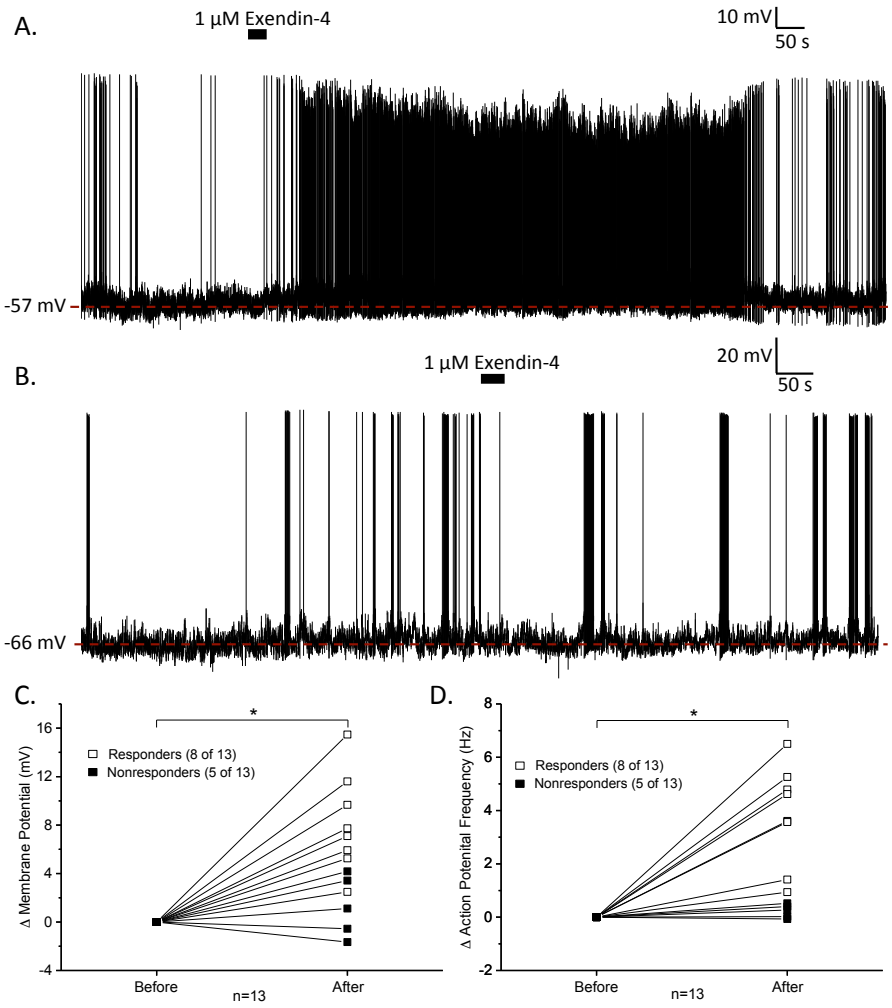

Figure 3.17 Response of TH neurons to 1 µM Exendin-4 application. Of 13 TH neurons tested with 1 µM Exendin-4, 8 responded and 5 showed no response according to pre-established criteria. **(A)** Example recording from a TH neuron that was depolarized. **(B)** Example recording from a TH neuron that did not respond. **(C)** Membrane potential significantly (paired-sample t-test; p= 0.0022) depolarized compared to baseline in TH neurons as a population (n=13). Neurons that responded are indicated by open squares (n=8), neurons that did not respond by closed squares (n=5). **(D)** Action potential frequency significantly (paired-sample t-test, p=0.0021) increased from baseline in TH neurons as a population (n=13). Neurons that responded are indicated by open squares (n=8), neurons that did not respond by closed squares (n=5).

population (n=13) after Exendin-4 treatment (Figure 3.17 D). Action potential frequency increased by 3.8 ± 0.7 Hz compared to baseline in TH neurons that responded (n=8), while in TH neurons that did not respond (n=5) action potential frequency increased by only 0.2 ± 0.1 Hz. Average lag time to response was 53.5 ± 10 s. Of the 8 TH neurons that responded, 5 TH neurons recovered. The average duration of effect in these TH neurons was 667.3 ± 135 s.

We next compared the response of TH neurons tested with 1 μM GLP-1 (n=6) to the response of TH neurons tested with 1 μM Exendin-4 (n=13). As expected, there was no difference in the percent of tested TH neurons that responded to either 1 μM GLP-1 or 1 μM Exendin-4 application (Fisher's exact test, p=1.0; Figure 3.18 B). Additionally, the magnitude of depolarization was similar (two-sample t-test, p=0.95) between TH neurons tested with 1 μM GLP-1 and those tested with 1 μM Exendin-4. Because of the similarities in response of TH neurons to 1 μM GLP-1 and 1 μM Exendin-4, we were able to pool this data in future comparisons.

3.3.4 Application of 1 μM GLP-1 to TH neurons in the presence of antagonist 1 μM Exendin-3 (9-39)

To ensure that responses we observed were due to the specific action of 1 μM GLP-1 and 1 μM Exendin-4 on the GLP-1 receptor, we next applied 1 μM GLP-1 in the presence of 1 μM of the GLP-1 receptor antagonist, Exendin-3 (9-39), to 10 TH neurons. Of the 10 TH neurons tested, 9 showed no response. An example current-clamp recording from a TH neuron that did not respond is depicted in Figure 3.19 A. The remaining TH

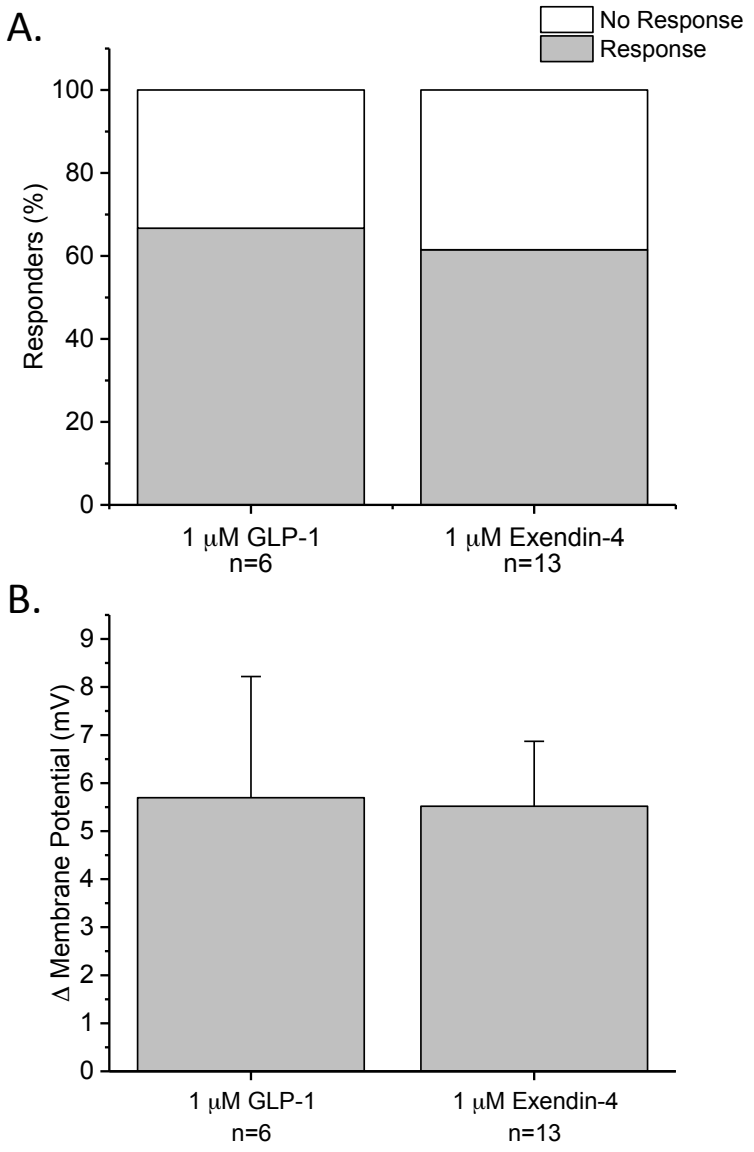

Figure 3.18 Comparison of GLP-1 receptor agonist response in TH neurons (A) The percentage of TH neurons (n=6) that responded to 1 μM GLP-1 was not significantly (Fisher's exact test, p=1.0) different from the percentage of TH neurons (n=13) that responded to 1 μM Exendin-4. **(B)** The magnitude of depolarization in TH neurons was similar following either GLP-1 or Exendin-4 (two-sample t-test, p=0.95).

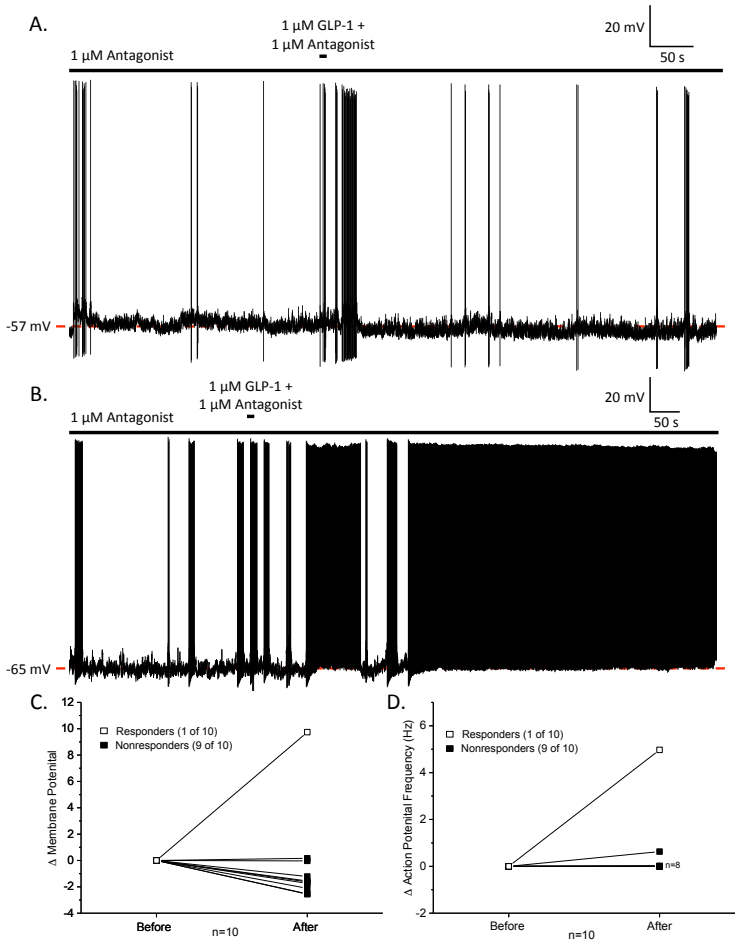

Figure 3.19 Response of TH neurons to 1 µM GLP-1 in the presence of 1 µM Exendin-3 (9-39). Of 10 TH neurons treated with 1 µM GLP-1 in the presence of 1 µM of the antagonist Exendin-3 (9-39), 9 showed no response, while 1 responded according to pre-established criteria. **(A)** Example recording from a TH neuron that did not respond. **(B)** Example recording from a TH neuron that responded. **(C)** Membrane potential was not significantly (paired-sample t-test; p=0.34) different compared to baseline in TH neurons as a population (n=10). Neurons that responded are indicated by open squares (n=1), neurons that did not respond by closed squares (n=9). **(D)** Action potential frequency was not significantly different (paired-sample t-test, p=0.28) from baseline in TH neurons as a population (n=13). Neurons that responded (n=1) are indicated by open squares, neurons that did not respond by closed squares (n=9).

neuron responded to 1 μM GLP-1 application (based on a membrane depolarization of at least 5 mV or an increase in action potential frequency of at least 1 Hz) despite the despite the presence of 1 μM Exendin-3 (9-39). The current-clamp recording from this TH neuron is shown in Figure 3.19 B. A change in membrane potential of -0.3 ± 1.2 mV in TH neurons as a population (n=10) was not significantly different (paired-sample t-test p=0.34) compared to baseline following treatment with 1 μM GLP-1 in the presence of 1 μM Exendin-3 (9-39) (Figure 3.19 C). In only the TH neurons that showed no response (n=9) membrane potential hyperpolarized by -1.5 ± 0.3 mV compared to baseline, while membrane potential depolarized by 9.7 mV compared to baseline in the TH neuron that responded. A change in action potential frequency of 0.6 ± 0.5 Hz in TH neurons as a population (n=10) was not significantly (paired-sample t-test, p=0.28) different from baseline following 1 μM GLP-1 application in the presence Exendin-3 (9-39) (Figure 3.19 D). Action potential frequency remained similar to baseline (0.1 ± 0.1 Hz) in only the TH neurons that did not respond (n=9), while it increased by 4.97 Hz compared to baseline in the TH neuron that responded (n=1). Finally, we compared the number of tested TH neurons that responded to 1 μM GLP-1 in the presence of antagonist to the number of tested TH neurons that response to 1 μM GLP-1 and 1 μM Exendin-4 (n=19, pooled data). We found that significantly (Fisher's exact test, p=0.0067) fewer tested TH neurons responded to GLP-1 in the presence of antagonist compared to the number of tested TH neurons responding to 1 μM GLP-1 and 1 μM Exendin-4 application, implying that 1 μM Exendin-3 (9-39) blocked the effects of GLP-1 and that the effects we observed in previous experiments were due to the specific action of GLP-1 and Exendin-4 on the GLP-1 receptor.

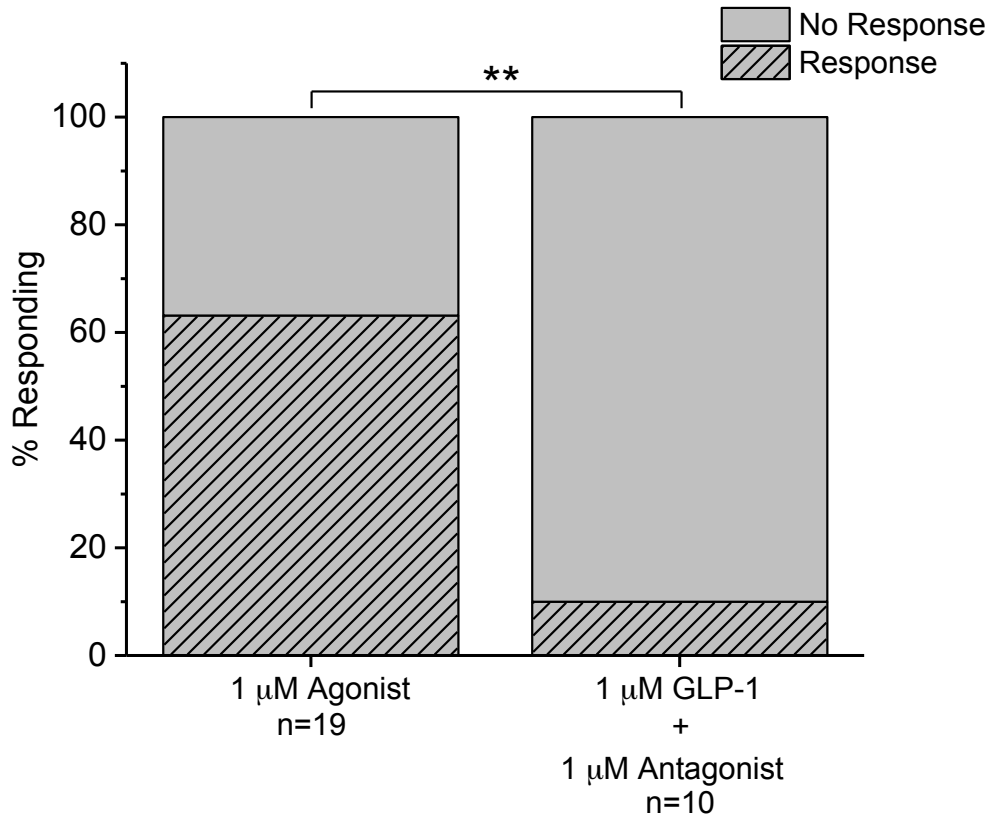

Figure 3.20 Number of TH neurons responding to GLP-1 and Exendin-4 compared to the number of TH neurons responding GLP-1 in the presence of Exendin-3 (9-39). A Fisher's exact test revealed that significantly (p=0.0067) fewer TH neurons responded to 1 μM GLP-1 in the presence of 1 μM of the antagonist Exendin-3 (n=10) than to 1 μM agonist (GLP-1 or 1 μM Exendin-4) (n-19, pooled data) alone.

3.3.5 Comparison of mean membrane potential change in TH and nonTH neurons

We next compared mean membrane potential change of all TH neurons treated with 1 μM GLP-1 or 1 μM Exendin-4 to the mean membrane potential change observed in TH and nonTH neurons treated with only ERS and to TH neurons treated with 1 μM GLP-1 in the presence of 1 μM of the antagonist Exendin-3 (9-39) using a one-way ANOVA with Tukey post hoc correction. Statistical analysis that a membrane potential change of 5.6 ± 1.2 mV in TH neurons treated with 1 μM GLP-1 or 1 μM Exendin-4 (n=19, pooled data) was significantly depolarized compared to a membrane potential change of -0.3 ± 0.5 mV observed in TH and nonTH neurons following application of only ERS (n=5) (p=0.032) and to a membrane potential change of -0.35 ± 1.2 mV in TH neurons following treatment with 1 μM GLP-1 in the presence of 1 μM Exendin-3 (9-39) (n=10) (p=0.0046) (Figure 3.21). Membrane potential change in TH neurons following application of 1 μM GLP-1 in the presence of 1 μM Exendin-3 (9-39) did not differ significantly from the membrane potential change following application of only ERS. Together, these results suggest GLP-1 receptor agonists significantly depolarize TH neurons.

3.3.6 Application of 1μM GLP-1 onto nonTH neurons

Previous literature suggests that a minority of nonTH neurons express the GLP-1 receptor (Yamamoto et al., 2003). Therefore, we investigated the response of 8 nonTH neurons to 1μM GLP-1. We found that 2 of the nonTH neurons responded to 1 μM GLP-1 treatment according to a membrane depolarization of at least 5 mV or an increase in

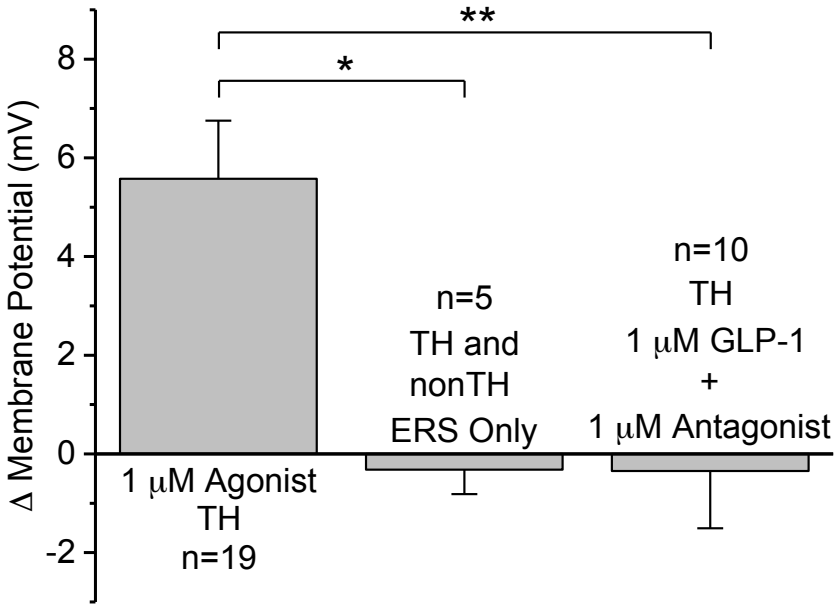

Figure 3.21 Comparison of mean membrane potential change of TH neurons treated with GLP-1 receptor agonists to ERS and antagonist control. A one-way ANOVA with Tukey post hoc correction was used to compare mean membrane potential change of all TH neurons treated with 1 μM agonist (GLP-1 or Exendin-4) to the mean membrane potential change observed in TH and nonTH neurons treated with only ERS and to TH neurons treated with 1 μM GLP-1 in the presence of 1 μM of the antagonist Exendin-3 (9-39). Membrane potential of TH neurons was significantly depolarized following GLP-1 receptor agonist application compared to application of only ERS and antagonist control.

action potential frequency of at least 1 Hz. An example recording from a nonTH neuron that responded is shown in Figure 3.22 A. The remaining 6 nonTH neurons did not respond to 1 μM GLP-1 application according to our criteria. An example recording from a nonTH neuron that did not respond is shown in Figure 3.22 B. A change in membrane potential of 0.9 ± 1.1 mV in nonTH neurons as a population (n=8) was not significantly (paired-sample t-test p=0.45) different from baseline following 1 μM GLP-1 application (Figure 3.22 C). In only the responding nonTH neurons (n=2) membrane potential depolarized by 4.9 ± 2.1 compared to baseline, while in only the nonTH neurons that showed no response (n=6) membrane potential hyperpolarized by -0.5 ± 0.7 mV compared to baseline. A change in action potential frequency of 1.0 ± 0.6 Hz in nonTH neurons as a population (n=8) was not significantly (paired-sample t-test, p=0.14) different compared to baseline following GLP-1 application (Figure 3.22 D). Action potential frequency increased by 3.3 ± 1.1 Hz compared to baseline in only the nonTH neurons that responded (n=2), while in only the nonTH neurons that did not respond (n=6) action potential frequency changed by 0.2 ± 0.2 Hz. Average latency to response was 165.7 ± 16 s. Both of the nonTH neurons that responded to GLP-1 application recovered after 393.5 ± 60 s.

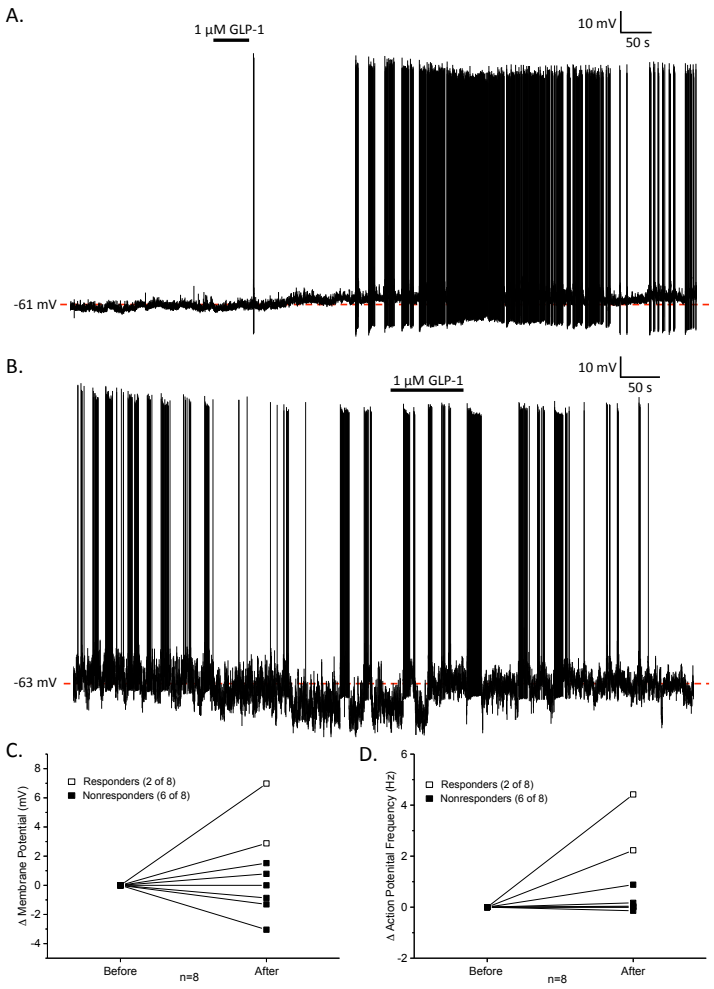

Figure 3.22 Response of nonTH neurons to 1 µM GLP-1 application. Of 8 nonTH neurons tested with 1 µM GLP-1, 2 responded while the remaining 6 showed no response according pre-established criteria. **(A)** Example recording from a nonTH neuron that responded. **(B)** Example recording from a nonTH neuron that did not respond. **(C)** Membrane potential significantly (paired-sample t-test; p= 0.45) depolarized compared to baseline in nonTH neurons as a population (n=8). Neurons that responded are indicated by open squares (n=2), neurons that did not respond by closed squares (n=6). **(D)** Action potential frequency was not significantly (paired-sample t-test, p=0.14) different from baseline in nonTH neurons as a population (n=8). Neurons that responded are indicated by open squares (n=2), neurons that did not respond by closed squares (n=6).

4. Discussion

This study is the first to characterize the intrinsic electrophysiological properties of mouse AP TH neurons. Voltage clamp recordings revealed subtle differences in K^+ current, Na^+ current, and I_H properties between TH and nonTH neurons. However, these electrical differences alone are not specific enough to distinguish TH neurons from nonTH neurons, as there is overlap in the properties of these ionic currents between these subpopulations. For the first time, we also investigated the direct response of TH neurons to GLP-1 receptor agonists. We observed that application of 1 μM GLP-1 or 1 μM Exendin-4 activated the majority of TH neurons tested. Additionally, we observed that a small minority of nonTH neurons were also activated by 1 μM GLP-1. Our observations indicate that TH neurons are an electrophysiologically heterogeneous population, and confirm an important role in the detection of circulating GLP-1 acting on the AP.

4.1 Immunohistochemistry

In the present study, a line of transgenic mice expressing GFP under control of the TH promoter was used to visually identify CA-containing neurons. Our immunochemistry results demonstrate that GFP can be used as an indicator of TH expression in the AP, as the majority of GFP-expressing neurons also contained TH. Specifically, we observed that 78% of GFP-expressing neurons also contained TH. This is similar to the GFP-expression efficiency of 60-80% initially reported in midbrain neurons of this line of mice (Matsushita et al., 2002) and to 70% GFP-expression efficiency reported in the ventral tegmental area of mice expressing GFP under the control of the human tyrosine hydroxylase promoter (Kessler et al., 2003). GFP

expression efficiency is higher in other lines of similar transgenic mice. For example, Matsushita et al. (2002) developed a second line of mice that also express GFP under the control of the TH promoter (termed GFP/21-31 mice). GFP expression efficiency in this second line of mice was reported to be as high as 85-94% in the midbrain. In mice expressing GFP under the control of the POMC promoter, a 99% GFP expression efficiency in ARC POMC neurons has been observed (Cowley et al., 2001). The results of this study provide further support to use of this TH-GFP mouse line as a visual tool for TH expression in multiple areas of the CNS, including the AP, with recognition of the possibility that a GFP neuron may not be TH and vice versa.

4.2 Neuronal culture of AP neurons

In this study, we utilized a dissociated neuronal preparation to investigate the electrical properties of AP neurons and their response to GLP-1. Dissociated cultures offer several unique advantages over acute slice preparations. First, the dissociation process removes most neurites from neurons, improving space clamp (Aston-Jones and Siggins, 1995; Kay and Krupa, 2001). Second, neurons are electrically isolated from one another in a dissociated culture, ensuring that any observed treatment effects are due to direct (postsynaptic) action rather than indirect (presynaptic) action. Finally, the use of dissociated cultures reduces the numbers of animals needed for experimentation. For example, up to 10 dissociated cultures can be generated from a single animal. Whereas in acute slice preparation, a new animal must be used every day and only 2-3 slices may be obtained from a single animal for a small nucleus like the AP.

The electrophysiology of neurons *in vivo* is well maintained in dissociated cultures. For example, Ferguson et al. (1997) have shown that the electrical properties of dissociated rat SFO neurons remain stable and that ANGII response is retained up to 1 week after culturing. Similarly, Hay and Lindsley (1995) reported that electrical properties and peptide response are maintained in dissociated rat AP cultures. Based on these previous studies, the electrical properties of mouse AP neurons we have measured *in vitro* likely provide an accurate representation of the *in vivo* electrophysiology.

4.3 Membrane properties of TH and nonTH neurons

The electrophysiological properties of AP neurons in this study are consistent with previously published observations. For example, we found that capacitance for TH neurons (n=87) of 7.2 ± 0.3 pF was significantly greater than the capacitance of 6.0 ± 0.3 pF measured in nonTH neurons (n=61) (two-sample t-test, p=0.0053; data not shown). These capacitance values are similar to mean capacitance values of 6.6 ± 1.9 pF and 7.7 ± 1.2 pF reported by Funahashi et al. (2006) for rat AP neurons. The resting membrane potential in TH neurons was -47.8 ± 1.2 mV and -49.2 ± 1.1 mV in nonTH neurons. A previous study reported resting membrane potential to be -48.7 ± 1.1 mV in rat AP neurons (Fry and Ferguson, 2009). Input resistance has been reported to range from 0.2 GΩ in rat brain slices (Hay and Lindsley, 1995) to 3.6 GΩ in dissociated rat AP neurons (Yang and Ferguson, 2002; Fry and Ferguson, 2009). In the present study, we observed input resistances of 6.3 ± 1.2 GΩ in TH neurons and 5.3 ± 1.1 GΩ in nonTH neurons. These high input resistances suggest that few leak channels are active in mouse AP neurons. The small size and simple architecture (McKinley et al., 2003; Funahashi et al.,

2006) of AP neurons also contributes to high input resistance. Finally, AP neurons are well known to fire spontaneous action potentials at low frequencies. In a previous study, dissociated rat AP neurons fired spontaneous action potentials at a rate of 0.2 to 9.9 Hz (Yang and Ferguson, 2002). In the present study, spontaneous action potential frequency was 0.89 Hz in TH neurons (n=11) and 1.11 Hz in nonTH neurons (n=15). Notwithstanding species differences, there are many similarities between the electrophysiological properties documented in our study and those in literature. Thus, we can be confident in the quality of our electrophysiological data.

4.4 K^+ current properties in TH and nonTH neurons

Voltage-gated K^+ current contributes to neuronal excitability and modulation of action potential properties (Hoyda and Ferguson, 2010; White et al., 2016). Specifically, I_{TO} contributes to delay of action potential firing, while I_K contributes to membrane repolarization during an action potential (Connor and Stevens, 1971).

Voltage-gated K^+ current has been well studied in sensory CVOs. In the SFO, K^+ current is composed of at least two components including I_K and I_{TO} and SFO neurons express different K^+ current properties (Anderson et al., 2001). For example, some SFO neurons exhibit a larger I_{TO}, smaller I_K, and greater degree of K^+ current inactivation.

In the rat AP, voltage-gated K^+ current is also composed of I_K and I_{TO} (Hay and Lindsley, 1995; Li and Hay, 2000) and rat AP neurons have been categorized into 3 groups based on I_{TO} properties and the presence of I_H (Funahashi et al., 2002a, 2006). Because Funahashi et al. (2002a, 2006a) have shown that AP neurons can be electrophysiologically grouped, we examined whether these properties correlate with

biochemical phenotype. In particular, we were interested in whether TH neurons have an electrophysiological "signature" that can be used for identification from surrounding nonTH neurons.

In the present study, we noted subtle differences in K^+ current properties between TH and nonTH neurons including decreased I_K density and a depolarizing shift in I_K activation in TH neurons. Decreases in I_K broaden action potentials (Aldrich et al., 1979) and a depolarizing shift in I_K activation could further potentiate the broadening of action potentials by delaying repolarization. Intriguingly, TH-containing neurons in other brain regions, such as the midbrain, exhibit broader action potential width compared to surrounding neurons (Grace and Onn, 1989; Richards et al., 1997). Lower I_K density suggests that fewer voltage-gated K^+ channels contributing to I_K are expressed in the TH neurons. We also observed lower I_{TO} density in TH neurons. Lower I_{TO} density can contribute to hyperpolarized action potential threshold and increased action potential height, contributing toward enhanced neuronal excitability.

To further investigate the properties of I_{TO}, we fitted this current to a double exponential decay function. We used a double exponential decay function because it provided the best fit for our data. Previous studies investigating I_{TO} properties in AP neurons used either a single exponential decay function (Funahashi et al., 2002a) or a triple exponential decay function (Hay and Lindsley, 1995). A double exponential decay function is advantageous compared to the single exponential function used by Funahashi et al., 2002a) because it allows partitioning of the current into fast and slow components that can be correlated to ion channel expression. Because previous studies used different exponential functions to fit their data, it is difficult to make direct comparisons with our

data. However, we can be confident in our fitting of I_{TO} as the τ values we have identified fall within the ranges of τ values described in these previous studies (Hay and Lindsley, 1995). For example, median τ_1 values of 19.8 ms and 20.3 ms identified for TH and nonTH neurons in this study are consistent with fast I_{TO} τ values of 13.6 ms to 28.5 ms described by Funahashi et al. (2002a, 2002b). As previously noted in the AP, these τ values are consistent with I_A current (Hay and Lindsley, 1995; Funahashi et al., 2002a). Similarly, our median τ_2 values of 125.9 ms in TH neurons and 137.6 ms in nonTH neurons correspond to the slow τ values of 56.2 ms to 150.7 ms described by Funahashi et al. (2002a). Slow I_{TO} has been hypothsized to belong to either a dendrotoxin-sensitive K^+ channel (I_D) (Funahashi et al., 2002a) or to represent remnant I_K that cannot be completely isolated from I_{TO} using voltage clamp alone (Budde et al., 1992; Albert and Nerbonne, 1995; Du and Meng, 2004). However, based on observations that slow I_{TO} contributes to unique action potenital firing properties in rat AP neurons (Funahashi et al., 2002a), it is likely that a large portion of this current is carried by voltage-gated K^+ channels other than those contributing to I_K. Additionally, our fittings suggest that I_{TO} inactivates more completely in TH neurons, as we observed a smaller median Y_0 in TH neurons compared to nonTH neurons.

AP neurons have previously been categorized as having a fast or slow I_{TO} based on a τ value obtained from fitting to a single exponential (Funahashi et al., 2002a). Because we fitted I_{TO} to a double exponential decay function, we separated this current into fast and slow components within individual neurons. Fast and slow components of I_{TO} are co-expressed in many other types of neurons including visual cortical (Gold et al., 1996), hippocampal (Du and Meng, 2004), and dorsal root ganglion (Everill et al., 1998)

neurons. Our results suggest that the proportion of ion channels contributing to either the fast or slow component of I_{TO} varies within neurons. For example, in TH neurons the fast proportion of I_{TO} ranged from 2.8% to 73.4 %, while in nonTH neurons it ranged from 4.3% to 60.8%. Although the difference in median percentage of I_{TO} made up by the fast component did not reach statistical significance between TH and nonTH neurons ($p=0.06936$), it did trend towards a larger value in TH neurons, suggesting that TH neurons tend to express more channels contributing to the fast component of I_{TO}. However, we found no difference in the overall percentage of TH neurons that could be categorized as having a predominantly fast I_{TO} compared to nonTH neurons.

Differences in K^+ current properties appear to contribute to different action potential firing patterns within AP neurons. For example, neurons that have a fast I_{TO} show delayed action potential firing in response to depolarizing current injections, while neurons that have a slow I_{TO} display an interruption between the first and second action potential in response to depolarizing current injections (Funahashi et al., 2002a). While we did not investigate specific action potential properties (such as action potential width), it is likely that the subtle the differences we observed in voltage-gated K^+ current properties between TH neurons and nonTH neurons help to fine tune the action potential properties of individual neurons. Further investigation is needed to determine the exact significance of these results.

The properties we have investigated of I_K and I_{TO} can be used to help begin correlating specific voltage-gated K^+ channels to these currents. A number of voltage-gated K^+ channel subfamilies are expressed in the AP including Kv1-Kv4 (Hindmarch et al., 2011). Specifically, the voltage-gated K^+ channels that are highly expressed in the AP

and expected to make a significant contribution to voltage-gated K^+ current include Kv1.4, Kv1.5, Kv3.2, Kv3.3, Kv4.2 and Kv4.3.

The voltage-gated K^+ channels Kv1.5 and Kv3.2 are well known to produce noninactivating K^+ currents in neurons (Hernández-Pineda et al., 1999; Tabarean, 2014) and heterologous expression systems (Vonderlin et al., 2014; Ahmed et al., 2016) and likely contribute to I_K in AP neurons as well. For example, Kv3 channels have a depolarized voltage dependence of activation (compared to other voltage-gated K^+ channels) (Conley et al., 1999), falling above 0 mV (McCormack et al., 1990), while voltage dependence of Kv1.5 channels is hyperpolarized compared to Kv3 channels with values reported near –10 mV (Snyders et al., 1993). The voltage dependence of activation we observed for I_{TO} density in TH ($V_{1/2ACT}$ = -3.6 ± 0.7 mV) and nonTH ($V_{1/2ACT}$ = -7.2 ± 0.8 mV) neurons is consistent with voltage dependent activation of Kv3.2 and Kv1.5 channels. Differential expression of these channels may help to fine tune I_K properties. For example, it is possible that more Kv3.2 channels are expressed in TH neurons than Kv1.5 channels, contributing to the depolarizing shift in voltage dependence of activation for I_K density we observed in these neurons.

The remaining voltage-gated K^+ channels Kv1.4, Kv3.3, Kv4.2 and Kv4.3 likely contribute to I_{TO} in AP neurons. Previous studies have compared I_{TO} to I_A based on current inactivation (Hay and Lindsley, 1995; Funahashi et al., 2002a). Time constants of inactivation for I_A-like current in cultured rat hippocampal neurons range from 10 ms to 40 ms (Segal and Barker, 1984; Segal et al., 1984). Similar inactivation time constants have been reported for Kv1.4 (Po et al., 1992; Xie et al., 2014) and Kv4.2 (Blair et al., 1991) in both *Xenopus* oocytes and HEK cells, and these time constants are consistent

with what we observed for τ_1. Kv4.3 channels often fit best to biphasic (double exponential decay) inactivation (Jerng et al., 2004) and in rat hippocampal neurons (Martina et al., 1998; Lien et al., 2002) exhibit a first time constant similar to that reported for I_A, and a second slower time constant with values similar to what we observed for τ_2. Finally, when expressed in heterologous systems such as CHO cells or HEK cells, Kv3.3 exhibit inactivation time constants that are slower than those observed for other fast inactivating K^+ channels, and are consistent with our observed τ_2 values. The possibility also exists that β-subunits, such as Kvb1.3 (Hindmarch et al., 2011), are interacting with slowly or noninactivating K^+ channels to create new inactivating channels with fast time constants (Rettig et al., 1994) or that KChIP channels are interacting with fast inactivating K^+ channels, such as Kv4.2 (An et al., 2000), resulting in slowed inactivation with τ values more closely resembling our observed τ_2 values.

While we have attempted to correlate some of the voltage-gated K^+ channels expressed in the AP with the biophysical properties we measured in our experiments, it is important to note that the behaviour of a given ion channel may vary among different neurons. This is in part due to interactions with other proteins (Rush et al., 2006). For example, endogenous expression of the K^+ channel β-subunit Kvβ2.1 in mouse L-cells hyperpolarizes voltage dependence of activation and slows inactivation of the voltage-gated K^+ channel Kv2.1 compared to HEK cells, which lack Kvβ2.1 (Uebele et al., 1996). Similarly, a mutation in Nav1.7 was found to depolarize membrane potential of both dorsal root ganglion and superior cervical ganglion neurons but lead to hyperexcitability of dorsal root ganglion neurons and hypoexcitability in superior cervical ganglion neurons. Hyperexcitability was due to specific expression of the voltage gated

Na^+ channel Nav1.8 in dorsal root ganglion neurons, which allowed action potential firing to continue at more depolarized potentials compared to superior cervical ganglion neurons, that lack Nav1.8 (Rush et al., 2006). So, while we have made an effort to correlate ion channels to a specific function, further electrophysiological experiments are needed to confirm their exact function within AP neurons.

4.5 Na^+ current properties in TH and nonTH neurons

In most neurons, voltage-gated Na^+ current consists of a rapidly-activating/rapidly-inactivating transient current, and non-inactivating persistent current. The transient current comprises most of the voltage-gated Na^+ current and is responsible for the rising phase of an action potential.

The voltage-dependence of activation and inactivation of I_{NaT} are strong indicators of neuronal excitability and are frequently investigated in electrophysiology experiments. In rat SFO and AP, I_{NaT} half activation occurs between -28 mV and -47 with slope factor k values of 4.5 to 7.2, while half inactivation of I_{NaT} occurs between -52 mV and -62 mV with slope factor k of 6.1 to 7.2 (Fry and Ferguson, 2007; Ingves and Ferguson, 2010; Kuksis and Ferguson, 2015).

Our results show that activation and inactivation of I_{NaT} are nearly identical in TH and nonTH neurons. The half activation and half inactivation we observed for TH and nonTH neurons are similar to previous studies in rat SFO and AP when junction potential is considered (Hay and Lindsley, 1995; Fry and Ferguson, 2007; Ingves and Ferguson, 2010; Kuksis and Ferguson, 2015). Additionally, slope factor k values of TH and nonTH neurons are also similar to those values reported literature.

We also investigated I_{NaT} density in TH and nonTH neurons. Density was significantly lower in TH neurons, suggesting that fewer sodium channels are present in TH neurons. As I_{NaT} drives action potentials, a lower density might suggest less driving force is available towards spontaneous action potential firing.

Lastly, we investigated the time dependent recovery of I_{NaT} in TH and nonTH neurons by fitting fractional recovery to a double exponential function to measure the fast and slow components of recovery. The fast time constants of 5.1 ± 0.6 ms in TH neurons, and 4.7 ± 0.7 in nonTH neurons, as well as the slow time constants of 325.7 ± 38.1 ms in TH neurons, and 231.5 ± 61.0 ms in nonTH neurons were similar, suggesting that I_{NaT} is carried by the same Na^+ channels in TH and nonTH neurons. The proportion of current made of up the fast component of recovery was also similar in TH and nonTH neurons. However, we observed that significantly more of the fractional recovery was made up of the slow component in TH neurons (A2 = -0.31 ± 0.02) versus nonTH neurons (A2 = -0.24 ± 0.02), implying that TH neurons contain a greater proportion of slowly recovering Na^+ channels, leading to slower recovery from inactivation. Slower recovery would tend to limit the rate of action potential firing and suggests that action potential firing may be slower in TH neurons compared to nonTH neurons. However, we observed no difference in spontaneous action potential frequency between TH and nonTH neurons. Limitations on maximum action potential firing frequency imposed by slower recovery of Na^+ channels in TH neurons may become apparent at more depolarized potentials when neurons are firing action potentials at higher rates.

We also investigated persistent Na^+ current, which has an amplitude of 1-5% of I_{NaT} (Stafstrom, 2007; Kiss, 2008). Despite it's small contribution, persistent current is

functionally significant in regulating neuronal excitability. For example, I_{NaP} contributes to bursting activity in rat SFO neurons by facilitating action potential firing (Washburn et al., 2000b; Fry and Ferguson, 2007). Persistent current is also recognized to potentiate excitatory post-synaptic potentials thereby facilitating neurotransmitter release (Stafstrom, 2007).

To our knowledge, this is the first study to record I_{NaP} in AP neurons. A previous study (Hay and Lindsley, 1995) attempted to elicit I_{NaP} in AP neurons, however, they were unsuccessful in recording this current in tested neurons. It is likely that the protocol they used was not optimal for recording I_{NaP} and thus prevented observation of this current. Voltage ramps that are too slow lead to time dependent inactivation of I_{NaP} before a significant amount of current can be measured (Magistretti and Alonso, 1999), preventing observation of I_{NaP}. I_{NaP} is most readily observed using a fast voltage ramp to prevent time-dependent inactivation of I_{NaP}, such as the one used in this study.

The properties of I_{NaP} in mouse AP neurons appear to be similar to those measured in rat SFO neurons. For example, we observed peak I_{NaP} to occur at a membrane potential of -36.1 ± 1.0 mV in TH neurons and -33.9 ± 1.0 mV in nonTH neurons. In rat SFO neurons, I_{NaP} is reported to occur near -40 mV (Kuksis and Ferguson, 2015). In mouse AP neurons, we observed an average I_{NaP} of -26.5 ± 3.0 pA in TH neurons and -26.2 ± 2.7 in nonTH neurons. A similarly small current of 68.5 ± 15.4 is observed in rat SFO neurons (Fry and Ferguson, 2007). Finally, we observed that I_{NaP} makes up 1.2 ± 0.1% of I_{NaT} in TH neurons and 0.8% ± 0.1% of I_{NaT} in nonTH neurons, which is smaller than 2.6% reported in SFO neurons (Fry and Ferguson, 2007).

It is not surprising that many of the transient and persistent Na^+ current properties we have measured in AP neurons are similar to those measured in SFO neurons, as many of the same voltage-gated Na^+ channels are expressed in these sensory CVOs including Nav1.1, Nav1.2, Nav1.3, and Nav1.7 (Hindmarch et al., 2008, 2011). For example, previous work from our lab (Huang, unpublished) has demonstrated that time dependent recovery of Na^+ channels from inactivation is relatively slow in SFO neurons with time constants of 6.29 ms to 6.82 ms for τ_1 and 102.2 ms to 107.3 ms for τ_2 when fitted to a double exponential equation. Our measurements of time dependent recovery of Na^+ channels in AP neurons are similarly slow, suggesting the similar Na^+ channels are contributing to I_{NaT} in the AP and SFO.

The Na^+ channels Nav1.1 and Nav1.7 recover more slowly (taking several hundreds of milliseconds to fully recover) than Nav1.2 and Nav1.3, which fully recover in just a few milliseconds. A previous study investigating Nav1.1 reported time constants of 8.5 ± 0.6 for τ_1 and 997.9 ± 308.7 for τ_2 (Thompson et al., 2011). Similar time constants of 19.6 ± 0.8 ms for τ_1 and 933.4 ± 54.6 ms have been observed for Nav1.7 (Vijayaragavan et al., 2001). Conversely, time constants of Nav1.2 and Nav1.3 are very fast and range from 2 ms to 11 ms when fitted with a single exponential function (Cummins et al., 2001; Rush et al., 2005). Based on these values, our results suggest that a large proportion of the Na^+ channels expressed in AP neurons are likely slowly recovering such as Nav1.1 and Nav1.7, as a large portion of I_{NaT} recovery consisted of slow recovery and because I_{NaT} took hundreds of milliseconds to reach near full recovery. Further, differential expression Na^+ channel isoforms and their splice variants (Smith and

Goldin, 1998; Thompson et al., 2011) could contribute to our observations of slower recovery in TH neurons.

It is widely accepted that I_{NaP} is carried by the same channels as I_{NaT}, but arises from different gating mechanisms including increased channel open times, decreased inactivation, or late channel openings (Alzheimer et al., 1993; Stafstrom, 2007). Given that the SFO and AP share many of the same voltage-gated Na^+ channels, it is not surprisingly that I_{NaP} properties are also similar between these CVOs.

4.6 I_H properties in TH and nonTH neurons

I_H current is best recognized for its role in generating pacemaker activity within the sinoatrial (Yanagihara and Irisawa, 1980) and atrioventricular nodes (Kokubun et al., 1982) of the heart. In the CNS, I_H has additional physiologically relevant roles including generating afterhyperpolarization potentials and contributing to resting membrane potential (Maccaferri et al., 1993; Funahashi et al., 2003).

In rats, a similar percentage (50-60%) of neurons within the AP and SFO express I_H (Washburn et al., 2000a; Funahashi et al., 2003, 2006). Within these sensory CVOs, I_H contributes to the generation of rebound potentials and a more depolarized resting membrane potential. Interestingly, rat AP neurons expressing I_H are thought to have a functionally distinct role in homeostasis (Funahashi et al., 2006). Specifically, rat AP neurons that express I_H are thought to participate in nausea and emesis (Shinpo et al., 2012). Conversely, rat AP neurons that are presynaptically modulated by the satiety signals cholecystokinin and amylin, and therefore likely involved in energy homeostasis, do not express I_H (Fukuda et al., 2013; Sugeta et al., 2015).

In the present study, we observed that most (95%) TH neurons do not express I_H. In contrast, 31.6% of nonTH neurons tested expressed I_H. Our observations of an overall lower rate of I_H compared to previous studies may be due to the use of a dissociated neuronal preparation, as it removes most processes from the neuron. Because of this, currents that are carried by channels predominately expressed in neuronal process may be attenuated or lost. Microarray analysis has revealed that HCN 1, 2, and 3 are expressed in the AP (Notomi and Shigemoto, 2004; Milligan et al., 2006; Hindmarch et al., 2011). Of these channels, only HCN1 has been confirmed to localize to the neuronal body (Notomi and Shigemoto, 2004). Other HCN isoforms are known to localize to neuronal processes in the thalamus (Abbas et al., 2006) and hippocampus (Notomi and Shigemoto, 2004). Thus, it is possible that one or more of the HCN isoforms in the AP localizes to neuronal processes and was therefore lost in the dissociation process. Species differences between mice and rats may also account for our observed difference in the rate of I_H expression. In mice, a significantly smaller proportion of neurons in the anterolateral bed nucleus of stria terminalis express I_H compared to the rat (Daniel et al., 2017).

Previous work has suggested that AP neurons expressing I_H play a significant role in initiating nausea and emesis (Funahashi et al., 2004; Shinpo et al., 2012) and other work has suggested that CA-containing AP neurons participate in emesis (Yoshikawa and Yoshida, 2002). Moreover, clinically relevant GLP-1 receptor agonists, such as exenatide (Byetta™) and liraglutide (Victoza™), induce nausea in some patients (Bettge et al., 2017; Horowitz et al., 2017). CA-containing AP neurons are thought to largely mediate the effects of circulating GLP-1 (a role supported by our whole-cell patch clamp results) suggesting that these neurons may in fact play a role in nausea induced by clinically used

GLP-1 receptor agonists. Together, the data suggest that TH neurons may belong to a neuronal circuit within the AP that functions to detect noxious compounds and initiate nausea and emesis.

4.7 GLP-1 receptor agonist application in TH and nonTH neurons

GLP-1 is an incretin hormone with powerful insulinotropic (Holst et al., 1987; Weir et al., 1989; Fehmann and Habener, 1992) and appetite-inhibiting effects (Turton et al., 1996). In particular, the appetite-reducing effects of GLP-1 are believed to be centrally mediated as GLP-1 receptors are widely distributed throughout the brain, including in key feeding areas such as the ARC and AP (Uttenthal et al., 1992; Göke et al., 1995; Richards et al., 2014), and ICV administration of GLP-1 in fasted (Turton et al., 1996) or schedule-fed (Meeran et al., 1999) rats reduces food intake. Previous literature suggests that the AP is important in detecting circulating GLP-1 as peripherally administered GLP-1 induces c-fos in the AP of mice (Parker et al., 2013) and ablation of the AP in rats alters exendin-4 response (Baraboi et al., 2010). Many AP neurons that are activated by GLP-1 contain CAs (Yamamoto et al., 2003; Holst, 2007), suggesting that this subpopulation is critical for GLP-1 detection at the level of the AP. While there is a growing body of literature implicating this neuronal population in the detection of circulating GLP-1, the direct electrophysiological response of these neurons to GLP-1 receptor agonists has never been investigated. Therefore, we sought to examine the response of AP CA-containing neurons to GLP-1 receptor agonists.

We began with preliminary experiments in cell-attached configuration to examine the effects of GLP-1 receptor agonists on spontaneous action potential frequency. A total

of 4 TH neurons were tested with either 1 μM GLP-1 or 1 μM Exendin-4. There was no obvious effect on spontaneous action potential frequency (data not shown) in any of the tested neurons. This is contradictory to previous literature that strongly suggests CA-containing neurons should respond to GLP-1 receptor agonists (Yamamoto et al., 2003; Holst, 2007). We hypothesized that the neurons may have been too active in cell-attached configuration to readily observe a response. Therefore, we switched to conducting our experiments in current clamp configuration so that we could maintain more control over membrane potential and action potential firing frequency.

In current clamp, we observed that the majority of TH neurons tested were activated by either 1 μM GLP-1 (n=4 of 6 neurons) or 1 μM Exendin-4 (n=8 of 13), while the remaining neurons showed no response. We observed a prolonged membrane depolarization and increase in action potential frequency in TH neurons that responded to GLP-1 receptor agonists. Membrane potential depolarized by 9.3 ± 1.6 mV following application of 1 μM GLP-1 onto TH neurons. This effect appeared to be very protracted as it took 1 of the responding neurons over 1500s to recover. The remaining responding neurons did not recover however, based on the recovery time we measured in the first neuron, it is possible that we did not maintain our recordings long enough to observe recovery in these neurons. Similarly, application of 1 μM Exendin-4 depolarized membrane potential by 8.2 ± 1.4 mV and this response lasted for 667.3 ± 135 s in the neurons that recovered (n=5). The duration of effect of 1 μM Exendin-4 application has been previously reported to last 10 minutes in acutely prepared mouse brain slices (Farkas et al., 2016).

Our observations that the majority of TH neurons responded to GLP-1 receptor agonists are consistent with previous c-Fos studies indicating that circulating GLP-1 activates CA-containing AP neurons (Schreihofer et al., 1997; Yamamoto et al., 2003). A significant drawback to studies utilizing c-Fos is that they are limited to only providing information about neuronal activation, as they are unable to detect neuronal inhibition. Our work builds upon these previous studies as our results indicate that GLP-1 receptor agonists do not inhibit CA-containing AP neurons.

A number of other studies have reported only observing membrane depolarization in the hypothalamic paraventricular nucleus, bed nucleus of the stria terminalis, and lateral hypothalamus following GLP-1 application (Acuna-Goycolea and van den Pol, 2004; Richards et al., 2014). Excitatory responses of similar magnitude and length to GLP-1 receptor agonist application have also been observed in other brain nuclei. One study reported that 100 nM GLP-1 depolarized membrane potential by 8 ± 1 mV in neurons of the bed nucleus of the stria terminalis, and by 8 ± 0.3 mV in hippocampal neurons (Richards et al., 2014). Another previous study reported that the effects of 1 μM Exendin-4 on action potential frequency of mouse gonadotropin-releasing hormone neurons lasted 10 minutes, which is similar in length to the response we observed in TH neurons treated with 1 μM Exendin-4 (Farkas et al., 2016).

In addition to the large majority of CA-containing neurons that express the GLP-1 receptor, GLP-1 receptor expression has been reported in a small percentage of nonCA AP neurons (Yamamoto et al., 2003). Therefore, we also applied 1 μM GLP-1 to this population and found that 2 of 8 nonTH neurons responded. Membrane potential significantly depolarized by 4.9 ± 2.1 mV in these 2 neurons. Action potential frequency

also increased in these neurons. The remaining nonTH neurons (n=6) showed no significant change in either of these properties following GLP-1 application.

Our observations that a minority of nonTH neurons respond to 1 μM GLP-1 suggest that this neuronal subpopulation also expresses the GLP-1 receptor. This is consistent with a previous study suggesting that a small number of nonCA AP neurons express the GLP-1 receptor (Yamamoto et al., 2003), as well as our immunochemistry results, which indicated that approximately 1 out of ever 10 nonTH neurons express the GLP-1 receptor.

4.8 Physiological relevance

The AP participates in emesis, cardiovascular regulation, and energy balance. Intriguingly, many of the central effects of GLP-1 including the induction of nausea and emesis, increased blood pressure and heart rate (Barragán et al., 1999), and decreased food intake (Tang-Christensen et al., 1996; Turton et al., 1996; Davis et al., 1998; Meeran et al., 1999) overlap with the roles of the AP. CA-containing AP neurons project to autonomic control sites such as the NTS, PBN, and VLM that are involved in these homeostatic functions (Shapiro and Miselis, 1985; Cunningham et al., 1994). Importantly, a previous study reported that 90% of CA-synthesizing AP neurons express the GLP-1 receptor (Yamamoto et al., 2003) and we have shown that a large proportion of CA-containing AP are directly activated by GLP-1 receptor agonists. Thus, this group of neurons is well situated to mediate the central effects of circulating GLP-1 through the first order detection of this peptide and subsequent signalling to higher brain nuclei. This notion is well supported by a previous observation that CA-containing projections from

the AP activate gastric sensory NTS neurons, resulting in reduced gastric motility and anorexia (Shapiro and Miselis, 1985; Yamamoto et al., 2003; Hollis et al., 2004),

In the present study, we have shown that there are subtle differences in the electrophysiological properties of CA and nonCA neurons, however these differences alone are not enough to identify CA neurons from nonCA neurons. Our observations that electrophysiological properties vary within CA-containing neurons suggest they are a heterogeneous population. This notion is supported by other studies that have shown CA-neurons have heterogeneous properties. CA-containing neurons of the AP are recognized to participate in a variety of homeostatic functions including emesis (Yoshikawa and Yoshida, 2002), cardiovascular regulation (Miller et al., 2015), and energy balance (Rinaman et al., 1998). However, CA-containing AP neurons do not appear to be specifically organized according to physiological function or projection area (Yamamoto et al., 2003), as neuronal subpopulations of the SFO are (McKinley et al., 2003). Neurons expressing specific K^+-current properties and I_H do not localize to specific areas of the AP (Funahashi et al., 2006) and our results show these properties cannot be used to identify CA-containing neurons. Additionally, some CA-containing neurons also contain serotonin (Miceli et al., 1987), suggesting that this is not a biochemically homogenous population. Finally, our results also imply that TH and nonTH neurons have an overlapping function in the detection of GLP-1, raising the question if these subpopulations participate in overlapping or distinct physiological roles.

4.9 Future Directions

Our results demonstrate that there are subtle differences in electrophysiological properties between CA and nonCA neurons. However, these differences alone are not enough to distinguish CA-containing from nonCA containing neurons. Further electrophysiological experiments are needed to determine if TH neurons can be electrically identified from nonTH neurons. Previously, Funahashi et al. (2002a) demonstrated that AP neurons could be grouped according to time to first action potential and first interspike interval, properties which strongly correlate with I_{TO}. Future experiments could examine these properties in TH and nonTH neurons using depolarizing current injections as described by Funahashi et al. (2002a). Because we did not find that K^+ current, Na^+ current, or I_H could be used to distinguish TH from nonTH neurons in the present study, if we were to observe a difference in time to first action potential and/or first interspike interval between TH and nonTH neurons, this would imply that additional ionic currents contribute to the modulation of these properties. Voltage-gated Ca^{2+} channels including CaV1.2, CaV1.3, and CaV2.2 are also expressed in the AP (Hindmarch et al., 2011). These channels are important for activation of Ca^{2+} dependent currents in AP neurons such as MaxiK current (Li and Hay, 2000).

Further studies could also utilize microarray experiments/next generation sequencing for comparison of CA-containing and nonCA neuron transcriptomes. In order to accomplish this, dissociated GFP-expressing TH-containing neurons could be separated from nonTH neurons using flow-assisted cell sorting (FACS). After cell sorting, cDNA would be extracted, reverse-transcribed, and hybridized to a microarray chip to determine gene-expression. Previous experiments in our lab have shown that

FACS is an effective way to separate dissociated GFP-expressing neurons from non-fluorescent neurons (unpublished data) and other previous studies have successfully used this technique for separation and gene-expression profiling of neuronal subpopulations (Lobo et al., 2006; Krolewski et al., 2013). If microarray analysis shows the specific expression of a peptide receptor in CA-containing neurons, this receptor could be used to identify these neurons in patch clamp experiments by applying the peptide and looking for a response.

Recently, Acuna-Goycolea and van den Pol, (2004) demonstrated that GLP-1 activates a nonselective cation current in a G-protein dependent manner within mouse hypothalamic neurons. This mechanism of action differs from the proposed mechanism of GLP-1 action in pancreatic β-cells, which includes inhibition of K_{ATP} channels (Holz et al., 1993), as well as in preganglionic neurons, where GLP-1 has been demonstrated to inhibit the opening of voltage-gated K^+ channels (Gaisano et al., 2010). The mechanism of GLP-1 action on AP neurons is currently unknown. Therefore, future experiments could work towards elucidating the intracellular pathway and ion channel(s) that lead to AP neuronal activation following GLP-1 application. Many previous studies have suggested that the GLP-1 receptor is coupled to the G_s pathway (Acuna-Goycolea and van den Pol, 2004). An initial set of experiments could investigate whether GLP-1 receptor activation is coupled to the G_s pathway in AP neurons by including GDPβS (a nonhydrolyzable GDP analog) in the recording pipet. If the GLP-1 receptor were coupled to the G_s pathway in AP neurons, GDPβS would prevent neuronal activation. If GDPβS did not prevent neuronal activation, it would suggest that the GLP-1 receptor is coupled to an alternative pathway in AP neurons, such as the $G_{i/o}$ pathway (Hällbrink et al., 2001).

A second set of experiments could examine what ion channel(s) might be responsible for depolarization of AP neurons following GLP-1 application. In these experiments, neurons would be subjected to a series of increasing current injections before and during GLP-1 application. Change in membrane potential would be plotted against injected current to generate a VI curve. VI curves would be compared before and during GLP-1 application to investigate any changes in input resistance and determine reversal potential of effect. If input resistance were to change following GLP-1 application, it would suggest that GLP-1 modulates ion channels. Specifically, an increase in input resistance would suggest that GLP-1 application leads to ion channel closing, while a decrease in input resistance would suggest that GLP-1 leads to ion channel opening. Reversal potential of effect is indicative of the ion channel being modulated according to the Nernst equation. For example, if GLP-1 were modulating K^+ channels in AP neurons, a reversal potential of effect near -90 mV would be expected.

A large body of evidence suggests the AP is important for detection of the circulating satiety signals, such as amylin (Rowland et al., 1997; Rowland and Richmond, 1999; Lutz et al., 2001; Barth et al., 2004). Interestingly, immunochemistry experiments show that GLP-1 sensitive AP neurons do not express receptors for amylin (Züger et al., 2013). Most AP neurons that express the GLP-1 receptor also contain CAs (Yamamoto et al., 2003a). Therefore, the question arises whether integration of hormonal energy balance information occurs at the level of the AP, or at higher levels; in other words, do amylin sensitive neurons interact with GLP-1 sensitive CA-synthesizing neurons within the AP. In order to investigate this hypothesis, electrophysiological experiments could be carried out to examine changes in the properties of post-synaptic and mini-postsynaptic

potentials in CA-containing neurons following amylin application that would suggest they are being pre-synaptically regulated by amylin-sensitive neurons. GLP-1 and amylin are both anorexigenic satiety signals. If amylin-sensitive neurons post-synaptically regulate GLP-1 sensitive CA-containing neurons, it is possible that these satiety signals will exert synergistic effects on the activity of GLP-1 sensitive CA-containing neurons. The dose response curve of CA-containing neurons to GLP-1, amylin, and to GLP-1 applied together with amylin could be constructed and compared to one another to determine if these peptides exert synergistic effects. If lower doses of these peptides were required when they are applied together, this would be suggestive of synergistic action.

4.10 Summary

The present study is the first to characterize the electrophysiological properties of TH-containing AP neurons. These experiments demonstrated that there are subtle differences in K^+ current, Na^+ current and I_H properties between TH-containing and nonTH neurons. However, these differences alone are not enough to electrically "fingerprint" this biochemical population. Nonetheless, this work represents a valuable step towards understanding the roles and subtypes of AP neurons. The possibility remains that specific differences exist in TH neurons that can be used to identify them and future experiments will work towards elucidating these differences. The present study also investigated the response of TH neurons to the satiety signal GLP-1. In the AP, GLP-1 elicits depolarizing effects on the majority TH neurons and a minority of nonTH neurons, suggesting that AP neurons participate in the detection of circulating GLP-1 and subsequent signalling of energy balance information to higher neuronal centres. Our

results contribute to our current understanding of the effects of GLP-1 acting on the AP. This information furthers our knowledge of how the CNS participates in energy balance regulation and has the potential to contribute to development of more effective treatments for obesity.

5. References

Abbas SY, Ying S-W, Goldstein PA (2006) Compartmental distribution of hyperpolarization-activated cyclic-nucleotide-gated channel 2 and hyperpolarization-activated cyclic-nucleotide-gated channel 4 in thalamic reticular and thalamocortical relay neurons. Neuroscience 141:1811–1825.

Abbott NJ, Rönnbäck L, Hansson E (2006) Astrocyte-endothelial interactions at the blood-brain barrier. Nat Rev Neurosci 7:41–53.

Acuna-Goycolea C, van den Pol A (2004) Glucagon-Like Peptide 1 Excites Hypocretin/Orexin Neurons by Direct and Indirect Mechanisms: Implications for Viscera-Mediated Arousal. J Neurosci 24:8141–8152.

Ahmed M, Fezai M, Uzcategui NL, Hosseinzadeh Z, Lang F (2016) SGK3 Sensitivity of Voltage Gated K+ Channel Kv1.5 (KCNA5). Cell Physiol Biochem 38:359–367.

Albert JL, Nerbonne JM (1995) Calcium-independent depolarization-activated potassium currents in superior colliculus-projecting rat visual cortical neurons. J Neurophysiol 73:2163–2178.

Aldrich RW, Getting PA, Thompson SH (1979) Mechanism of frequency-dependent broadening of molluscan neurone soma spikes. J Physiol 291:531–544.

Alhadeff AL, Rupprecht LE, Hayes MR (2012) GLP-1 neurons in the nucleus of the solitary tract project directly to the ventral tegmental area and nucleus accumbens to control for food intake. Endocrinology 153:647–658.

Allen MA, Smith PM, Ferguson A V (1997) Adrenomedullin microinjection into the area postrema increases blood pressure. Am J Physiol 272:R1698-1703.

Alzheimer C, Schwindt PC, Crill WE (1993) Modal gating of Na+ channels as a mechanism of persistent Na+ current in pyramidal neurons from rat and cat sensorimotor cortex. J Neurosci 13:660–673.

An WF, Bowlby MR, Betty M, Cao J, Ling H-P, Mendoza G, Hinson JW, Mattsson KI, Strassle BW, Trimmer JS, Rhodes KJ (2000) Modulation of A-type potassium channels by a family of calcium sensors. Nature 403:553–556.

Anand BK, Brobeck JR (1951) Localization of a "Feeding Center" in the Hypothalamus of the Rat. Exp Biol Med 77:323–325.

Anderson JW, Smith PM, Ferguson A V (2001) Subfornical organ neurons projecting to paraventricular nucleus: whole-cell properties. Brain Res 921:78–85.

Andrews PL, Kovacs M, Watson JW (2001) The anti-emetic action of the neurokinin(1) receptor antagonist CP-99,994 does not require the presence of the area postrema in the dog. Neurosci Lett 314:102–104.

Aston-Jones GS, Siggins GR (1995) Electrophysiology. In: Psychopharmacology: The Fourth Generation of Progress. Raven Press, New York.

Bagnasco M, Tulipano G, Melis MR, Argiolas A, Cocchi D, Muller EE (2003) Endogenous ghrelin is an orexigenic peptide acting in the arcuate nucleus in response to fasting. Regul Pept 111:161–167.

Banks WA, Burney BO, Robinson SM (2008) Effects of triglycerides, obesity, and starvation on ghrelin transport across the blood-brain barrier. Peptides 29:2061–2065.

Banks WA, Kastin AJ, Huang W, Jaspan JB, Maness LM (1996) Leptin enters the brain

by a saturable system independent of insulin. Peptides 17:305–311.

Banks WA, Tschöp M, Robinson SM, Heiman ML (2002) Extent and direction of ghrelin transport across the blood-brain barrier is determined by its unique primary structure. J Pharmacol Exp Ther 302:822–827.

Bannon AW, Seda J, Carmouche M, Francis JM, Norman MH, Karbon B, McCaleb ML (2000) Behavioral characterization of neuropeptide Y knockout mice. Brain Res 868:79–87.

Baraboi E-D, Smith P, Ferguson A V, Richard D (2010) Lesions of area postrema and subfornical organ alter exendin-4-induced brain activation without preventing the hypophagic effect of the GLP-1 receptor agonist. Am J Physiol Regul Integr Comp Physiol 298:R1098-1110.

Barnes K, Ferrario C (1980) Characterization of the sympatho-facilitative area postrema path way. Clin Sci 59:255–251.

Barragán JM, Eng J, Rodríguez R, Blázquez E (1999) Neural contribution to the effect of glucagon-like peptide-1-(7-36) amide on arterial blood pressure in rats. Am J Physiol 277:E784-791.

Barth SW, Riediger T, Lutz TA, Rechkemmer G (2004) Peripheral amylin activates circumventricular organs expressing calcitonin receptor a/b subtypes and receptor-activity modifying proteins in the rat. Brain Res 997:97–102.

Berglund ED, Vianna CR, Donato J, Kim MH, Chuang J-C, Lee CE, Lauzon DA, Lin P, Brule LJ, Scott MM, Coppari R, Elmquist JK (2012) Direct leptin action on POMC neurons regulates glucose homeostasis and hepatic insulin sensitivity in mice. J Clin

Invest 122:1000–1009.

Berthoud H-R (2002) Multiple neural systems controlling food intake and body weight. Neurosci Biobehav Rev 26:393–428.

Bettge K, Kahle M, Abd El Aziz MS, Meier JJ, Nauck MA (2017) Occurrence of nausea, vomiting and diarrhoea reported as adverse events in clinical trials studying glucagon-like peptide-1 receptor agonists: A systematic analysis of published clinical trials. Diabetes, Obes Metab 19:336–347.

Bhargava KP, Gupta PC, Chandra O (1961) Effect of ablation of the chemoreceptor trigger zone (CT zone) on the emetic response to intraventricular injection of apomorphine and emetine in the dog. J Pharmacol Exp Ther 134:329–331.

Bian J, Bai XM, Zhao YL, Zhang L, Liu ZJ (2013) Lentiviral vector-mediated knockdown of Lrb in the arcuate nucleus promotes diet-induced obesity in rats. J Mol Endocrinol 51:27–35.

Bjørbæk C, Elmquist JK, Michl P, Ahima RS, van Bueren A, McCall AL, Flier JS (1998) Expression of Leptin Receptor Isoforms in Rat Brain Microvessels. Endocrinology 139:3485–3491.

Blair TA, Roberds SL, Tamkun MM, Hartshorne RP (1991) Functional characterization of RK5, a voltage-gated K+ channel cloned from the rat cardiovascular system. FEBS Lett 295:211–213.

Borison HL (1959) Effect of ablation of medullary emetic chemoreceptor trigger zone on vomiting responses to cerebral intraventricular injection of adrenaline, apomorphine and pilocarpine in the cat. J Physiol 147:172–177.

Budde T, Mager R, Pape H-C (1992) Different Types of Potassium Outward Current in Relay Neurons Acutely Isolated from the Rat Lateral Geniculate Nucleus. Eur J Neurosci 4:708–722.

Butler AA, Kesterson RA, Khong K, Cullen MJ, Pelleymounter MA, Dekoning J, Baetscher M, Cone RD (2000) A unique metabolic syndrome causes obesity in the melanocortin-3 receptor-deficient mouse. Endocrinology 141:3518–3521.

Canadian Institute for Health Information (2015) National Health Expenditure Trends, 1975 to 2015 Report.

Carpenter DO, Briggs DB, Knox AP, Strominger N (1988) Excitation of area postrema neurons by transmitters, peptides, and cyclic nucleotides. J Neurophysiol 59:358–369.

Chalfie M, Tu Y, Euskirchen G, Ward WW, Prasher DC (1994) Green fluorescent protein as a marker for gene expression. Science 263:802–805.

Chatelier A, Zhao J, Bois P, Chahine M (2010) Biophysical characterisation of the persistent sodium current of the Nav1.6 neuronal sodium channel: a single-channel analysis. Pflügers Arch - Eur J Physiol 460:77–86.

Cheung CC, Clifton DK, Steiner RA (1997) Proopiomelanocortin neurons are direct targets for leptin in the hypothalamus. Endocrinology 138:4489–4492.

Christopoulos G, Paxinos G, Huang XF, Beaumont K, Toga AW, Sexton PM (1995) Comparative distribution of receptors for amylin and the related peptides calcitonin gene related peptide and calcitonin in rat and monkey brain. Can J Physiol Pharmacol 73:1037–1041.

Collister JP, Osborn JW (1998) Area postrema lesion attenuates the long-term hypotensive effects of losartan in salt-replete rats. Am J Physiol - Regul Integr Comp Physiol 274:R357–R366.

Conley EC, Brammar WJ, Conley EC (1999) VLG K Kv3-Shaw: Vertebrate K+ channels related to Drosophila Shaw (Kvα subunits encoded by gene subfamily Kv3). In: Ion Channel Factsbook, pp 559–616. Academic Press.

Connor JA, Stevens CF (1971) Prediction of repetitive firing behaviour from voltage clamp data on an isolated neurone soma. J Physiol 213:31–53.

Contreras RJ, Stetson PW (1981) Changes in salt intake lesions of the area postrema and the nucleus of the solitary tract in rats. Brain Res 211:355–366.

Cooper E, Shrier A (1989) Inactivation of A currents and A channels on rat nodose neurons in culture. J Gen Physiol 94:881–910.

Cowley MA et al. (2003) The Distribution and Mechanism of Action of Ghrelin in the CNS Demonstrates a Novel Hypothalamic Circuit Regulating Energy Homeostasis. Neuron 37:649–661.

Cowley MA, Smart JL, Rubinstein M, Cerdan MG, Diano S, Horvath TL, Cone RD, Low MJ (2001) Leptin activates anorexigenic POMC neurons through a neural network in the arcuate nucleus. Nature 411:480–484.

Criscione L, Rigollier P, Batzl-Hartmann C, Rüeger H, Stricker-Krongrad A, Wyss P, Brunner L, Whitebread S, Yamaguchi Y, Gerald C, Heurich RO, Walker MW, Chiesi M, Schilling W, Hofbauer KG, Levens N (1998) Food intake in free-feeding and energy-deprived lean rats is mediated by the neuropeptide Y5 receptor. J Clin

Invest 102:2136–2145.

Cummings DE, Purnell JQ, Frayo RS, Schmidova K, Wisse BE, Weigle DS (2001) A Preprandial Rise in Plasma Ghrelin Levels Suggests a Role in Meal Initiation in Humans. Diabetes 50:1714–1719.

Cummins TR, Aglieco F, Renganathan M, Herzog RI, Dib-Hajj SD, Waxman SG (2001) Nav1.3 Sodium Channels: Rapid Repriming and Slow Closed-State Inactivation Display Quantitative Differences after Expression in a Mammalian Cell Line and in Spinal Sensory Neurons. J Neurosci 21:5952–5961.

Cunningham ET, Miselis RR, Sawchenko PE (1994) The relationship of efferent projections from the area postrema to vagal motor and brain stem catecholamine-containing cell groups: an axonal transport and immunohistochemical study in the rat. Neuroscience 58:635–648.

Curtis KS, Krause EG, Contreras RJ (2003) Cardiovascular function and circadian patterns in rats after area postrema lesions or prolonged food restriction. Neurosci Lett 350:46–50.

Daniel SE, Guo J, Rainnie DG (2017) A Comparative Analysis of the Physiological Properties of Neurons in the Anterolateral Bed Nucleus of the Stria Terminalis in the Mus musculus, Rattus norvegicus, and Macaca mulatta. J Comp Neurol 525:2235–2248.

Daousi C, Casson IF, Gill G V, MacFarlane IA, Wilding JPH, Pinkney JH (2006) Prevalence of obesity in type 2 diabetes in secondary care: association with cardiovascular risk factors. Postgrad Med J 82:280–284.

Date Y, Kojima M, Hosoda H, Sawaguchi A, Mondal MS, Suganuma T, Matsukura S, Kangawa K, Nakazato M (2000) Ghrelin, a novel growth hormone-releasing acylated peptide, is synthesized in a distinct endocrine cell type in the gastrointestinal tracts of rats and humans. Endocrinology 141:4255–4261.

Davis HR, Mullins DE, Pines JM, Hoos LM, France CF, Compton DS, Graziano MP, Sybertz EJ, Strader CD, Van Heek M (1998) Effect of chronic central administration of glucagon-like peptide-1 (7-36) amide on food consumption and body weight in normal and obese rats. Obes Res 6:147–156.

De Jonghe BC, Horn CC (2009) Chemotherapy agent cisplatin induces 48-h Fos expression in the brain of a vomiting species, the house musk shrew (Suncus murinus). Am J Physiol Regul Integr Comp Physiol 296:R902-911.

Druce MR, Neary NM, Small CJ, Milton J, Monteiro M, Patterson M, Ghatei MA, Bloom SR (2006) Subcutaneous administration of ghrelin stimulates energy intake in healthy lean human volunteers. Int J Obes (Lond) 30:293–296.

Drucker DJ, Brubaker PL (1989) Proglucagon gene expression is regulated by a cyclic AMP-dependent pathway in rat intestine. Proc Natl Acad Sci 86:3953–3957.

Drucker DJ, Philippe J, Mojsov S, Chick WL, Habener JF (1987) Glucagon-like peptide I stimulates insulin gene expression and increases cyclic AMP levels in a rat islet cell line. Proc Natl Acad Sci 84:3434–3438.

Du Z, Meng Z (2004) Effects of derivatives of sulfur dioxide on transient outward potassium currents in acutely isolated hippocampal neurons. Food Chem Toxicol 42:1211–1216.

Eckel LA, Ossenkopp KP (1993) Novel diet consumption and body weight gain are reduced in rats chronically infused with lithium chloride: mediation by the chemosensitive area postrema. Brain Res Bull 31:613–619.

Edwards GL, Ritter RC (1981) Ablation of the area postrema causes exaggerated consumption of preferred foods in the rat. Brain Res 216:265–276.

Edwards GL, Ritter RC (1986) Area postrema lesions: cause of overingestion is not altered visceral nerve function. Am J Physiol 251:R575-81.

Eissele R, Göke R, Willemer S, Harthus HP, Vermeer H, Arnold R, Göke B (1992) Glucagon-like peptide-1 cells in the gastrointestinal tract and pancreas of rat, pig and man. Eur J Clin Invest 22:283–291.

Erickson KR, Ronnekleiv OK, Kelly MJ (1993) Electrophysiology of guinea-pig supraoptic neurones: role of a hyperpolarization-activated cation current in phasic firing. J Physiol 460:407–425.

Everill B, Rizzo MA, Kocsis JD (1998) Morphologically identified cutaneous afferent DRG neurons express three different potassium currents in varying proportions. J Neurophysiol 79:1814–1824.

Farkas I, Vastagh C, Farkas E, Bálint F, Skrapits K, Hrabovszky E, Fekete C, Liposits Z (2016) Glucagon-Like Peptide-1 Excites Firing and Increases GABAergic Miniature Postsynaptic Currents (mPSCs) in Gonadotropin-Releasing Hormone (GnRH) Neurons of the Male Mice via Activation of Nitric Oxide (NO) and Suppression of Endocannabinoid Signaling Pathways. Front Cell Neurosci 10:214.

Faulconbridge LF, Cummings DE, Kaplan JM, Grill HJ (2003) Hyperphagic effects of

brainstem ghrelin administration. Diabetes 52:2260–2265.

Fehmann HC, Habener JF (1992) Insulinotropic hormone glucagon-like peptide-I(7-37) stimulation of proinsulin gene expression and proinsulin biosynthesis in insulinoma beta TC-1 cells. Endocrinology 130:159–166.

Ferguson AV, Bicknell RJ, Carew MA, Mason WT (1997) Dissociated Adult Rat Subfornical Organ Neurons Maintain Membrane Properties and Angiotensin Responsiveness for up to 6 Days. Neuroendocrinology 66:409–415.

Ferguson A V, Marcus P (1988) Area postrema stimulation induced cardiovascular changes in the rat. Am J Physiol 255:R855-60.

Ferrario CM, Barnes KL, Szilagyi JE, Brosnihan KB (1979) Physiological and pharmacological characterization of the area postrema pressor pathways in the normal dog. Hypertension 1:235–245.

Fink GD, Bruner CA, Mangiapane ML (1987) Area postrema is critical for angiotensin-induced hypertension in rats. Hypertension 9:355–361.

Fridolf T, Böttcher G, Sundler F, Ahrén B (1991) GLP-1 and GLP-1(7-36) amide: influences on basal and stimulated insulin and glucagon secretion in the mouse. Pancreas 6:208–215.

Fry M, Ferguson A V (2007) Subthreshold oscillations of membrane potential of rat subfornical organ neurons. Neuroreport 18:1389–1393.

Fry M, Ferguson A V (2009) Ghrelin modulates electrical activity of area postrema neurons. Am J Physiol Regul Integr Comp Physiol 296:R485-492.

Fukuda T, Hirai Y, Maezawa H, Kitagawa Y, Funahashi M (2013) Electrophysiologically

identified presynaptic mechanisms underlying amylinergic modulation of area postrema neuronal excitability in rat brain slices. Brain Res 1494:9–16.

Funahashi M, Mitoh Y, Akaike T, Matsuo R (2006) Variety of morphological and electrophysiological properties of area postrema neurons in adult rat brain slices. Neurosci Res 54:43–48.

Funahashi M, Mitoh Y, Kohjitani A, Matsuo R (2003) Role of the hyperpolarization-activated cation current (Ih) in pacemaker activity in area postrema neurons of rat brain slices. J Physiol 552:135–148.

Funahashi M, Mitoh Y, Matsuo R (2002a) Two distinct types of transient outward currents in area postrema neurons in rat brain slices. Brain Res 942:31–45.

Funahashi M, Mitoh Y, Matsuo R (2002b) Electrophysiological properties of the rat area postrema neurons displaying both the transient outward current and the hyperpolarization-activated inward current. Brain Res Bull 58:337–343.

Funahashi M, Mitoh Y, Matsuo R (2004) The sensitivity of hyperpolarization-activated cation current (Ih) to propofol in rat area postrema neurons. Brain Res 1015:198–201.

Gaisano GG, Park SJ, Daly DM, Beyak MJ (2010) Glucagon-like peptide-1 inhibits voltage-gated potassium currents in mouse nodose ganglion neurons. Neurogastroenterol Motil 22:470–479, e111.

Gatti PJ, Dias Souza J, Gillis RA (1988) Increase in coronary vascular resistance produced by stimulating neurons in the region of the area postrema of the cat. Brain Res 448:313–319.

Gean PW, Shinnick-Gallagher P (1989) The transient potassium current, the A-current, is involved in spike frequency adaptation in rat amygdala neurons. Brain Res 480:160–169.

Geerling JC, Shin J-W, Chimenti PC, Loewy AD (2010) Paraventricular hypothalamic nucleus: axonal projections to the brainstem. J Comp Neurol 518:1460–1499.

Gilg S, Lutz TA (2006) The orexigenic effect of peripheral ghrelin differs between rats of different age and with different baseline food intake, and it may in part be mediated by the area postrema. Physiol Behav 87:353–359.

Glanowska KM, Moenter SM (2015) Differential Regulation of GnRH Secretion in the Preoptic Area (POA) and the Median Eminence (ME) in Male Mice. Endocrinology 156:231–241.

Glenn Stanley B, Kyrkouli SE, Lampert S, Leibowitz SF (1986) Neuropeptide Y chronically injected into the hypothalamus: A powerful neurochemical inducer of hyperphagia and obesity. Peptides 7:1189-1192.

Göke R, Larsen PJ, Mikkelsen JD, Sheikh SP (1995) Distribution of GLP-1 binding sites in the rat brain: evidence that exendin-4 is a ligand of brain GLP-1 binding sites. Eur J Neurosci 7:2294–2300.

Gold MS, Shuster MJ, Levine JD (1996) Characterization of six voltage-gated K+ currents in adult rat sensory neurons. J Neurophysiol 75:2629–2646.

Goto M, Arima H, Watanabe M, Hayashi M, Banno R, Sato I, Nagasaki H, Oiso Y (2006) Ghrelin increases neuropeptide Y and agouti-related peptide gene expression in the arcuate nucleus in rat hypothalamic organotypic cultures. Endocrinology

147:5102–5109.

Government of Canada PHA of C (2011) Obesity in Canada - Healthy Living - Public Health Agency of Canada.

Grace AA, Onn SP (1989) Morphology and electrophysiological properties of immunocytochemically identified rat dopamine neurons recorded in vitro. J Neurosci 9:3463–3481.

Green ED, Maffei M, Braden V V, Proenca R, DeSilva U, Zhang Y, Chua SC, Leibel RL, Weissenbach J, Friedman JM (1995) The human obese (OB) gene: RNA expression pattern and mapping on the physical, cytogenetic, and genetic maps of chromosome 7. Genome Res 5:5–12.

Greenman Y, Kuperman Y, Drori Y, Asa SL, Navon I, Forkosh O, Gil S, Stern N, Chen A (2013) Postnatal Ablation of POMC Neurons Induces an Obese Phenotype Characterized by Decreased Food Intake and Enhanced Anxiety-Like Behavior. Mol Endocrinol 27:1091–1102.

Gromada J, Holst JJ, Rorsman P (1998) Cellular regulation of islet hormone secretion by the incretin hormone glucagon-like peptide 1. Pflugers Arch 435:583–594.

Gross PM, Weindl A (1987) Peering through the windows of the brain. J Cereb Blood Flow Metab 7:663–672.

Grouselle D, Chaillou E, Caraty A, Bluet-Pajot M-T, Zizzari P, Tillet Y, Epelbaum J (2008) Pulsatile Cerebrospinal Fluid and Plasma Ghrelin in Relation to Growth Hormone Secretion and Food Intake in the Sheep. J Neuroendocrinol 20:1138–1146.

Gu G, Roland B, Tomaselli K, Dolman CS, Lowe C, Heilig JS (2013) Glucagon-like

peptide-1 in the rat brain: distribution of expression and functional implication. J Comp Neurol 521:2235–2261.

Hagbom M, Istrate C, Engblom D, Karlsson T, Rodriguez-Diaz J, Buesa J, Taylor JA, Loitto V-M, Magnusson K-E, Ahlman H, Lundgren O, Svensson L (2011) Rotavirus stimulates release of serotonin (5-HT) from human enterochromaffin cells and activates brain structures involved in nausea and vomiting. PLoS Pathog 7:e1002115.

Håkansson ML, Hulting AL, Meister B (1996) Expression of leptin receptor mRNA in the hypothalamic arcuate nucleus--relationship with NPY neurones. Neuroreport 7:3087–3092.

Halaas JL, Gajiwala KS, Maffei M, Cohen SL, Chait BT, Rabinowitz D, Lallone RL, Burley SK, Friedman JM (1995) Weight-reducing effects of the plasma protein encoded by the obese gene. Science 269:543–546.

Hällbrink M, Holmqvist T, Olsson M, Östenson C-G, Efendic S, Langel Ü (2001) Different domains in the third intracellular loop of the GLP-1 receptor are responsible for Gαs and Gαi/Gαo activation. Biochim Biophys Acta - Protein Struct Mol Enzymol 1546:79–86.

Hansen AB, Gespach CP, Rosselin GE, Holst JJ (1988) Effect of truncated glucagon-like peptide 1 on cAMP in rat gastric glands and HGT-1 human gastric cancer cells. FEBS Lett 236:119–122.

Harvard Health Publications (2007) Weigh less, live longer: strategies for successful weight loss.

Hay M, Bishop VS (1991a) Effects of area postrema stimulation on neurons of the nucleus of the solitary tract. Am J Physiol 260:H1359-1364.

Hay M, Bishop VS (1991b) Interactions of area postrema and solitary tract in the nucleus tractus solitarius. Am J Physiol 260:H1466-1473.

Hay M, Lindsley KA (1995) Membrane properties of area postrema neurons. Brain Res 705:199–208.

Hendel MD, Collister JP (2005) Contribution of the subfornical organ to angiotensin II-induced hypertension. Am J Physiol Heart Circ Physiol 288:H680-685.

Hernández-Pineda R, Chow A, Amarillo Y, Moreno H, Saganich M, Vega-Saenz de Miera EC, Hernández-Cruz A, Rudy B (1999) Kv3.1-Kv3.2 channels underlie a high-voltage-activating component of the delayed rectifier K+ current in projecting neurons from the globus pallidus. J Neurophysiol 82:1512–1528.

Hetherington AW, Ranson SW (1940) Hypothalamic lesions and adiposity in the rat. Anat Rec 78:149–172.

Hindmarch C, Fry M, Yao ST, Smith PM, Murphy D, Ferguson A V (2008) Microarray analysis of the transcriptome of the subfornical organ in the rat: regulation by fluid and food deprivation. Am J Physiol Regul Integr Comp Physiol 295:R1914-1920.

Hindmarch CCT, Fry M, Smith PM, Yao ST, Hazell GGJ, Lolait SJ, Paton JFR, Ferguson A V, Murphy D (2011) The transcriptome of the medullary area postrema: the thirsty rat, the hungry rat and the hypertensive rat. Exp Physiol 96:495–504.

Hollis JH, Lightman SL, Lowry CA (2004) Integration of systemic and visceral sensory information by medullary catecholaminergic systems during peripheral

inflammation. Ann N Y Acad Sci 1018:71–75.

Holst JJ (2007) The physiology of glucagon-like peptide 1. Physiol Rev 87:1409–1439.

Holst JJ, Ørskov C, Vagn Nielsen O, Schwartz TW (1987) Truncated glucagon-like peptide I, an insulin-releasing hormone from the distal gut. FEBS Lett 211:169–174.

Holz GG, Kühtreiber WM, Habener JF (1993) Pancreatic beta-cells are rendered glucose-competent by the insulinotropic hormone glucagon-like peptide-1(7-37). Nature 361:362–365.

Holz GG, Leech CA, Habener JF (1995) Activation of a cAMP-regulated Ca(2+)-signaling pathway in pancreatic beta-cells by the insulinotropic hormone glucagon-like peptide-1. J Biol Chem 270:17749–17757.

Holz GG, Leech CA, Heller RS, Castonguay M, Habener JF (1999) cAMP-dependent mobilization of intracellular Ca2+ stores by activation of ryanodine receptors in pancreatic beta-cells. A Ca2+ signaling system stimulated by the insulinotropic hormone glucagon-like peptide-1-(7-37). J Biol Chem 274:14147–14156.

Horn CC (2009) Brain Fos expression induced by the chemotherapy agent cisplatin in the rat is partially dependent on an intact abdominal vagus. Auton Neurosci 148:76–82.

Horowitz M, Aroda VR, Han J, Hardy E, Rayner CK (2017) Upper and/or lower gastrointestinal adverse events with glucagon-like peptide-1 receptor agonists: Incidence and consequences. Diabetes, Obes Metab 19:672–681.

Hoyda TD, Ferguson A V (2010) Adiponectin modulates excitability of rat paraventricular nucleus neurons by differential modulation of potassium currents. Endocrinology 151:3154–3162.

Huang S (2014) The Role of Voltage-Gated Sodium Channel 1.3 on Subfornical Organ Neurons.

Huang S, Lee SA, Oswald KE, Fry M (2015) Ghrelin alters neurite outgrowth and electrophysiological properties of mouse ventrolateral arcuate tyrosine hydroxylase neurons in culture. Biochem Biophys Res Commun 466:682–688.

Huang W, Sved AF, Stricker EM (2000) Vasopressin and oxytocin release evoked by NaCl loads are selectively blunted by area postrema lesions. Am J Physiol Regul Integr Comp Physiol 278:R732-740.

Huszar D, Lynch CA, Fairchild-Huntress V, Dunmore JH, Fang Q, Berkemeier LR, Gu W, Kesterson RA, Boston BA, Cone RD, Smith FJ, Campfield LA, Burn P, Lee F (1997) Targeted Disruption of the Melanocortin-4 Receptor Results in Obesity in Mice. Cell 88:131–141.

Hyde TM, Miselis RR (1983) Effects of area postrema/caudal medial nucleus of solitary tract lesions on food intake and body weight. Am J Physiol 244:R577-587.

Ingalls AM, Dickie MM, Snell GD (1950) Obese, a new mutation in the house mouse. J Hered 41:317–318.

Ingves M V., Ferguson A V. (2010) Prokineticin 2 modulates the excitability of area postrema neurons in vitro in the rat. Am J Physiol - Regul Integr Comp Physiol 298:R617-626.

Jacobowitz DM, O'Donohue TL (1978) alpha-Melanocyte stimulating hormone: immunohistochemical identification and mapping in neurons of rat brain. Proc Natl Acad Sci U S A 75:6300–6304.

Jerng HH, Pfaffinger PJ, Covarrubias M (2004) Molecular physiology and modulation of somatodendritic A-type potassium channels. Mol Cell Neurosci 27:343–369.

Kalia M, Sullivan JM (1982) Brainstem projections of sensory and motor components of the vagus nerve in the rat. J Comp Neurol 211:248–264.

Kay AR, Krupa DJ (2001) Acute isolation of neurons from the mature mammalian central nervous system. Curr Protoc Neurosci Chapter 6:Unit 6.5.

Kessler MA, Yang M, Gollomp KL, Jin H, Iacovitti L (2003) The human tyrosine hydroxylase gene promoter. Mol Brain Res 112:8–23.

Kishi T, Aschkenasi CJ, Choi BJ, Lopez ME, Lee CE, Liu H, Hollenberg AN, Friedman JM, Elmquist JK (2005) Neuropeptide Y Y1 receptor mRNA in rodent brain: distribution and colocalization with melanocortin-4 receptor. J Comp Neurol 482:217–243.

Kiss T (2008) Persistent Na-channels: Origin and function. Acta Biol Hung 59:1–12.

Kohno D, Nakata M, Maekawa F, Fujiwara K, Maejima Y, Kuramochi M, Shimazaki T, Okano H, Onaka T, Yada T (2007) Leptin suppresses ghrelin-induced activation of neuropeptide Y neurons in the arcuate nucleus via phosphatidylinositol 3-kinase- and phosphodiesterase 3-mediated pathway. Endocrinology 148:2251–2263.

Koistinen HA, Karonen SL, Iivanainen M, Koivisto VA (1998) Circulating leptin has saturable transport into intrathecal space in humans. Eur J Clin Invest 28:894–897.

Kojima M, Hosoda H, Date Y, Nakazato M, Matsuo H, Kangawa K (1999) Ghrelin is a growth-hormone-releasing acylated peptide from stomach. Nature 402:656–660.

Kokubun S, Nishimura M, Noma A, Irisawa H (1982) Membrane currents in the rabbit

atrioventricular node cell. Pflugers Arch Eur J Physiol 393:15–22.

Komatsu R, Matsuyama T, Namba M, Watanabe N, Itoh H, Kono N, Tarui S (1989) Glucagonostatic and insulinotropic action of glucagonlike peptide I-(7-36)-amide. Diabetes 38:902–905.

Kopp J, Xu Z-Q, Zhang X, Pedrazzini T, Herzog H, Kresse A, Wong H, Walsh JH, Hökfelt T (2002) Expression of the neuropeptide Y Y1 receptor in the CNS of rat and of wild-type and Y1 receptor knock-out mice. Focus on immunohistochemical localization. Neuroscience 111:443–532.

Korol S V., Jin Z, Babateen O, Birnir B (2014) GLP-1 and Exendin-4 Transiently Enhance GABAA Receptor–Mediated Synaptic and Tonic Currents in Rat Hippocampal CA3 Pyramidal Neurons. Diabetes 64:79–89.

Kosten T, Contreras RJ, Stetson PW, Ernest MJ (1983) Enhanced saline intake and decreased heart rate after area postrema ablations in rat. Physiol Behav 31:777–785.

Krolewski RC, Packard A, Schwob JE (2013) Global expression profiling of globose basal cells and neurogenic progression within the olfactory epithelium. J Comp Neurol 521:833–859.

Kuksis M, Ferguson A V (2015) Actions of a hydrogen sulfide donor (NaHS) on transient sodium, persistent sodium, and voltage-gated calcium currents in neurons of the subfornical organ. J Neurophysiol 114:1641–1651.

Lamont EW, Bruton J, Blum ID, Abizaid A (2013) Ghrelin receptor-knockout mice display alterations in circadian rhythms of activity and feeding under constant lighting conditions. Eur J Neurosci 39:207–217.

Langlet F, Levin BE, Luquet S, Mazzone M, Messina A, Dunn-Meynell AA, Balland E, Lacombe A, Mazur D, Carmeliet P, Bouret SG, Prevot V, Dehouck B (2013a) Tanycytic VEGF-A boosts blood-hypothalamus barrier plasticity and access of metabolic signals to the arcuate nucleus in response to fasting. Cell Metab 17:607–617.

Langlet F, Mullier A, Bouret SG, Prevot V, Dehouck B (2013b) Tanycyte-like cells form a blood-cerebrospinal fluid barrier in the circumventricular organs of the mouse brain. J Comp Neurol 521:3389–3405.

Larsen PJ, Tang-Christensen M, Holst JJ, Orskov C (1997a) Distribution of glucagon-like peptide-1 and other preproglucagon-derived peptides in the rat hypothalamus and brainstem. Neuroscience 77:257–270.

Larsen PJ, Tang-Christensen M, Holst JJ, Orskov C (1997b) Distribution of glucagon-like peptide-1 and other preproglucagon-derived peptides in the rat hypothalamus and brainstem. Neuroscience 77:257–270.

Leech CA, Habener JF (1997) Insulinotropic glucagon-like peptide-1-mediated activation of non-selective cation currents in insulinoma cells is mimicked by maitotoxin. J Biol Chem 272:17987–17993.

Leech CA, Habener JF (1998) A role for Ca2+-sensitive nonselective cation channels in regulating the membrane potential of pancreatic beta-cells. Diabetes 47:1066–1073.

Leslie RA (1986) Comparative aspects of the area postrema: fine-structural considerations help to determine its function. Cell Mol Neurobiol 6:95–120.

Levin BE (2005) Factors promoting and ameliorating the development of obesity. Physiol

Behav 86:633–639.

Levin BE (2007) Why some of us get fat and what we can do about it. J Physiol 583:425–430.

Li Y, Wu X, Zhao Y, Chen S, Owyang C (2006) Ghrelin acts on the dorsal vagal complex to stimulate pancreatic protein secretion. Am J Physiol Gastrointest Liver Physiol 290:G1350-1358.

Li Z, Hay M (2000) 17-beta-estradiol modulation of area postrema potassium currents. J Neurophysiol 84:1385–1391.

Liberini CG, Boyle CN, Cifani C, Venniro M, Hope BT, Lutz TA (2016) Amylin receptor components and the leptin receptor are co-expressed in single rat area postrema neurons. Eur J Neurosci 43:653–661.

Lien C-C, Martina M, Schultz JH, Ehmke H, Jonas P (2002) Gating, modulation and subunit composition of voltage-gated K(+) channels in dendritic inhibitory interneurones of rat hippocampus. J Physiol 538:405–419.

Lin L, Saha PK, Ma X, Henshaw IO, Shao L, Chang BHJ, Buras ED, Tong Q, Chan L, McGuinness OP, Sun Y (2011) Ablation of ghrelin receptor reduces adiposity and improves insulin sensitivity during aging by regulating fat metabolism in white and brown adipose tissues. Aging Cell 10:996–1010.

Lobo MK, Karsten SL, Gray M, Geschwind DH, Yang XW (2006) FACS-array profiling of striatal projection neuron subtypes in juvenile and adult mouse brains. Nat Neurosci 9:443–452.

Lund PK, Goodman RH, Montminy MR, Dee PC, Habener JF (1983) Anglerfish islet

pre-proglucagon II. Nucleotide and corresponding amino acid sequence of the cDNA. J Biol Chem 258:3280–3284.

Luther JA, Halmos KC, Tasker JG (2000) A slow transient potassium current expressed in a subset of neurosecretory neurons of the hypothalamic paraventricular nucleus. J Neurophysiol 84:1814–1825.

Lutz TA, Mollet A, Rushing PA, Riediger T, Scharrer E (2001) The anorectic effect of a chronic peripheral infusion of amylin is abolished in area postrema/nucleus of the solitary tract (AP/NTS) lesioned rats. Int J Obes Relat Metab Disord 25:1005–1011.

Maccaferri G, Mangoni M, Lazzari A, DiFrancesco D (1993) Properties of the hyperpolarization-activated current in rat hippocampal CA1 pyramidal cells. J Neurophysiol 69:2129–2136.

Magistretti J, Alonso A (1999) Biophysical properties and slow voltage-dependent inactivation of a sustained sodium current in entorhinal cortex layer-II principal neurons: a whole-cell and single-channel study. J Gen Physiol 114:491–509.

Mangiapane ML, Skoog KM, Rittenhouse P, Blair ML, Sladek CD (1989) Lesion of the area postrema region attenuates hypertension in spontaneously hypertensive rats. Circ Res 64:129–135.

Marsh DJ, Hollopeter G, Kafer KE, Palmiter RD (1998) Role of the Y5 neuropeptide Y receptor in feeding and obesity. Nat Med 4:718–721.

Martina M, Schultz JH, Ehmke H, Monyer H, Jonas P (1998) Functional and molecular differences between voltage-gated K+ channels of fast-spiking interneurons and pyramidal neurons of rat hippocampus. J Neurosci 18:8111–8125.

Matsushita N, Okada H, Yasoshima Y, Takahashi K, Kiuchi K, Kobayashi K (2002) Dynamics of tyrosine hydroxylase promoter activity during midbrain dopaminergic neuron development. J Neurochem 82:295–304.

McCormick DA, Pape HC (1990) Properties of a hyperpolarization-activated cation current and its role in rhythmic oscillation in thalamic relay neurones. J Physiol 431:291–318.

McKinley MJ, McAllen RM, Davern P, Giles ME, Penschow J, Sunn N, Uschakov A, Oldfield BJ (2003) The sensory circumventricular organs of the mammalian brain. Adv Anat Embryol Cell Biol 172:1–122.

McMinn JE, Wilkinson CW, Havel PJ, Woods SC, Schwartz MW (2000) Effect of intracerebroventricular α-MSH on food intake, adiposity, c-Fos induction, and neuropeptide expression. Am J Physiol - Regul Integr Comp Physiol 279:R695–R703.

Meeran K, O'Shea D, Edwards CM, Turton MD, Heath MM, Gunn I, Abusnana S, Rossi M, Small CJ, Goldstone AP, Taylor GM, Sunter D, Steere J, Choi SJ, Ghatei MA, Bloom SR (1999) Repeated intracerebroventricular administration of glucagon-like peptide-1-(7-36) amide or exendin-(9-39) alters body weight in the rat. Endocrinology 140:244–250.

Mentlein R (1999) Dipeptidyl-peptidase IV (CD26)--role in the inactivation of regulatory peptides. Regul Pept 85:9–24.

Merchenthaler I, Lane M, Shughrue P (1999) Distribution of pre-pro-glucagon and glucagon-like peptide-1 receptor messenger RNAs in the rat central nervous system.

J Comp Neurol 403:261–280.

Miceli MO, Post CA, van der Kooy D (1987) Catecholamine and serotonin colocalization in projection neurons of the area postrema. Brain Res 412:381–385.

Michel S, Becskei C, Erguven E, Lutz TA, Riediger T (2007) Diet-derived nutrients modulate the effects of amylin on c-Fos expression in the area postrema and on food intake. Neuroendocrinology 86:124–135.

Miller AD, Leslie RA (1994) The area postrema and vomiting. Front Neuroendocrinol 15:301–320.

Miller RL, Denny GO, Knuepfer MM, Kleyman TR, Jackson EK, Salkoff LB, Loewy AD (2015) Blockade of ENaCs by amiloride induces c-Fos activation of the area postrema. Brain Res 1601:40–51.

Miller RL, Wang MH, Gray PA, Salkoff LB, Loewy AD (2013) ENaC-expressing neurons in the sensory circumventricular organs become c-Fos activated following systemic sodium changes. Am J Physiol - Regul Integr Comp Physiol 305:R1141-1152.

Milligan CJ, Edwards IJ, Deuchars J (2006) HCN1 ion channel immunoreactivity in spinal cord and medulla oblongata. Brain Res 1081:79–91.

Mizuno TM, Kleopoulos SP, Bergen HT, Roberts JL, Priest CA, Mobbs C V (1998) Hypothalamic pro-opiomelanocortin mRNA is reduced by fasting and [corrected] in ob/ob and db/db mice, but is stimulated by leptin. Diabetes 47:294–297.

Mollet A, Gilg S, Riediger T, Lutz TA (2004) Infusion of the amylin antagonist AC 187 into the area postrema increases food intake in rats. Physiol Behav 81:149–155.

Morest DK (1967) Experimental study of the projections of the nucleus of the tractus solitarius and the area postrema in the cat. J Comp Neurol 130:277–299.

Morita S, Miyata S (2012) Different vascular permeability between the sensory and secretory circumventricular organs of adult mouse brain. Cell Tissue Res 349:589–603.

Morrison CD, Morton GJ, Niswender KD, Gelling RW, Schwartz MW (2005) Leptin inhibits hypothalamic Npy and Agrp gene expression via a mechanism that requires phosphatidylinositol 3-OH-kinase signaling. Am J Physiol Endocrinol Metab 289:E1051-1057.

Mullier A, Bouret SG, Prevot V, Dehouck B (2010) Differential distribution of tight junction proteins suggests a role for tanycytes in blood-hypothalamus barrier regulation in the adult mouse brain. J Comp Neurol 518:943–962.

Nagamori K, Ishibashi M, Shiraishi T, Oomura Y, Sasaki K (2003) Effects of leptin on hypothalamic arcuate neurons in Wistar and Zucker rats: an in vitro study. Exp Biol Med (Maywood) 228:1162–1167.

Näslund E, Gutniak M, Skogar S, Rössner S, Hellström PM (1998) Glucagon-like peptide 1 increases the period of postprandial satiety and slows gastric emptying in obese men. Am J Clin Nutr 68:525–530.

Nichol KA, Morey A, Couzens MH, Shine J, Herzog H, Cunningham AM (1999) Conservation of expression of neuropeptide Y5 receptor between human and rat hypothalamus and limbic regions suggests an integral role in central neuroendocrine control. J Neurosci 19:10295–10304.

Notomi T, Shigemoto R (2004) Immunohistochemical localization of Ih channel subunits, HCN1-4, in the rat brain. J Comp Neurol 471:241–276.

Novak U, Wilks A, Buell G, McEwen S (1987) Identical mRNA for preproglucagon in pancreas and gut. Eur J Biochem 164:553–558.

O'Halloran DJ, Nikou GC, Kreymann B, Ghatei MA, Bloom SR (1990) Glucagon-like peptide-1 (7-36)-NH2: a physiological inhibitor of gastric acid secretion in man. J Endocrinol 126:169–173.

Orskov C, Poulsen SS, Møller M, Holst JJ (1996) Glucagon-like peptide I receptors in the subfornical organ and the area postrema are accessible to circulating glucagon-like peptide I. Diabetes 45:832–835.

Osaka T, Endo M, Yamakawa M, Inoue S (2005) Energy expenditure by intravenous administration of glucagon-like peptide-1 mediated by the lower brainstem and sympathoadrenal system. Peptides 26:1623–1631.

Palkovits M (1985) Distribution of neuroactive substances in the dorsal vagal complex of the medulla oblongata. Neurochem Int 7:213–219.

Papas S, Smith P, Ferguson A V (1990) Electrophysiological evidence that systemic angiotensin influences rat area postrema neurons. Am J Physiol 258:R70-76.

Pape HC (1996) Queer current and pacemaker: the hyperpolarization-activated cation current in neurons. Annu Rev Physiol 58:299–327.

Parker JA, McCullough KA, Field BCT, Minnion JS, Martin NM, Ghatei MA, Bloom SR (2013) Glucagon and GLP-1 inhibit food intake and increase c-fos expression in similar appetite regulating centres in the brainstem and amygdala. Int J Obes (Lond)

37:1391–1398.

Pedrazzini T, Seydoux J, Künstner P, Aubert J-F, Grouzmann E, Beermann F, Brunner HR (1998) Cardiovascular response, feeding behavior and locomotor activity in mice lacking the NPY Y1 receptor. Nat Med 4:722–726.

Pelletier G, Dube D (1977) Electron microscopic immunohistochemical localization of a-MSH in the rat brain. Am J Anat 150:201–205.

Percie du Sert N, Rudd JA, Moss R, Andrews PLR (2009) The delayed phase of cisplatin-induced emesis is mediated by the area postrema and not the abdominal visceral innervation in the ferret. Neurosci Lett 465:16–20.

Perfetti R, Zhou J, Doyle ME, Egan JM (2000) Glucagon-like peptide-1 induces cell proliferation and pancreatic-duodenum homeobox-1 expression and increases endocrine cell mass in the pancreas of old, glucose-intolerant rats. Endocrinology 141:4600–4605.

Peruzzo B, Pastor FE, Blázquez JL, Schöbitz K, Peláez B, Amat P, Rodríguez EM (2000) A second look at the barriers of the medial basal hypothalamus. Exp brain Res 132:10–26.

Petrov T, Howarth AG, Krukoff TL, Stevenson BR (1994) Distribution of the tight junction-associated protein ZO-1 in circumventricular organs of the CNS. Mol Brain Res 21:235–246.

Pirnik Z, Bundziková J, Holubová M, Pýchová M, Fehrentz JA, Martinez J, Zelezná B, Maletínská L, Kiss A (2011) Ghrelin agonists impact on Fos protein expression in brain areas related to food intake regulation in male C57BL/6 mice. Neurochem Int

59:889–895.

Po S, Snyders DJ, Baker R, Tamkun MM, Bennett PB (1992) Functional expression of an inactivating potassium channel cloned from human heart. Circ Res 71:732–736.

Pollick FE, Barnes KL, Ferrario CM (1987) Effect of area postrema lesion on low-frequency arterial pressure oscillations in dogs. Am J Physiol 253:H524-30.

Potes CS, Lutz TA, Riediger T (2010) Identification of central projections from amylin-activated neurons to the lateral hypothalamus. Brain Res 1334:31–44.

Privitera PJ, Beckstead RM, Yates P, Walgren R (2003) Autoradiographic localization of [125I-Tyr0]bradykinin binding sites in brains of Wistar-Kyoto and spontaneously hypertensive rats. Cell Mol Neurobiol 23:805–815.

Quirion R, Dalpé M, Dam T V (1986) Characterization and distribution of receptors for the atrial natriuretic peptides in mammalian brain. Proc Natl Acad Sci U S A 83:174–178.

Raufmansq J-P, Singhs L, Engll J (1991) Exendin-3, a novel peptide from Heloderma horridurn venom, interacts with vasoactive intestinal peptide receptors and a newly described receptor on dispersed acini from guinea pig pancreas. J Biol Chem 266:2897–2902.

Reese TS, Karnovsky MJ (1967) Fine structural localization of a blood-brain barrier to exogenous peroxidase. J Cell Biol 34:207–217.

Rettig J, Heinemann SH, Wunder F, Lorra C, Parcej DN, Oliver Dolly J, Pongs O (1994) Inactivation properties of voltage-gated K+ channels altered by presence of β-subunit. Nature 369:289–294.

Richards C., Shiroyama T, Kitai S. (1997) Electrophysiological and immunocytochemical characterization of GABA and dopamine neurons in the substantia nigra of the rat. Neuroscience 80:545–557.

Richards P, Parker HE, Adriaenssens AE, Hodgson JM, Cork SC, Trapp S, Gribble FM, Reimann F (2014) Identification and characterisation of glucagon-like peptide-1 receptor expressing cells using a new transgenic mouse model. Diabetes 63:1224–1233.

Riediger T, Zuend D, Becskei C, Lutz TA (2004) The anorectic hormone amylin contributes to feeding-related changes of neuronal activity in key structures of the gut-brain axis. Am J Physiol Regul Integr Comp Physiol 286:R114-122.

Rinaman L, Baker EA, Hoffman GE, Stricker EM, Verbalis JG (1998) Medullary c-Fos activation in rats after ingestion of a satiating meal. Am J Physiol 275:R262–R268.

Rodríguez EM, Rodríguez S, Hein S (1998) The subcommissural organ. Microsc Res Tech 41:98–123.

Rossi M, Kim MS, Morgan DG, Small CJ, Edwards CM, Sunter D, Abusnana S, Goldstone AP, Russell SH, Stanley SA, Smith DM, Yagaloff K, Ghatei MA, Bloom SR (1998) A C-terminal fragment of Agouti-related protein increases feeding and antagonizes the effect of alpha-melanocyte stimulating hormone in vivo. Endocrinology 139:4428–4431.

Rowland NE, Crews EC, Gentry RM (1997) Comparison of Fos induced in rat brain by GLP-1 and amylin. Regul Pept 71:171–174.

Rowland NE, Richmond RM (1999) Area postrema and the anorectic actions of

dexfenfluramine and amylin. Brain Res 820:86–91.

Rush AM, Dib-Hajj SD, Liu S, Cummins TR, Black JA, Waxman SG (2006) A single sodium channel mutation produces hyper- or hypoexcitability in different types of neurons. Proc Natl Acad Sci U S A 103:8245–8250.

Rush AM, Dib-Hajj SD, Waxman SG (2005) Electrophysiological properties of two axonal sodium channels, Nav1.2 and Nav1.6, expressed in mouse spinal sensory neurones. J Physiol 564:803–815.

Salam RA, Hooda M, Das JK, Arshad A, Lassi ZS, Middleton P, Bhutta ZA (2016) Interventions to improve adolescent nutrition: a systematic review and meta-analysis. J Adolesc Health 59:S29–S39.

Sandhu H, Wiesenthal SR, MacDonald PE, McCall RH, Tchipashvili V, Rashid S, Satkunarajah M, Irwin DM, Shi ZQ, Brubaker PL, Wheeler MB, Vranic M, Efendic S, Giacca A (1999) Glucagon-like peptide 1 increases insulin sensitivity in depancreatized dogs. Diabetes 48:1045–1053.

Schirra J, Göke B (2005) The physiological role of GLP-1 in human: incretin, ileal brake or more? Regul Pept 128:109–115.

Schirra J, Nicolaus M, Roggel R, Katschinski M, Storr M, Woerle HJ, Göke B (2006) Endogenous glucagon-like peptide 1 controls endocrine pancreatic secretion and antro-pyloro-duodenal motility in humans. Gut 55:243–251.

Schreihofer DA, Cameron JL, Verbalis JG, Rinaman L (1997) Cholecystokinin induces Fos expression in catecholaminergic neurons of the macaque monkey caudal medulla. Brain Res 770:37–44.

Scrocchi LA, Brown TJ, Maclusky N, Brubaker PL, Auerbach AB, Joyner AL, Drucker DJ (1996) Glucose intolerance but normal satiety in mice with a null mutation in the glucagon–like peptide 1 receptor gene. Nat Med 2:1254–1258.

Segal M, Barker JL (1984) Rat hippocampal neurons in culture: potassium conductances. J Neurophysiol 51:1409–1433.

Segal M, Rogawski M, Barker J (1984) A transient potassium conductance regulates the excitability of cultured hippocampal and spinal neurons. J Neurosci 4:604–609.

Serre V, Dolci W, Schaerer E, Scrocchi L, Drucker D, Efrat S, Thorens B (1998) Exendin-(9–39) Is an Inverse Agonist of the Murine Glucagon-Like Peptide-1 Receptor: Implications for Basal Intracellular Cyclic Adenosine 3′,5′-Monophosphate Levels and β-Cell Glucose Competence [1]. Endocrinology 139:4448–4454.

Sexton PM, Paxinos G, Kenney MA, Wookey PJ, Beaumont K (1994) In vitro autoradiographic localization of amylin binding sites in rat brain. Neuroscience 62:553–567.

Shapiro RE, Miselis RR (1985) The central neural connections of the area postrema of the rat. J Comp Neurol 234:344–364.

Shi P, Stocker SD, Toney GM (2007) Organum vasculosum laminae terminalis contributes to increased sympathetic nerve activity induced by central hyperosmolality. AJP Regul Integr Comp Physiol 293:R2279–R2289.

Shi W-X (2009) Electrophysiological characteristics of dopamine neurons: a 35-year update. J Neural Transm Suppl:103–119.

Shibata R, Nakahira K, Shibasaki K, Wakazono Y, Imoto K, Ikenaka K (2000) A-Type K+ Current Mediated by the Kv4 Channel Regulates the Generation of Action Potential in Developing Cerebellar Granule Cells. J Neurosci 20:4145–4155.

Shinpo K, Hirai Y, Maezawa H, Totsuka Y, Funahashi M (2012) The role of area postrema neurons expressing H-channels in the induction mechanism of nausea and vomiting. Physiol Behav 107:98–103.

Shintani M, Ogawa Y, Ebihara K, Aizawa-Abe M, Miyanaga F, Takaya K, Hayashi T, Inoue G, Hosoda K, Kojima M, Kangawa K, Nakao K (2001) Ghrelin, an endogenous growth hormone secretagogue, is a novel orexigenic peptide that antagonizes leptin action through the activation of hypothalamic neuropeptide Y/Y1 receptor pathway. Diabetes 50:227–232.

Simoes D, Riva P, Peliciari-Garcia RA, Cruzat VF, Graciano MF, Munhoz AC, Taneda M, Cipolla-Neto J, Carpinelli AR (2016) Melatonin modifies basal and stimulated insulin secretion via NADPH oxidase. J Endocrinol 231:235–244.

Skoog KM, Mangiapane ML (1988) Area postrema and cardiovascular regulation in rats. Am J Physiol 254:H963-969.

Smith PM, Brzezinska P, Hubert F, Mimee A, Maurice DH, Ferguson A V. (2016) Leptin influences the excitability of area postrema neurons. Am J Physiol - Regul Integr Comp Physiol 310:R440-448.

Smith RD, Goldin AL (1998) Functional analysis of the rat I sodium channel in Xenopus oocytes. J Neurosci 18:811–820.

Spain WJ, Schwindt PC, Crill WE (1991) Two transient potassium currents in layer V

pyramidal neurones from cat sensorimotor cortex. J Physiol 434:591–607.

Stafstrom CE (2007) Persistent sodium current and its role in epilepsy. Epilepsy Curr 7:15–22.

Stanić D, Mulder J, Watanabe M, Hökfelt T (2011) Characterization of NPY Y2 receptor protein expression in the mouse brain. II. Coexistence with NPY, the Y1 receptor, and other neurotransmitter-related molecules. J Comp Neurol 519:1219–1257.

Statistics Canada (2014) Overweight and obese adults (self-reported), 2014.

Sugeta S, Hirai Y, Maezawa H, Inoue N, Yamazaki Y, Funahashi M (2015) Presynaptically mediated effects of cholecystokinin-8 on the excitability of area postrema neurons in rat brain slices. Brain Res 1618:83–90.

Suzuki S, Kawai K, Ohashi S, Mukai H, Yamashita K (1989) Comparison of the effects of various C-terminal and N-terminal fragment peptides of glucagon-like peptide-1 on insulin and glucagon release from the isolated perfused rat pancreas. Endocrinology 125:3109–3114.

Tabarean I V (2014) Electrical remodeling of preoptic GABAergic neurons involves the Kv1.5 subunit. PLoS One 9:e96643.

Takaya K, Ogawa Y, Hiraoka J, Hosoda K, Yamori Y, Nakao K, Koletsky RJ (1996) Nonsense mutation of leptin receptor in the obese spontaneously hypertensive Koletsky rat. Nat Genet 14:130–131.

Takayama K, Johno Y, Hayashi K, Yakabi K, Tanaka T, Ro S (2007) Expression of c-Fos protein in the brain after intravenous injection of ghrelin in rats. Neurosci Lett 417:292–296.

Tang-Christensen M, Larsen PJ, Göke R, Fink-Jensen A, Jessop DS, Møller M, Sheikh SP (1996) Central administration of GLP-1-(7-36) amide inhibits food and water intake in rats. Am J Physiol 271:R848-856.

Tang-Christensen M, Vrang N, Larsen PJ (1998) Glucagon-like peptide 1(7-36) amide's central inhibition of feeding and peripheral inhibition of drinking are abolished by neonatal monosodium glutamate treatment. Diabetes 47:530–537.

Tartaglia LA, Dembski M, Weng X, Deng N, Culpepper J, Devos R, Richards GJ, Campfield LA, Clark FT, Deeds J, Muir C, Sanker S, Moriarty A, Moore KJ, Smutko JS, Mays GG, Wool EA, Monroe CA, Tepper RI (1995) Identification and expression cloning of a leptin receptor, OB-R. Cell 83:1263–1271.

Thomas EA, Bechtell JL, Vestal BE, Johnson SL, Bessesen DH, Tregellas JR, Cornier M-A (2013) Eating-related behaviors and appetite during energy imbalance in obese-prone and obese-resistant individuals. Appetite 65:96–102.

Thompson CH, Kahlig M, George YL (2011) SCN1A splice variants exhibit divergent sensitivity to commonly used antiepileptic drugs. Epilepsia 52:1000–1009.

Tolessa T, Näslund E, Hellström PM (2001) The inhibitory mechanism of GLP-1, but not glucagon, on fasted gut motility is dependent on the L-arginine/nitric oxide pathway. Regul Pept 98:33–40.

Tong Y, Pelletier G (1992) Role of dopamine in the regulation of proopiomelanocortin (POMC) mRNA levels in the arcuate nucleus and pituitary gland of the female rat as studied by in situ hybridization. Brain Res Mol Brain Res 15:27–32.

Tschöp M, Smiley DL, Heiman ML (2000) Ghrelin induces adiposity in rodents. Nature

407:908–913.

Turton MD, O'Shea D, Gunn I, Beak SA, Edwards CM, Meeran K, Choi SJ, Taylor GM, Heath MM, Lambert PD, Wilding JP, Smith DM, Ghatei MA, Herbert J, Bloom SR (1996) A role for glucagon-like peptide-1 in the central regulation of feeding. Nature 379:69–72.

Tuso P (2014) Prediabetes and lifestyle modification: time to prevent a preventable disease. Perm J 18:88–93.

Uebele VN, England SK, Chaudhary A, Tamkun MM, Snyders DJ (1996) Functional differences in Kv1.5 currents expressed in mammalian cell lines are due to the presence of endogenous Kv beta 2.1 subunits. J Biol Chem 271:2406–2412.

Uttenthal LO, Blázquez E (1990) Characterization of high-affinity receptors for truncated glucagon-like peptide-1 in rat gastric glands. FEBS Lett 262:139–141.

Uttenthal LO, Toledano A, Blázquez E (1992) Autoradiographic localization of receptors for glucagon-like peptide-1 (7-36) amide in rat brain. Neuropeptides 21:143–146.

van den Top M, Lee K, Whyment AD, Blanks AM, Spanswick D (2004) Orexigen-sensitive NPY/AgRP pacemaker neurons in the hypothalamic arcuate nucleus. Nat Neurosci 7:493–494.

Vijayaragavan K, O 'leary ME, Chahine M (2001) Gating Properties of Na v 1.7 and Na v 1.8 Peripheral Nerve Sodium Channels. J Neurosci 21:7909–1918.

Vonderlin N, Fischer F, Zitron E, Seyler C, Scherer D, Thomas D, Katus HA, Scholz EP (2014) Inhibition of cardiac Kv1.5 potassium current by the anesthetic midazolam: mode of action. Drug Des Devel Ther 8:2263–2271.

Wang J-H, Wang F, Yang M-J, Yu D-F, Wu W-N, Liu J, Ma L-Q, Cai F, Chen J-G (2008) Leptin regulated calcium channels of neuropeptide Y and proopiomelanocortin neurons by activation of different signal pathways. Neuroscience 156:89–98.

Wang Y, Lavond DG, Chambers KC (1997) Cooling the area postrema induces conditioned taste aversions in male rats and blocks acquisition of LiCl-induced aversions. Behav Neurosci 111:768–776.

Washburn DL, Anderson JW, Ferguson A V (2000a) The calcium receptor modulates the hyperpolarization-activated current in subfornical organ neurons. Neuroreport 11:3231–3235.

Washburn DLS, Anderson JW, Ferguson A V. (2000b) A subthreshold persistent sodium current mediates bursting in rat subfornical organ neurones. J Physiol 529:359–371.

Watson WE (1985) The effect of removing area postrema on the sodium and potassium balances and consumptions in the rat. Brain Res 359:224–232.

Weigle DS, Duell PB, Connor WE, Steiner RA, Soules MR, Kuijper JL (1997) Effect of fasting, refeeding, and dietary fat restriction on plasma leptin levels. J Clin Endocrinol Metab 82:561–565.

Weir GC, Mojsov S, Hendrick GK, Habener JF (1989) Glucagonlike peptide I (7-37) actions on endocrine pancreas. Diabetes 38:338–342.

Wen J, Phillips SF, Sarr MG, Kost LJ, Holst JJ (1995) PYY and GLP-1 contribute to feedback inhibition from the canine ileum and colon. Am J Physiol 269:G945-952.

White SH, Sturgeon RM, Magoski NS (2016) Nicotine inhibits potassium currents in

Aplysia bag cell neurons. J Neurophysiol 115:2635–2648.

WHO (2016) WHO | Obesity and overweight. WHO.

Willesen MG, Kristensen P, Rømer J (1999) Co-localization of growth hormone secretagogue receptor and NPY mRNA in the arcuate nucleus of the rat. Neuroendocrinology 70:306–316.

Williams KW, Margatho LO, Lee CE, Choi M, Lee S, Scott MM, Elias CF, Elmquist JK (2010) Segregation of acute leptin and insulin effects in distinct populations of arcuate proopiomelanocortin neurons. J Neurosci 30:2472–2479.

Wu R-L, Barish ME (1999) Modulation of a slowly inactivating potassium current, ID, by metabotropic glutamate receptor activation in cultured hippocampal pyramidal neurons. J Neurosci 19:6825–6837.

Xie C, Su H, Guo T, Yan Y, Peng X, Cao R, Wang Y, Chen P, Wang X, Liang S (2014) Synaptotagmin I delays the fast inactivation of Kv1.4 channel through interaction with its N-terminus. Mol Brain 7:4.

Xue B, Gole H, Pamidimukkala J, Hay M (2003) Role of the area postrema in angiotensin II modulation of baroreflex control of heart rate in conscious mice. Am J Physiol Heart Circ Physiol 284:H1003-1007.

Yamamoto H, Kishi T, Lee CE, Choi BJ, Fang H, Hollenberg AN, Drucker DJ, Elmquist JK (2003) Glucagon-like peptide-1-responsive catecholamine neurons in the area postrema link peripheral glucagon-like peptide-1 with central autonomic control sites. J Neurosci 23:2939–2946.

Yamamoto H, Lee CE, Marcus JN, Williams TD, Overton JM, Lopez ME, Hollenberg

AN, Baggio L, Saper CB, Drucker DJ, Elmquist JK (2002) Glucagon-like peptide-1 receptor stimulation increases blood pressure and heart rate and activates autonomic regulatory neurons. J Clin Invest 110:43–52.

Yanagihara K, Irisawa H (1980) Inward current activated during hyperpolarization in the rabbit sinoatrial node cell. Pflugers Arch Eur J Physiol 385:11–19.

Yang B, Ferguson A V. (2002) Orexin-A Depolarizes Dissociated Rat Area Postrema Neurons through Activation of a Nonselective Cationic Conductance. J Neurosci 22:6303–6308.

Yang C-G, Wang W-G, Yan J, Fei J, Wang Z-G, Zheng Q (2013) Gastric motility in ghrelin receptor knockout mice. Mol Med Rep 7:83–88.

Yang M-J, Wang F, Wang J-H, Wu W-N, Hu Z-L, Cheng J, Yu D-F, Long L-H, Fu H, Xie N, Chen J-G (2010) PI3K integrates the effects of insulin and leptin on large-conductance Ca2+-activated K+ channels in neuropeptide Y neurons of the hypothalamic arcuate nucleus. Am J Physiol Endocrinol Metab 298:E193-201.

Yang S-J, Lee K-Z, Wu C-H, Lu K-T, Hwang J-C (2006) Vasopressin produces inhibition on phrenic nerve activity and apnea through V(1A) receptors in the area postrema in rats. Chin J Physiol 49:313–325.

Yao ST, Antunes VR, Bradley PMJ, Kasparov S, Ueta Y, Paton JFR, Murphy D (2011) Temporal profile of arginine vasopressin release from the neurohypophysis in response to hypertonic saline and hypotension measured using a fluorescent fusion protein. J Neurosci Methods 201:191-195.

Yoshikawa T, Yoshida N (2002) Effect of 6-hydroxydopamine treatment in the area

postrema on morphine-induced emesis in ferrets. Jpn J Pharmacol 89:422–425.

Yuan W, Burkhalter A, Nerbonne JM (2005) Functional role of the fast transient outward K+ current IA in pyramidal neurons in (rat) primary visual cortex. J Neurosci 25:9185–9194.

Yue C, Yaari Y (2004) KCNQ/M channels control spike afterdepolarization and burst generation in hippocampal neurons. J Neurosci 24:4614–4624.

Zigman JM, Jones JE, Lee CE, Saper CB, Elmquist JK (2006) Expression of ghrelin receptor mRNA in the rat and the mouse brain. J Comp Neurol 494:528–548.

Zobel EH, Hansen TW, Rossing P, von Scholten BJ (2016) Global changes in food supply and the obesity epidemic. Curr Obes Rep:1–7.

Züger D, Forster K, Lutz TA, Riediger T (2013) Amylin and GLP-1 target different populations of area postrema neurons that are both modulated by nutrient stimuli. Physiol Behav 112:61–69.